Effects of Thermal Aging on Plastic Ball Grid Array Microprocessor Life under Power and Mechanical Cycling

by

Md. Kamruzzaman

MASTER OF SCIENCE IN MECHANICAL ENGINEERING

Department of Mechanical Engineering

BANGLADESH UNIVERSITY OF ENGINEERING AND TECHNOLOGY

Dhaka – 1000, Bangladesh

September 2019

Effects of Thermal Aging on Plastic Ball Grid Array Microprocessor Life under Power and Mechanical Cycling

by

Md. Kamruzzaman

Submitted to

DEPARTMENT OF MECHANICAL ENGINEERING

in partial fulfillment of the requirements for the degree of

MASTER OF SCIENCE IN MECHANICAL ENGINEERING

Department of Mechanical Engineering

BANGLADESH UNIVERSITY OF ENGINEERING AND TECHNOLOGY

Dhaka – 1000, Bangladesh

September 2019

Certificate of Approval

The thesis titled "**Effects of Thermal Aging on Plastic Ball Grid Array Microprocessor Life under Power and Mechanical Cycling**" submitted by **Md. Kamruzzaman**, Roll No.: **0416102009 P**, Session: **April, 2016**, has been accepted as satisfactory in partial fulfillment of the requirement for the degree of Master of Science in Mechanical Engineering on **September 4, 2019.**

BOARD OF EXAMINERS

Dr. Mohammad Abdul Motalab Associate Professor Department of Mechanical Engineering, BUET, Dhaka – 1000	Chairman (Supervisor)
Dr. Md. Ashraful Islam Professor and Head Department of Mechanical Engineering, BUET, Dhaka – 1000	Member (Ex- officio)
Dr. Md. Afsar Ali Professor Department of Mechanical Engineering, BUET, Dhaka – 1000	Member
Dr. Ahmed Sahrif Professor Department of Materials and Metallurgical Engineering, BUET, Dhaka – 1000	Member (External)

CANDIDATE'S DECLARATION

It is hereby declared that this thesis or any part of it has not been submitted elsewhere for the award of any degree.

Md. Kamruzzaman

Author

DEDICATION

Dedicated to My Family

Table of Contents

List of Tables

List of Figures

List of Abbreviations of Technical Symbols and Terms

Abbreviations

PBGA	Plastic Ball Grid Array
RoHS	Restriction of Hazardous Substances
WEEE	Waste from Electrical and Electronic Equipment
PCB	Printed Circuit Board
ENIG	Electroless Nickel Immersion Gold
SMT	Surface Mount Technology
PLWK	Plastic Work (MPa)
CTE	Coefficient of Thermal Expansion (ppm/°C)

Symbols

Ag	Silver
Cu	Copper
Pb	Lead
Sn	Tin
W_{pl}	Plastic Work (MPa)
ΔW	Plastic Work per Cycle (MPa)
P	Power (Js^{-1}/watt(W))
σ	Normal Stress (MPa)
τ	Shear Stress (MPa)
s_o	Initial value of Deformation resistance (MPa)
Q/R	Activation Energy (kJ/mole)/Universal Gas Constant (kJ/(mole-K))
A	Pre-exponential Factor (1/s)
ξ	Multiple of Stress
m	Strain Rate Sensitivity of Stress
h_o	Hardening/Softening constant (MPa)
$\hat{s}$	Coefficient for Deformation Resistance Saturation Value (MPa)
n	Strain rate Sensitivity of Saturation (Deformation resistance) Value
a	Strain Rate Sensitivity of Hardening or softening

Acknowledgment

At the very first, I would like to show my gratitude to Allah Sub-ha-na-hu-wa-ta-ala without Whose mercy it is not possible to complete a single good deed in this world. I would like to express my gratitude toward Him for His blessings upon me to complete this arduous task.

After that, the most important person in doing this strenuous job is my supervisor, Dr. Mohammad Abdul Motalab, Associate Professor, Department of Mechanical Engineering, Bangladesh University of Engineering and Technology. I am very much debtful to him for his kind supervision, constant guidance, encouragement, support and thoughtful discussion throughout the entire research.

I am also grateful to the Department of Mechanical Engineering for allowing me to use the "Postgraduate Computer Lab" for the research. Also to friends/colleagues for their valuable support.

Finally, I wish to thank my parents, wife, friends, relatives, colleagues and all my well-wishers for their help and mental support.

Abstract

Traditional finite element based predictions for solder joint reliability of electronic packages use the accelerated thermal cycling life testing method and are based on solder constitutive equations (e.g. Anand viscoplastic model) and failure models (e.g. energy dissipation per cycle model). The Accelerated thermal testing method has the drawback that it considers uniform temperature distribution in the entire package during operation which is not the actual case. Also, the constitutive equations and failure models are subject to change with thermal aging which is a common phenomenon in electronic assemblies that causes great changes in the microstructure, mechanical response, and failure behavior of Lead-Free solder joints, which are not considered in the traditional finite element analysis of thermal cycling method. Besides, in commercially available solders, the percentage of silver is generally varied between 1 ~ 4%, which in turn affects the mechanical properties of solder joints. In this study, finite element analysis of a 3D plastic ball grid array (PBGA) package has been performed firstly for the power cycling simulations to observe the effects of variation of aging time (between 0 to 365 days) and specified range of Ag % of solder materials. The non uniform temperature distribution of the package is first obtained by a non-linear transient heat transfer analysis for this purpose. In next, another cycling named as mechanical bend cycling is considered in this study. Electronic packages may be subjected to mechanical cycling during manufacturing or assembly processes, in transportation, and in application stages that can pose a threat to the package life. Three different loading frequencies 1, 3, and 5 Hz with three different testing temperatures (25, 75, and 125 °C) have been used in mechanical cycling simulations. Effects of solder aging (0 to 365 days) and variation of Ag (1 ~ 4 %) on the mechanical cycling life has also been investigated. Results show that solder aging enhances power cycling life of the PBGA packages while it becomes detrimental in case of mechanical bend cycling. Similarly, a boost up of the power cycling life has been observed with changing the Ag % from 1 to 4% while it has proven to deteriorate the mechanical cycling life of the PBGA package.

CHAPTER 1

Introduction

1.1 General

Electronic Packaging is the housing and interconnection of integrated circuits (also referred to as ICs, silicon chips, chips, or die) to form electronic systems ranging from individual semiconductor devices up to complete systems such as a mainframe computer. The functions that a package must provide include a structure to physically support the chip, a physical housing to protect the chip from the environment, an adequate means of removing heat generated by the chips or system, electrical connections to allow signal and power access to and from the chip, and a wiring structure to provide interconnection between the chips of an electronic system. Besides, an electronic package must also function at its designed performance level while still allowing for a product that is high quality, reliable, serviceable, and economical. Thus electronic packaging technology is becoming more and more challenging as they are getting increasingly complex due to the requirement of reduce power, down-size, high density and multi-functionality products. The three breakthroughs in packaging technology are shown in Figure 1.1 [1]. The first breakthrough in the packaging technology was the through-hole mounting technology that involves the use of leads on the components that are inserted into holes drilled in printed circuit boards (PCB) and soldered to pads on the opposite side. The drawback of this technology was that it requires the drilling of holes, which is expensive and time consuming. The hole also limits the density of interconnections as it needs to pass through all layers of the PCB. To overcome the limitations of through-hole mounting, surface mount technology (SMT) emerged in which components are mounted directly onto the surface of the PCB and so there is no need of hole. Another technology which is not new but miniaturization of SMT is chip-scale packaging in which the passive components surrounding the chips must also be miniaturized. The Ball Grid Array or BGA is a type of surface mount technology that is used for integrated circuits. PBGA is sometimes referred to as Motorola's Over Molded Pad Array Carrier or OMPAC package, is a subset of BGA. It was developed by Motorola in the late 1980's for use in Motorola products such as radios, pagers and cellular telephones. Nowadays, it is also being used in other applications e.g. automobiles, spaceships, etc. for logical operations.

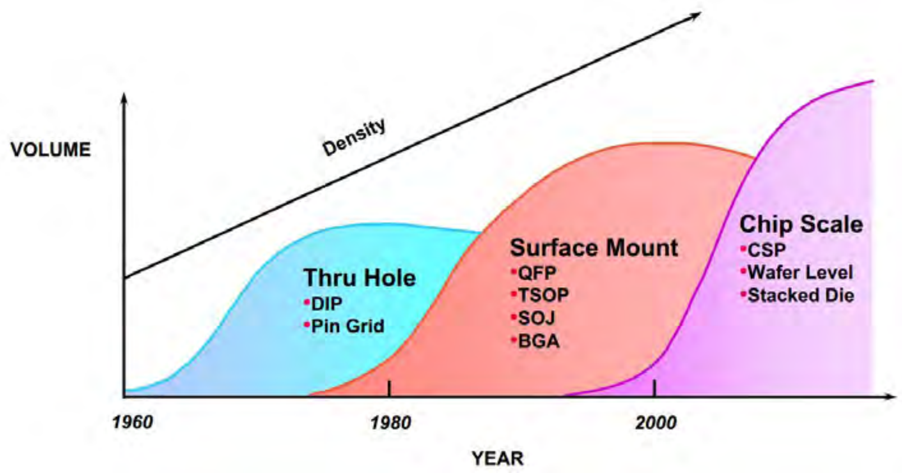

Figure 1.1 Showing the Evolution in Electronic Packaging Technologies

PBGA uses plastic substrates with copper traces to transmit electronic signals between chip and PCB for processing of data. Due to more interconnections compared to other types of packages, reduced size and weight and reduced manufacturing cost, PBGA has become one of the most popular packaging alternatives for high I/O devices in the packaging industry. The orientation of different layers in a typical PBGA microprocessor package is shown in Figure 1.2. In the center of the package, silicon chip (die) is located. The chip is encapsulated by a molding compound. The purpose of the molding compound is to protect the silicon chip from damage due to harsh environments. The material under the die is called substrate material. Its function is to support the silicon chip and transmit electronic signals from the die to the printed circuit board (PCB). A die attach material is used to attach the silicon die with substrates. Between the substrate and the PCB, BGA solder balls are located. Solder balls are used to transmit electronic signal from the silicon die to the PCB for effective and efficient performance and computation. The bottom-most layer is called the PCB board. The Printed Circuit Board (PCB) mechanically supports and electrically connects electronic components using conductive tracks, pads and other features etched from copper sheets laminated onto a non-conductive substrate. Components (e.g. capacitors, resistors or active devices) are generally soldered on the PCB.

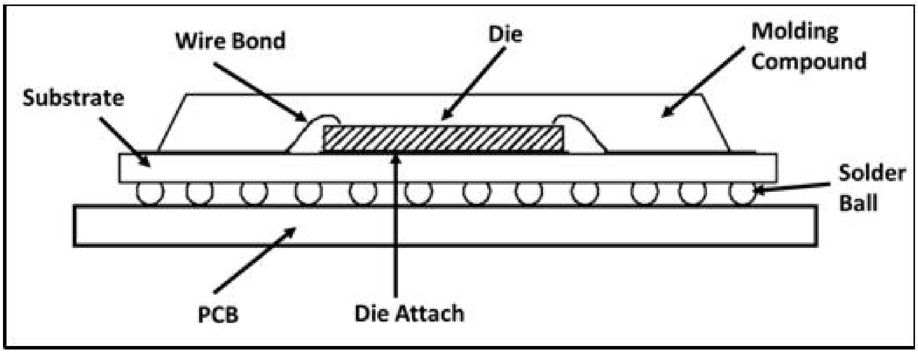

Figure 1.2 Schematic Diagram of a PBGA Package

1.2 Advantages of BGA Packages

The Ball Grid Array provides several number of benefits to IC and equipment manufacturers as well as providing benefits to the eventual users of equipment. Some of the BGA benefits over other technologies include:

(i) Efficient use of PCB space, allowing connections to be made under the SMD package and not just around its periphery, leading to more interconnections.

(ii) Better thermal and electrical performance. BGA packages offer power and ground planes for low inductances and controlled impedance traces for signals as well as being able to remove heat via the pads, etc.

(iii) Improvements in manufacturing yields as a result of the improved soldering. BGAs allow wide spacing between connections as well as a better level of solderability.

(iv) Reduction in package thickness which is a great advantage when many assemblies need to be made much thinner, e.g. mobile phones, etc.

(v) Reduction in weight of microprocessor components.

1.3 Different Types of BGA Packages

In order to meet the variety of requirements for different types of assembly and equipment, several number of BGA variants have been developed.

(i) MAPBGA - Molded Array Process Ball Grid Array: This BGA package is suitable for low-performance to mid-performance devices that require packaging with low inductance, ease of surface mounting. It provides a low-cost option with a high level of reliability.

(ii) PBGA - Plastic Ball Grid Array: This BGA package is suitable for mid-to-high-performance devices that require low inductance, ease of surface mounting, relatively low cost, while also retaining high levels of reliability. It has some additional copper layers in the substrate that enable increased power dissipation levels to be handled.

(iii) TEPBGA - Thermally Enhanced Plastic Ball Grid Array: This package is used for much higher heat dissipation application. It uses thick copper planes in the substrate to draw heat from the die to the customer board.

(iv) TBGA - Tape Ball Grid Array: Solution for applications needing an external heatsink. This BGA provides a mid-to-high-end high thermal performance without an external heatsink.

(v) PoP - Package on Package: This package is used in applications where space is at a real premium. It allows for stacking a memory package on top of a base device.

(vi) MicroBGA: This type of BGA package is smaller than the standard BGA package. Three pitches are prevalent in the industry: 0.65, 0.75 and 0.8mm.

1.4 Lead-Free Solders in Electronic Packaging Industry

The reflow process and other manufacturing parameters of electronic packaging are dependent on the material used as solder. The material of choice in this case was the Tin-Lead (Sn-Pb) eutectic alloy which had proved to be highly useful due to their relatively low melting temperature (183 °C), excellent ductility, good reliability, and for their superior wettability and compatibility with most substrates and devices [2]. However environmental research indicated that the presence of lead in the environment, even in small quantities could have severe effects. Lead is harmful in very small amounts (as are most heavy metals); once absorbed into the body lead combines with and inhibits the functioning of certain enzymes often with severe physiological or neurological consequences. Lead is an element hence it cannot be degraded or transformed into some other material, and it is extremely difficult to clean up after dispersal in the environment. The problem arises when old electronic devices are disposed using the usual solid waste management processes and ultimately end up in landfills. The acidity of the rain water washes the solder lead out from these crushed PCBs, which eventually ends up in the drinking water. Although electronic devices contain a very small amount of lead, the sheer number of devices being disposed off is a cause for concern.

In order to prevent the spread of lead in the environment measures were taken to reduce the amount of lead being used in industries around the world. In June 2000, the EU adopted two directives, the Waste of Electrical and Electronic Equipment (WEEE) and the Directive of the Restriction of the Use of Certain Hazardous Substances (RoHS) [3]. The WEEE directive requires that lead has to be removed from any end-of-life electrical or electronic components. The RoHS specifically bans lead from electrical and electronic components manufactured after July 1, 2006. As a result of the enforcement of the directives, all electrical or electronic equipment and devices produced in or imported to E.U. member states must comply with these lead-free standards except those items that are exempted from the bans. So due to the general push towards the eco-efficiency and green electronics, manufacturers are motivated for the adoption of Lead-Free electronics. Therefore, the conversion to Lead-Free solders in the global electronic market appears imminent.

Replacing it with another material meant that this new material would have to be close to the original in terms of its mechanical and thermal properties so that there would be a minimum amount of restructuring required by manufacturers. As an alternative to

Sn-Pb solder, researchers tried to use pure tin since it formed the major portion of the Sn-Pb alloy. But using tin had its own problems and did not prove to be the best alternative. Others tried to use Sn-Zn alloy but the study of this composition is still in progress and further research is needed for its useful application. Much of the research was directed towards finding an appropriate composition of tin-silver-copper which was expected to give properties close to the original material. However, the actual composition of the Sn-Ag-Cu (SAC) alloy varies among manufacturers and to date there are few compositions which are considered as benchmarks.

In selecting a suitable alternative of Sn-Pb soldering materials, it is important to take into consideration that the properties of the alternative solders are comparable or superior to Sn-Pb solders. Compatible candidates of the Sn-Pb solders must have the following behaviors [4]:

- Melting temperature similar to eutectic Sn-Pb for a similar reflow profile
- Sufficient wettability for good metallization process
- Good electrical properties for transmitting electrical signals
- Strong mechanical properties for good fatigue resistance and reliability
- Inexpensive and easier manufacturability

1.5 Sn-Ag-Cu Lead-Free Solder Alloys

Among different lead-free solders, SnAgCu (SAC) has been the most popular, widely used in today's market. A variety of SAC alloys with different chemical compositions have been proposed by various user groups and industry experts. These include: SAC105 (98.5Sn-1.0Ag-0.5Cu), SAC205 (97.5Sn-2.0Ag-0.5Cu), SAC305 (96.5Sn-3.0Ag-0.5Cu), and SAC405 (95.5Sn-4.0Ag-0.5Cu), known as the SACN05 series; SAC387 (95.5Sn-3.8Ag-0.7Cu), SAC396 (95.5Sn-3.9Ag-0.6Cu), and SAC357 (95.2Sn-3.5Ag-0.7Cu), identified as near eutectic SAC choices; SAC3810 (95.2Sn-3.8Ag-1.0Cu), SAC3595 (95.55Sn-3.5Ag-0.95Cu), SAC0307 (9Sn-0.3Ag-0.7Cu), and SAC107 (98.3Sn-1.0Ag-0.7Cu), designed for special needs such as high temperature application, drop and shock optimization, etc. The main benefits of the various SAC alloy systems are their relatively low melting temperatures compared with the 96.5Sn- 3.5Ag binary eutectic alloy, as well as their superior mechanical and manufacturability properties when compared to other Lead-Free solders [5].

In SAC alloys, the formation of intermetallic compounds between the primary elements Sn and Ag, and Cu affect all the properties of the alloys. There are three possible intermetallic compounds that may be formed: Ag_3Sn forms due to the reaction between Sn and Ag and Cu_6Sn_5 forms due to the Sn and Cu reaction. The compound Cu_3Sn will not form at the eutectic point unless the Cu content is high enough for the formation of Cu_3Sn at higher temperatures, so in bulk specimens, Cu_3Sn is not presented. There is no reaction between Ag and Cu to form any kind of intermetallic compounds. The particles of intermetallic compounds possess much higher strength than the bulk material. Fine intermetallic particles in the Sn matrix can, therefore, strengthen the alloys. However, due to the brittleness of intermetallic compound, fatigue life of electronic components can also be reduced.

1.6 Mechanical Properties of Lead-Free Solders

Electronic equipments are somewhat unusual as all categories of engineering materials may exist in close proximity. The properties of these materials are also different from each other. So, each components will have different effect. Solder joints are used to mount chips and components onto printed circuit boards (PCB) and thus create an electrical circuit. Therefore, an ideal solder material needs both excellent conductivity to transmit signals and adequate strength to provide mechanical support and connection. The mechanical properties of solder alloys are therefore critically important in producing reliable products. Among the all mechanical properties of solders, tensile properties and shear properties are of particular concern.

1.6.1 Tensile Properties (Stress-Strain Behavior)

Under the action of increasing stress, metals usually exhibit elasticity, plasticity, and a maximum value of stress that is followed by necking and fracture. The slope of the linear elastic portion of the stress vs. strain plot is the modulus, and the stress at the termination of elastic behavior is the yield stress. The extent of deformation prior to fracture is known as ductility.

Figure 1.3 shows a typical engineering stress-strain curve for a solder alloy. Tensile properties are generally described by stress-strain curves. A typical engineering stress-strain curve for solder alloys consists of an elastic region and a plastic region. In the elastic region, when the stress is reduced, the material will return to its original shape. In this linear region, the material obeys the relationship defined by Hoke's Law. However, since the effective modulus includes small inelastic deformations or time-dependent deformations, it is usually smaller than the dynamic modulus measured by acoustic or ultrasonic wave methods, which largely eliminates the inelastic deformation due to rapid wave propagation [6-8].

When the load is high enough to exceed the elastic limits the material will experience plastic deformation, which is permanent. At this stage, the material is undergoing a rearrangement of its internal molecular or microscopic structure, in which atoms are being moved to new equilibrium positions. Specimens subject to plastic deformation will simultaneously elongate and decrease in diameter. The Yield Stress (YS) is defined as the stress level that causes the onset of plastic deformation. However, the precise YS is difficult to measure. In engineering practice, a specified small amount of plastic deformation is used, with 0.2% being the widely accepted value [9]. This is determined by a line parallel to the elastic slope that passes through a strain level of 0.0% (Figure 1.3). When the load is removed at a point above the yield stress, the stress-strain curve will unload along a line approximately parallel to the initial modulus. The ultimate tensile strength (UTS) is the maximum engineering stress level reached in a stress-strain test. In ductile materials similar to solders, the UTS levels are usually well outside of the elastic portion, and the elastic strain is very small compared to the plastic strain. When necking occurs, the engineering stress decreases and the specimen eventually fails.

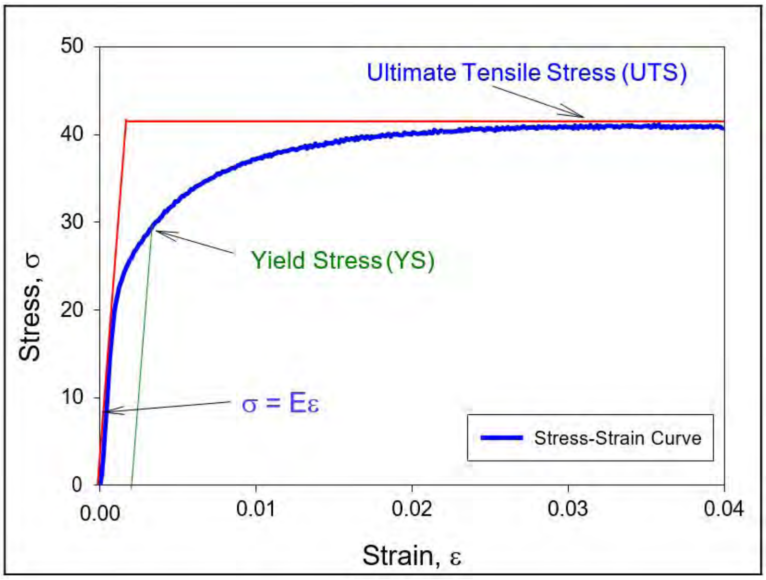

Figure 1.3 Typical Stress-Strain Curve of Solder Alloy

1.6.2 Shear Properties

Solder joints in microelectronics systems are often subjected to shear loading due to the thermal cycling conditions and CTE mismatches of the materials in an assembly (i.e. due to the CTE mismatch between substrate and PCB in Figure 1.2). A typical shear stress-strain diagram is shown in Figure 1.4. Similar to tension (Figure 1.3), when a material is subjected to shear loading, it will have a linear elastic region and a proportional limit τ_{pl}. In the elastic region, when the stress is reduced, the material will return to its original shape.

After yielding, plastic deformation and strain hardening take place, for stress levels between the proportional limit to the ultimate shear stress τ_u. Then, the stress starts to decrease until failure. Hooke's Law also holds for shear stress-strain responses at small shear strains, and the slope of the initial region of the curve G is called the shear modulus or modulus of rigidity. In isotropic materials, the shear modulus can also be expressed in terms of the elastic modulus and Poisson's ratio.

Electronic assemblies often are subjected to combined shear deformation, warpage, and distortion under the action of thermal or power cycling. Combined tension and shear loading can act on solder joints in these operating conditions.

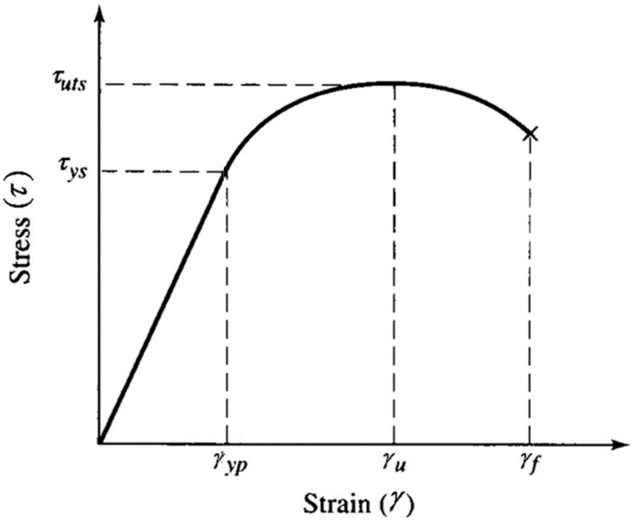

Figure 1.4 Typical Shear Stress-Strain Response for Ductile Materials

1.7 Fatigue

Electronic equipment rarely experiences a single constant or continuously increasing stress. More common are stress or strain fluctuations induced by the service conditions, and these give rise to fatigue (failure due to a number of cycles, the magnitude of which is insufficient to cause failure in a single application). The key design parameters are the stress/strain, amplitude, and the number of cycles, N_f, necessary for failure. The fatigue process involves the initiation and gradual growth of cracks until the remaining section of the material can no longer support the applied load. It is by far the most common mode of failure in engineering applications.

When subjected to temperature changes, stresses or strains in electronic assemblies are typically developed due to the mismatches in the coefficients of thermal expansion (CTE) of the soldered components and the PCB. Cyclic temperature changes, either due to the external environment or power switching, can, therefore, lead to substantial alternating stresses and strains within the solder joints. During cyclic loading, micro-cracks form within the solder material followed by macro cracks which lead to damage and ultimately to fatigue failure.

A hysteresis loop is a convenient means of depicting cyclic stress-strain relationships during fatigue as shown in Figure 1.5. The width of the loop is equal to the total strain range, $\Delta\varepsilon$, which is made up of a small elastic strain range and a larger plastic strain range. The area enclosed by the loop is a measure of the plastic strain energy, which is also called plastic work per cycle (ΔW), required to produce the observed deformation. This type of representation is very convenient when considering more complex and real cycles. During strain-controlled fatigue, the stress range necessary to maintain the strain limits may increase (cycling hardening) or decrease (cycling softening). These changes may be due to the deformation process or cracking. Similarly, for stress-controlled fatigue, the strain range necessary to maintain the stress level may increase or decrease.

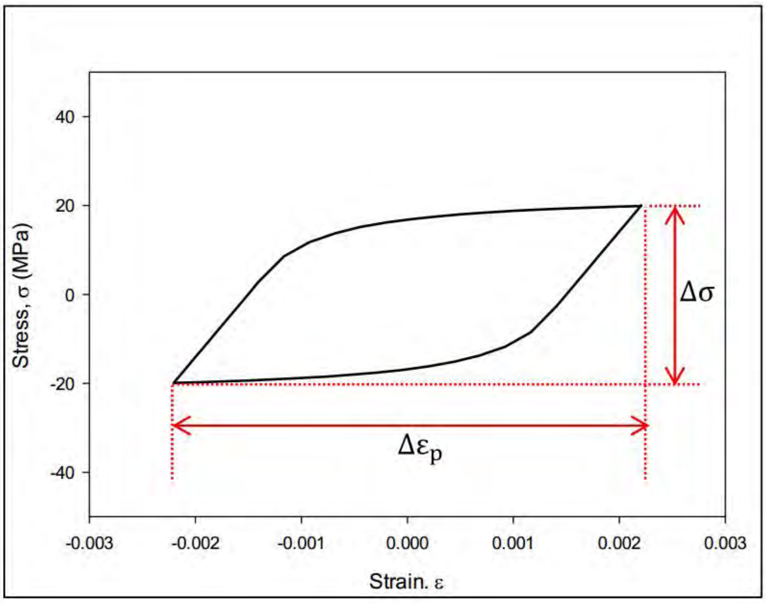

Figure 1.5 A Typical Hysteresis Loop

It has been observed that for a strain-controlled fatigue test, the peak stress drops continuously during cyclic loading due to damage accumulation. The plastic strain range also increases due to material softening. During the test, cyclic tension-compression loading causes damage accumulation eventually resulting in crack initiation. Different stages of peak stress drop during a fatigue test is shown in Figure 1.6. It is seen that the stress drops rapidly during the initial cycles due to damage accumulation and material softening. A steady-state stage is then attained where grain growth progresses, re-crystallization occurs in the microstructure, and micro-voids form as shown in Figure 1.7. In the tertiary region, the stress drops rapidly when macro cracks initiate and crack growth progresses to final rupture of the material. The number of cycles until fracture is commonly defined as the fatigue life of the material. Generally, the number of cycles at 50% drop of the tensile load is taken to be the fatigue life as recommended by ASTM [10, 11]. After crack initiation, the crack growth rate depends on the dissipation of plastic strain energy per cycle in the solder joint.

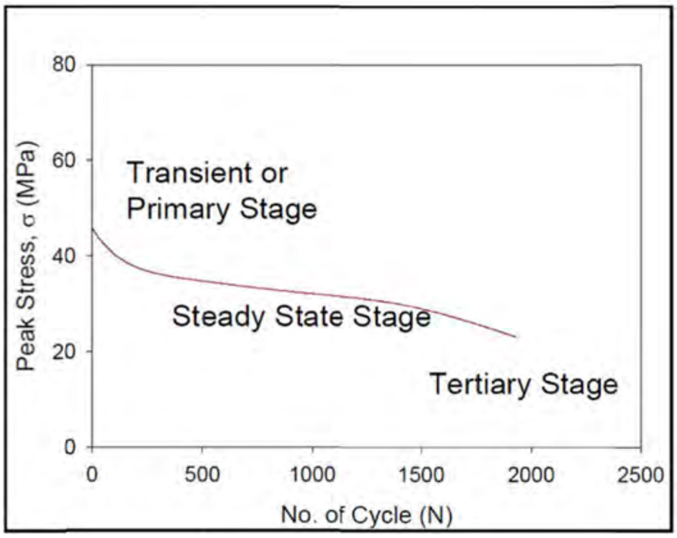

Figure 1.6 Different Stages of Stress Drop during Fatigue Test [11]

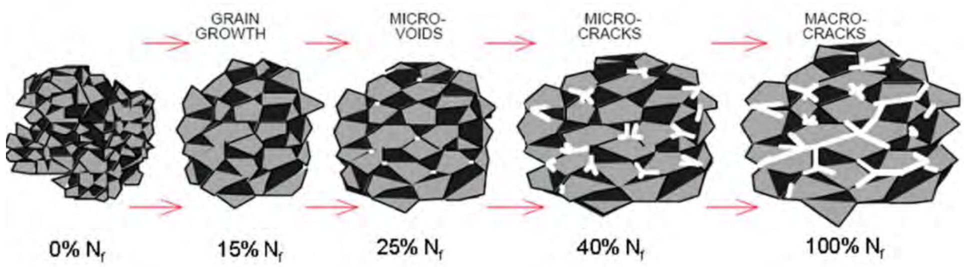

Figure 1.7 Depiction of the Effects of the Accumulating Fatigue Damage [11]

1.8 Effects of Aging on Solder Properties

Isothermal aging is a common phenomenon that occurs in the electronic packaging components. In thermal aging, the package component is subjected to an elevated temperature for a period of time. Thermal aging has significant effects on the structural properties of the aged materials. In electronic packaging, aging of solder material is important because the package usually fails in the solder joint. During aging, the intermetallic compounds of the solder material are dispersed to form a new microstructure that causes the change in the structural properties of the solder material. Generally, the strength and hardness of the solder material decreases with aging due to the dispersion of brittle intermetallic compound and grain coarsening and the material becomes soft. The effects of aging on stress-strain curve and creep behavior of SAC305 solder are depicted in Figure 1.8 and Figure 1.9 [82].

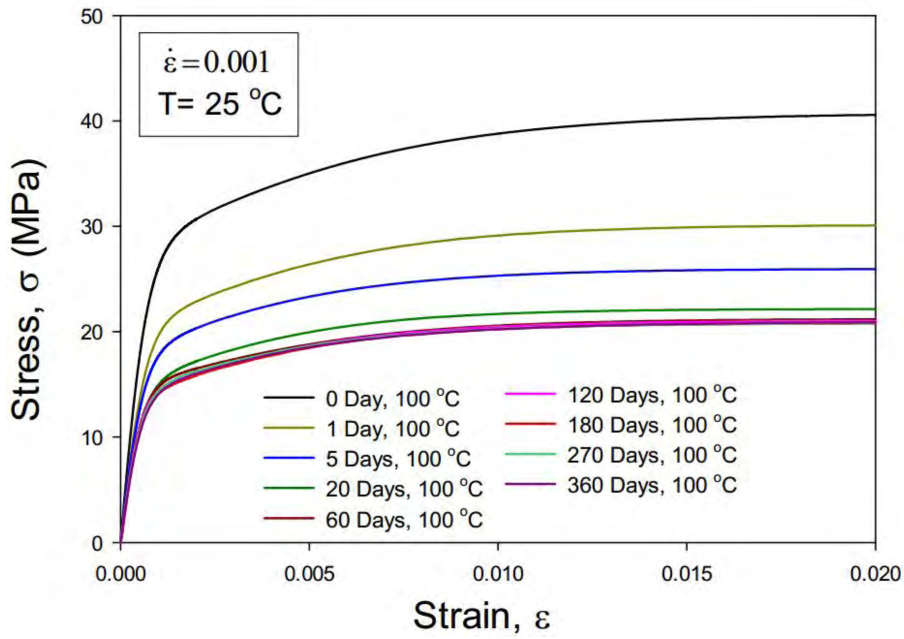

Figure 1.8 Stress-Strain Curves of SAC305 Solder for Different Aging Times [82]

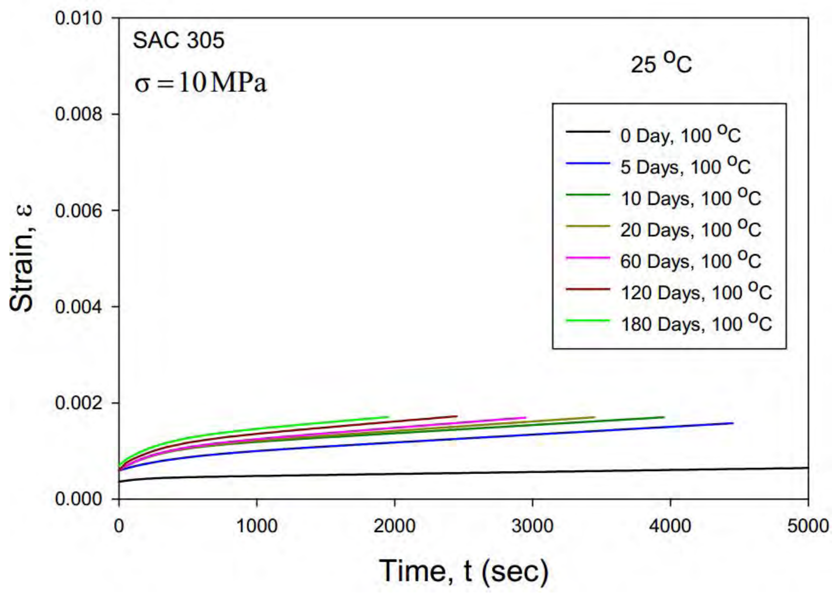

Figure 1.9 Creep Curves for SAC305 Solder for Different Aging Times [82]

1.9 Reliability Testing of Lead-Free Assemblies

Reliability testing is an integral part of the product development process and especially in the field of electronics reliability testing is a key factor in the success or failure of a new product. The consumer expects electronic devices to get smaller and more portable without decreasing in functionality, and the manufacturers compete to fabricate smaller chips with smaller footprints to gain the advantage. While there seems to be no end to this trend it is a fact that factors that were previously non-issues are now important in the context of product life. For instance, low-frequency vibrations that are common in cell phone buzzers are actually capable of affecting the solder joints within the phone over an extended period of time. Devices may be exposed to temperature extremes and portable devices will suffer handling damage and mechanical shocks.

The current reliability of products is such that they are more likely to be replaced by their owners well before the end of their useful life. For example, the break-even point of a common cell phone is approximately seven years, yet people change their cell phones for a newer model in just one or two years. This indicates a shift in the trend of consumer products, whereby the consumer is not looking for a long life from the product but rather short term reliability with a low cost. All these come back to the product design and development where the engineer is interested in the loads over a particular useful life and under a variety of conditions. Based on real-life usage an electronic device can undergo one or more of several available tests such as

- Thermal cycling
- Power cycling
- Thermal shock
- Cyclic Bending
- Drop testing
- Vibration testing

Each of these tests is designed to simulate the same kind of stresses that the product would undergo in its useful life. In real-life situations, the factors affecting the product work together and not alone, but it is necessary for these tests to isolate the effects of each one of these failure mechanisms. However, in recent times researchers have conducted combinations of these such as vibration testing coupled with thermal cycling, etc. In all cases, the results of these tests are specific to the particular material being tested and while the industry had a vast knowledge base for Sn-Pb solder there is still a lot of work required to determine the effect of Lead-Free solder on the reliability of package to board interconnects. This task is further compounded by the variety of Lead-Free compositions floating in the market since each one of them will have its own characteristics and effect on reliability.

1.9.1 Thermal Cycling

Thermal cycling testing method of life testing of electronic packages is the most popular method in accelerated life testing (ALT) system due to its ease in testing. In this testing method the package is subjected to harsh change in temperature in a short period of time. Although the temperature of the package is varied with time, the temperature is considered uniform at any specific time. The rate at which the temperature changes is called the ramp rate. The time period at which the temperature is held constant is known as dwell time and the temperature is called dwell temperature. There are two time period in a cycle where the temperature is held constant. One is at high temperature and named as high temperature dwell. Another is at low temperature and named as low temperature dwell. Typical temperature range is varied from -40 to 125 °C temperature. A typical thermal cycling temperature profile is shown in figure 1.10. Here, solder solidification temperature is considered as 220 °C.

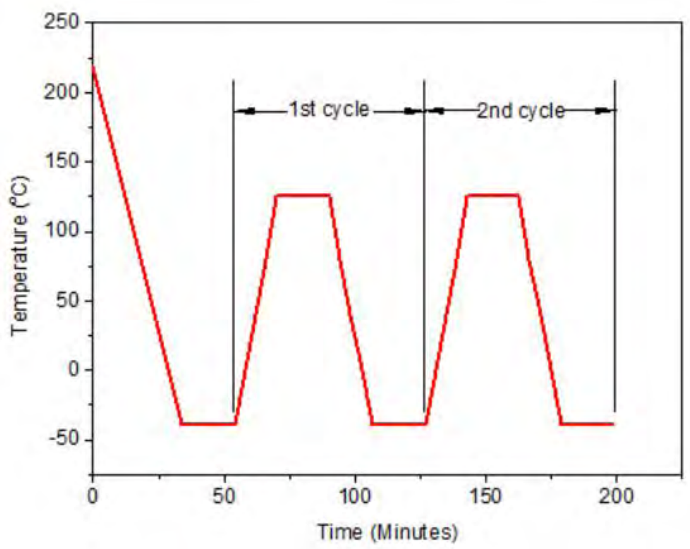

Figure 1.10 A Typical Thermal Cycling Temperature Profile

1.9.2 Power Cycling

The main drawback of thermal cycling is that it considers uniform temperature distribution in the entire package during operation at any specific time which is not the actual case. In actual case, the silicon die generates heat due to the I/O signal processing and all other package components act as heat dissipater. So, the temperature of the die will be maximum and will decrease with the distance from the center of the die. Power cycling simulates this actual phenomenon by considering the die as heat source and all other package components as heat dissipater. The temperature of the package increases with time due to the heat generation from the die when the power is 'on' and decreases by natural convection in the surrounding medium when the power is ‘off’. A typical power cycling input profile with square wave input history is shown in Figure 1.11.

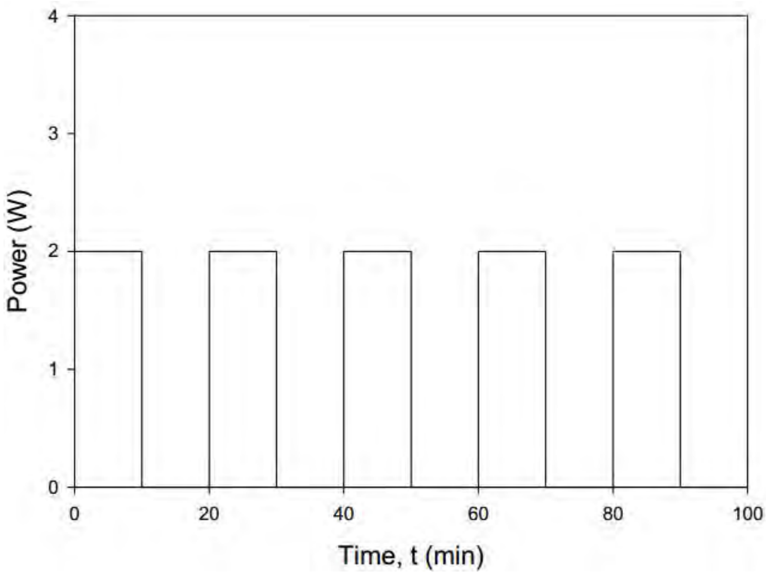

Figure 1.11 A Typical Power Cycling Input Profile

1.9.3 Mechanical Bend Cycling

Besides thermal and power cycling test, mechanical bend cycling test is also performed to assess the package life in bend cycle. A package can experience cyclic bending during manufacturing or assembly process, in transportation, and in application. For example, package used in vehicle can be subjected to cycling bending due to the low frequency vibration of the vehicle body. Typing on the keypads in laptop can also induce cyclic bending in the microprocessor component. In this bend cycling test, the package is subjected to cyclic bending load at low frequency (e.g. 1 Hz) [63]. Mechanical bend cycling differs from vibration test in which the frequency is considered very high and amplitude is considered low. The load can be displacement or force and the load profile may be sinusoidal, triangular, etc. in nature in mechanical cycling test. A typical sinusoidal displacement load profile for bend cycle analysis is shown in Figure 1.12.

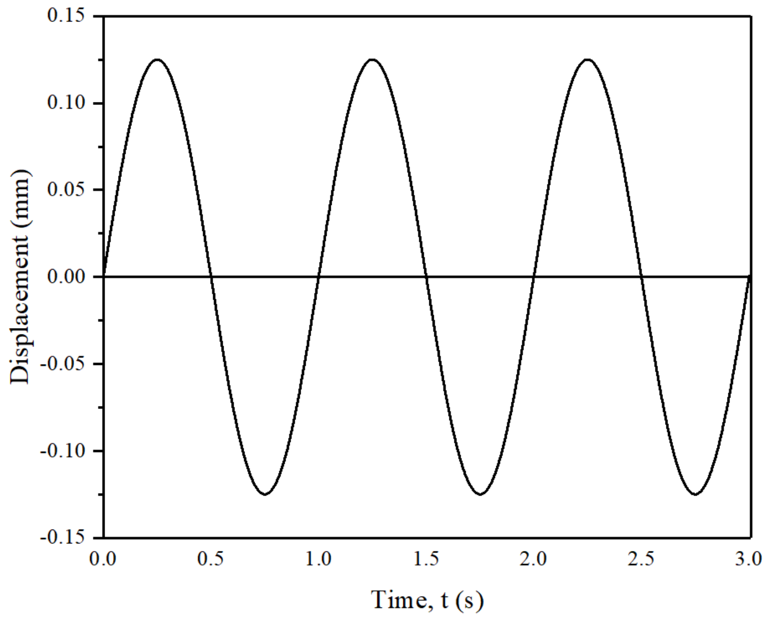

Figure 1.12 A Typical Sinusoidal Displacement Load Profile

1.10 Outlines of the Thesis

In this work, effects of thermal aging and variation of silver percentage of lead free SAC solder materials on the power and mechanical bend cycling life have been investigated. The outlines of this thesis are as follows:

Chapter 1: Introduction of lead-free SAC solder alloy and its mechanical properties along with different reliability testing methods.

Chapter 2: Literature review on thermal cycling, power cycling, and mechanical bend cycling, isothermal aging effects on material properties and thermal cycling life, silver percentage effects on material properties and thermal cycling life.

Chapter 3: Description of package configuration, finite element modeling for the analysis of power and mechanical bend cycling, material properties, and life prediction model.

Chapter 4: Results and discussions of the finite element analysis of power cycling and mechanical bend cycling that explores the effects of thermal aging and silver percentage on the life of the PBGA package component.

Chapter 5: Concludes the entire work by summarizing the key finding of the analysis.

CHAPTER 2

Literature Review

2.1 Introduction

Fatigue failure of solder interconnect is a major reliability concern in electronics packaging. Temperature fluctuations caused by either power consumption or environmental changes, along with the resulting thermal expansion mismatch between the various package materials result in deformation and stresses in packages/assemblies especially in solder interconnects. Accelerated Life Testing (ALT) using thermal cycling (TC) test have long been performed [12-20] along with energy dissipation based fatigue model [21] to assess the reliability of solder interconnects. In all these thermal cycling studies, detailed experimental and finite element analysis of the microstructural evolution of solder ball, the fatigue life of the package, effect of the temperature profile, effects of material properties, effects of the solder and other package component geometry on the fatigue life of the package have been performed. However, in thermal cycling test, the entire assembly is subjected to uniform temperature change in an environment chamber (heating/cooling), whereas, the actual package (or assembly) is experiencing non uniform temperature distribution in the assembly having the chip as the source of heat generation. Consequently, it is obvious that the thermal cycling test does not truly represent real service conditions.

2.2 Thermal Cycling vs. Power Cycling

Power cycling reliability (heat generation from power dissipation) has to be addressed with power cycling (PC) tests, which simulate as closely as possible actual operational conditions by increasing the temperature of the die when the power is “on” and allowing natural temperature decrease when the power is “off.” The importance of power cycling over thermal cycling has been reported by many researchers. Popp et al. [22] performed a comparative study of thermal cycling and power cycling of a flip-chip PBGA package and found great deviation between the results. The location of the critical solder ball and the failure mechanics are also different from each other. The location of the critical solder ball is found in the center of the package for thermal cycling whereas the location of the critical solder ball for power cycling is found in the outer side of the package. In thermal cycling, the failure is due to the flexing of the unbalanced package during transitions from hot to cold whereas in power cycling the failure is due to the shear strain caused by the mismatch of coefficient of thermal expansion of the package components. The characteristic life was found more than 45% greater for power cycling compared to thermal cycling. Ham et al. [23] studied the thermal deformation of CSP package under both thermal cycling and power cycling and found that the assembly bends in the opposite direction in power cycling as compared to its bending during thermal cycling. In the finite element analysis of Rodgers et al. [24] by substructuring and submodelling technique, they investigated a 9x9 ball grid array under three cases, (i) isothermal temperature cycling, (ii) isothermal temperature cycling with constant heat generation in the die and (iii) power cycling (transient heat generation in die). They found that in the first two cases, the center solder joint fails first and that the superimposed constant heat generation in the die has little effect on fatigue life. In the case of power cycling, the outermost diagonal joint is predicted to fail first. This variation occurs due to the difference in the temperature distribution of the package for the two cases.

Li et al. [25] studied experimentally and numerically the reliability of a thin fine-pitch ball grid array (BGA) package under both thermal and power cycling showing that power cycling has an absolute fatigue life 2.3 times longer than that of thermal cycling. The dominant failure mode was found to be the recrystallization-assisted crack nucleation and propagation. Failure mechanisms of lead-free solder interconnections in power cycling and thermal shock tests have been investigated by Laurila et al. [26] showing that the failures in both cases were induced by recrystallization assisted crack nucleation and propagation. However, in the power cycling test, the recrystallization occurred earlier than in the thermal shock test, mainly owing to the higher average temperature, and the enhanced growth of intermetallic compound layer at the anode side due to the electromigration was observed during power cycling. Park and Ahmed

[27] reported that in case of a flip-chip plastic ball grid array (FC-PBGA) package, the non-uniform temperature distribution in power cycling makes the package deform differently than the case of uniform temperature in thermal cycling. They found about 14% shorter life in case of power cycling than in thermal cycling.

2.3 Influence of Silver Percentage in Solder

Along with the difference in life obtained between thermal and power cycling tests, previous studies also revealed that the cycle to failure largely depends on the mechanical/microstructural properties of the Lead-Free solder alloy. There are mainly two phenomena that lead to the change of the solder alloy properties. One is the change of the constituents of the SAC alloy (i.e. change in percentage of silver in the solder alloy) and another is the isothermal aging of the solder alloy. Kariya et al. [28] have reported that with increasing the silver percentage of SAC solder, the strength of the solder alloy increases due to the formation of brittle intermetallic compound Ag_3Sn and thus preventing shear plastic deformation of the solder bump. However, the fatigue endurance of 1% Ag solder is superior to other solders over the plastic strain range of 3%, even though the strength of the solder is the lowest. Kang et al. [29] have reported from their experimental investigation that the thermal cycling life of CBGA assemblies is improved if lower silver content solder joints are used due to its greater ductility and lower hardness. Henshall et al. [30] studied experimentally the accelerated thermal cycling test reliability of three common BGA ball alloy and found that SAC105 has the lowest thermal fatigue resistance among the alloys tested, with SAC 305 having superior performance. Zhang and Lee [31] have done a detailed computational analysis of the effect of material properties of the solder alloy and temperature profile on thermal fatigue life and found that increase of Young's modulus of the solder material leads to a decrease of the fatigue life of PBGA solder joints. Although numerous studies are performed to investigate the effects of variation of Ag % on thermal cycling life, studies are hardly found for investigating these effects on power cycling life of packages.

2.4 Solder Aging

In real applications, solder joints are continuously exposed to thermal aging during service. It has been well documented that the microstructure, mechanical response, and failure behavior of solder materials are constantly evolving under such circumstances [32-62].

Xiao et al. [32] investigated the stress-strain behavior of SAC396 solder alloy which was subjected to aging at 25 and 180 ℃ for various amount of time. They have shown that the strength reduces by 25% for aging at room temperature for 35 days and a 33% reduction for aging at 180 ℃ for 9 days. Ding et al. [33] investigated the influence of aging on fracture behavior of Sn-Ag solder in tensile tests. They have shown that the solder samples tensile strength reduces very quickly for isothermal aging at 180 ℃ for 120 hours. Ma et al. [34] studied the evolution of elastic modulus, yield strength, and ultimate tensile strength of SAC305 and SAC405 solder alloys under various aging conditions. They have shown that the material properties decreased dramatically in the first 20 days for both room temperature aging as well as elevated temperature aging. After 20 days of aging, the properties change slowly and linearly and it continues for a longer aging time. Zhang et al. [35] also studied the aging effects on tensile properties of SACN05 (N = 1%, 2%, 3% and 4% silver) series solders for different amount of aging at temperatures 25-125 ℃. They have demonstrated that the mechanical properties degraded more dramatically when the aging temperature was increased. The data also shows that the degradation becomes linear with longer aging time. Cai et al. [36] have also shown that the aging effects are significant for Lead-Free solders (SAC105, SAC205, SAC305 and SAC405) for room temperature aging as well as elevated temperature aging. They have also shown that the aging effects can be reduced by using certain dopants to (e.g. Bi, In, Ni, La, Mg, Mn, Ce, Co, Ti, Zn, etc.) SAC solder alloys to enhance the reliability of Lead-Free solders. Basit et al. [37] have studied in detail the change in mechanical properties of SAC305 solder material due to aging by performing tensile tests at different aging time and testing temperature. They found that significant degradation of the mechanical properties occurs due to aging for both water quenched and reflowed sample. Finally, Mustafa et al. [38] have demonstrated that the hysteresis loop area in cyclic (tension/compression) loading of various SAC solder alloys changes significantly with aging. For strain-controlled tests, the hysteresis loop area deceases and for the stress-controlled tests, the loop area increases with aging time.

Researchers also investigated the effects of aging on the strength of solder joint in package components. Kim et al. [39] found that the shear strength of SAC305 solder decreased during isothermal aging for all the test temperatures considered. Coyle et al. [40] reported 20% shearing strength reduction in BGA solder joints after 240 hours of aging at room temperature. In the investigation of Lee and coworkers [41], aging has been shown to degrade the Thermal Cycling Reliability (TCR) of Lead-Free Plastic Ball Grid Array (PBGA) assemblies subjected to Accelerated Life Testing (ALT). They have shown dramatic degradation in fatigue life of BGA components with SAC 305 solders, which were subjected to thermal cycling from 0 to 100 °C with prior aging at either 100 or 150 °C. The amount of life degradation was found to be dependent on the surface finish of the PCB substrates, with 44% degradation observed for ENIG surface finish and 20% degradation observed for OSP surface finish under the most severe aging conditions (1000 hours at 150 °C) prior to thermal cycling accelerated life testing. Motalab et al. [42] studied the effects of aging on the reliability prediction model and found that predicted life by modified model that considers aging differs significantly than the life that does not consider aging. Package life found from modified model conforms better to the experiment results. The effects of aging on the degradation of the thermal cycling reliability of Lead-Free BGA assemblies have been studied by Zhang et al. [43]. In their studies, PBGA daisy chain test assemblies were subjected to up to 2 years of aging (25, 55, 85, and 125 °C), followed by thermal cycling from -40 to 125 °C or -40 to 85 °C to failure. They have shown that for all component sizes and Lead-Free solder alloys, the solder joint thermal cycling reliabilities of the BGA components were severely reduced by prior aging. For up to 360 days prior aging for the components with Im-Ag PCB surface finish and thermal cycling from -40 to 125 °C, they have observed clear degradation in life for aged components relative to non-aged components and the amount of degradation was exacerbated with higher aging temperatures. Zhang, et al. [44] have investigated the effects of isothermal aging on the thermal-cycling reliability of PBGA components. They found that for 180 days of prior aging at 125 °C the reliability of SAC105 components dropped by 53%. Smetana, et al. [45] have performed an extensive study on the effects of prior isothermal preconditioning (aging) on the thermal cycling lifetime for a variety of components. Similar to the investigations discussed above, it was observed that prior aging reduced the thermal cycling characteristic life of some of the SAC BGA assemblies subjected to 0 to 100 °C cycling. However, improvement of thermal cycling life was also observed in case of 2512 resistors and certain QFNs.

Li et al. [46] studied elevated temperature aging effects on flip-chip packages with SAC solders. They have shown that the shear strength of solder bumps subjected to aging at 80 °C decreased gradually with aging. Also, for elevated aging temperatures of 150 and 175 °C, the degradations of shear strengths of the bumps were much faster. Darveaux [47] found at a 10% to 30% reduction in solder joint strength for 24 hours of aging at 125 °C. The lifetime of wafer-level chip scale packages with SAC305 solder interconnects was investigated by Lee et al. [48]. It was found that the life was reduced by 29% for 500 hours of aging at 150 °C.

From the above reviews, it is evident that the effect of isothermal aging on the microstructure and mechanical properties of solder alloy and the thermal cycling fatigue life of the solder as well as of the packages with lead free solder joints are well established. Also, the effect of aging is mostly detrimental but not always. Sometimes it also increases the thermal cycling fatigue life. Although a number of studies have been performed on aging effects with thermal cycling, the effect of isothermal aging on the power cycling life is yet to be investigated. It is of utmost importance for the reliability study of the packages at the real conditions.

2.5 Work on Mechanical Cycling

There is another type of cycling test in which the package is subjected to cyclic bending load. This is called mechanical cycling test.

Skipor and Leicht [63] investigated the mechanical bending cycle fatigue for an area array package. They reported that the failure of the solder ball occurs at the corner location, unlike the thermal cycling test where failure occurs in the die edge solder location. Also, the solder failure took place on the PCB side unlike the package side failure of thermal cycling. They also found that at 100 °C temperature, fatigue life can be reduced as much as ten times compared to room temperature. Finally, they studied the effects of substrate thickness and elastic modulus on mechanical bending fatigue life and found that reduced substrate elastic modulus has a positive impact on fatigue life and a thinner substrate is preferred when the modulus is high. Leicht and Skipor [64] found in their study of low-frequency mechanical cycling fatigue of PBGA package interconnects, that failure occurs in the PCB side of the solder interconnects and the crack propagates through the solder material rather than in the intermetallic formed at the surface of the pad, which is in contrary to the thermal cycling tests. Pang and Che [65] studied the isothermal cyclic bending of very-thin quad flat no-lead (VQFN) package with two different board finish and two different isothermal temperature conditions. They found that bending fatigue resistance of VQFN with OSP finish is slightly better than ENIG finish case and the acceleration factor of failure at high temperature (125°C) is higher than that at room temperature (25°C). Other researchers also performed different studies on the mechanical cycling of electronic packages [66-69]. However, the effects of solder aging as well as variation of Ag percentage are yet to be explored.

2.6 Objectives of This Research

The objectives of the study can be summarized as follows:

(i) To develop a 3D finite element model of a PBGA microprocessor component for the simulations of power and mechanical cycling tests and to validate it by comparing the obtained results with the experimental power and mechanical cycling tests results that are available in the literature.

(ii) To identify and analyze the locations of critical solder joints in the PBGA package subjected to the power and mechanical cycling tests.

(iii) To study the effects of different SAC solder materials (by varying only the Ag percentages) on the power cycling and mechanical cycling life of the PBGA component.

(iv) To investigate how thermal aging affects the power and mechanical cycling life of the PBGA component.

CHAPTER 3

Finite Element Modeling

3.1 General

A finite element analysis (FEA) of a Plastic Ball Grid Array microprocessor to investigate the effects of isothermal aging and variation of silver percentage of the SAC solder ball on the package life has been performed. The study consists of two major parts, one is the power cycling analysis and another one is the mechanical bend cycling analysis. The power cycling analysis is further subdivided into two parts: a transient heat transfer analysis followed by the nonlinear structural analysis. For the power cycling analysis, first, the temperature distribution of the package is found by transient heat transfer analysis for three different input power. Temperatures obtained from the transient thermal analysis is saved for subsequent loading for the FE-structural analysis. From the structural analysis results, the inelastic energy dissipation in each solder joint is calculated and the critical solder joint is identified. By combining the life prediction theory available in the literature with the finite element results, the life of the critical solder joint is predicted for this package. The above procedure is repeated for different SAC alloys by varying the percentages of silver from 1% to 4%. For isothermal aging studies, thermal aging data of SAC solder from no aging upto 365 days aging at 100 °C (severe aging) has been utilized in the simulations. Finally, for the mechanical cycling simulation, a displacement control bending load cycle has been applied on the package at three different isothermal test temperatures and at three different loading frequencies. The effects of Ag percentage a variation and aging have been also investigated following the same protocol that has been used in power cycling tests.

3.2 Package Configuration

The 196 I/O PBGA microprocessor used in this analysis is shown in Figure 3.1 [81]. It has a dimension of 15×15 mm. The package consists of different components. Figure

3.4 (a) shows the model view of the package and Figure 3.2 shows a unit cell of the model with different components labelled. At the bottom of the package is the PCB with dimensions of 37.5×37.5×1 mm. Molding compound and substrate have dimensions of 15×15×0.53 mm and 15×15×0.25 mm respectively. Die attach material is placed between the silicon die and substrate with a thickness of 0.03 mm. The height of the solder ball is 0.46 mm with a maximum diameter or width of 0.6 mm and neck diameter or width of 0.2 mm. The pitch and outer solder ball locations are shown in Figure 3.3. The silicon die has dimensions of 5×5×0.1778 mm. Since the package has a total of 196 solder balls, the quarter model consists of an array of 49 solder balls.

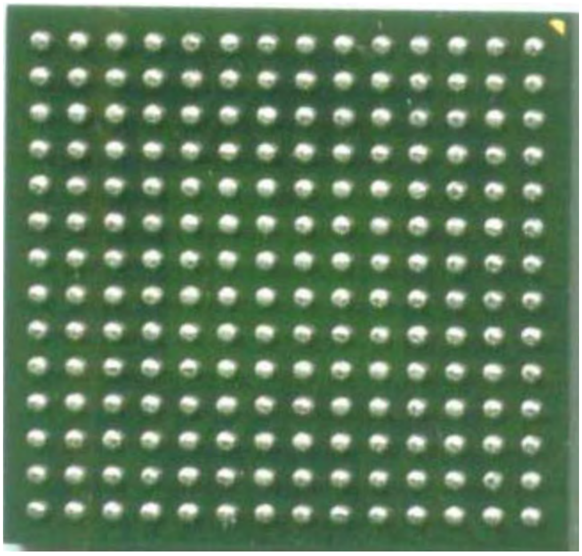

Figure 3.1 196 I/O PBGA Microprocessor Component

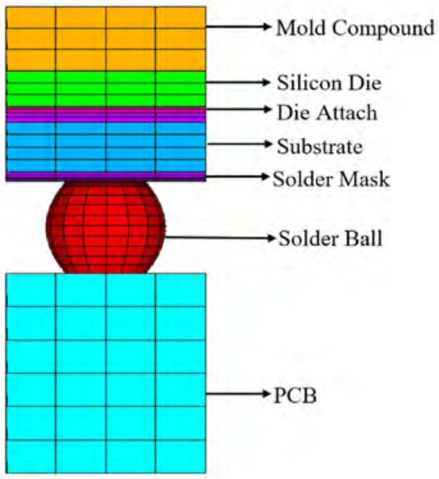

Figure 3.2 Unit Cell of the Package Model Showing Its Various Component

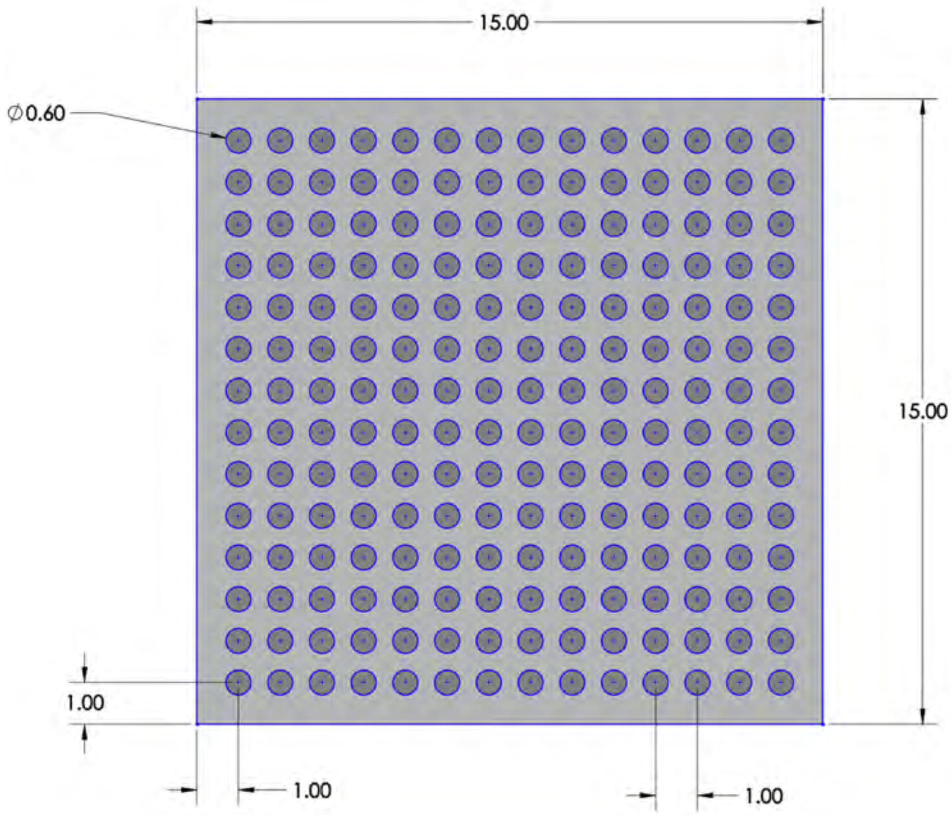

Figure 3.3 Layout of the Microprocessor Showing the Pitch and Outer Solder Ball Locations

3.3 Finite Element Model

A three-dimensional nonlinear finite element modeling of the package has been developed in the commercially available finite element software ANSYS. Figure 3.4 shows the quarter symmetry model of the PBGA package that was developed and solved using ANSYS finite element software. The entire model utilized a structured finite element mesh with 241060 elements and 256432 nodes for the power cycling analysis and 239704 elements and 257152 nodes for mechanical bend cycling analysis. This variation in element and node number is caused by the variation in grid independence test results in power cycling and mechanical bend cycling which is discussed in Section 4.5

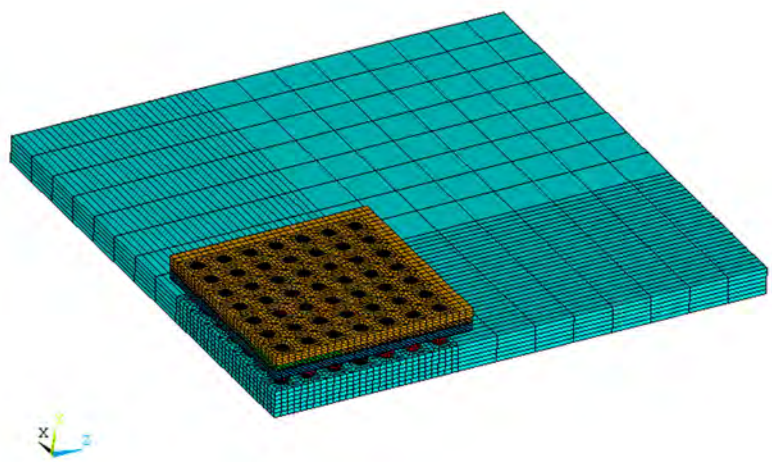

(a)

(b)

Figure 3.4 Finite Element Model of the Package (a) Isometric View (b) Front View

All the materials are modeled in ANSYS with SOLID70 element for transient heat transfer analysis and for structural analysis equivalent SOLID185 element is used. The thermal element SOLID70 has 8 nodes having one degree of freedom at each node for temperature whereas the SOLID185 structural element also has 8 nodes with three degrees of freedom at each node for displacement in each primary axes. The element is shown in Figure 3.5. Iterative solution procedures have been used due to the nonlinear material properties of the model. Typical solution run time for each run was about 6 hours using a workstation with Intel Core i7 processor and 16 GB of memory.

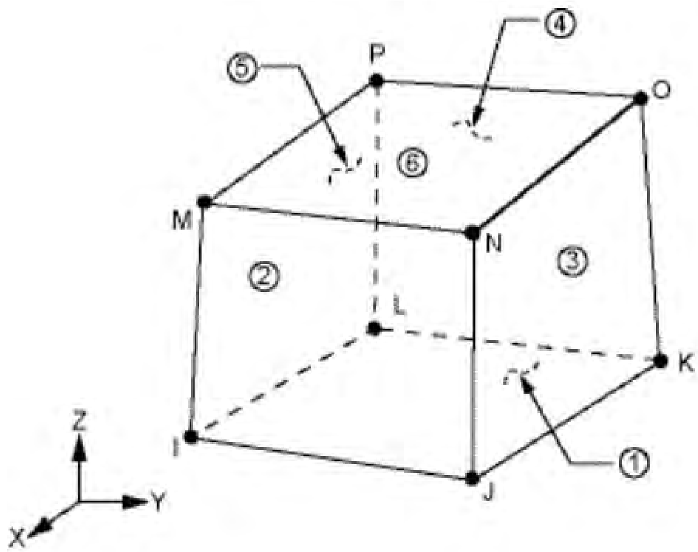

Figure 3.5 SOLID70 and SOLID185 Element

3.4 Power Cycling Analysis

The power cycling analysis consists of the sequential study of transient heat transfer followed by the structural analysis. For transient heat transfer analysis, the die is considered as the only heat source and other components of the package are considered as heat dissipater. The boundary condition applied is shown in Figure 3.6. The symmetry condition exists at the symmetry of the model which imply that the heat flux is zero on the symmetry planes. The chosen transient power dissipation profile is shown in Figure 3.7. A square wave cycle is utilized, with peak excitation of 0.4, 0.5

and 0.6 Watts, and a cycle length of 20 minutes (10 minutes at full excitation and ten minutes at no excitation) is repeated three times to complete three cycles [70]. All other surfaces are at free convection boundary condition with a convective heat transfer coefficient of 0.6 W/m^2K found from [70]. With the results of the thermal analysis as applied temperature load, the structural analysis is performed for the three power cycle. For the structural analysis, the model has been appropriately constrained along the axes of symmetry so that the displacement component perpendicular to the symmetry plane becomes zero. In addition, all three displacements at the bottom center node are constrained to prevent rigid body motion. These boundary conditions are shown in Figure 3.8. The room temperature is considered as the stress-free condition for the structural analysis [25]. From the structural analysis results, stresses, strains, and the inelastic or plastic work results are extracted in the post processing step. The plastic work (PLWK) or more precisely plastic work per volume (ΔW) is related to the life prediction model of solder materials by which package life can be predicted. The analyses are performed for various aging duration (0 to 365 days at 100 °C) and for different silver percentages of SAC alloy (1~4%).

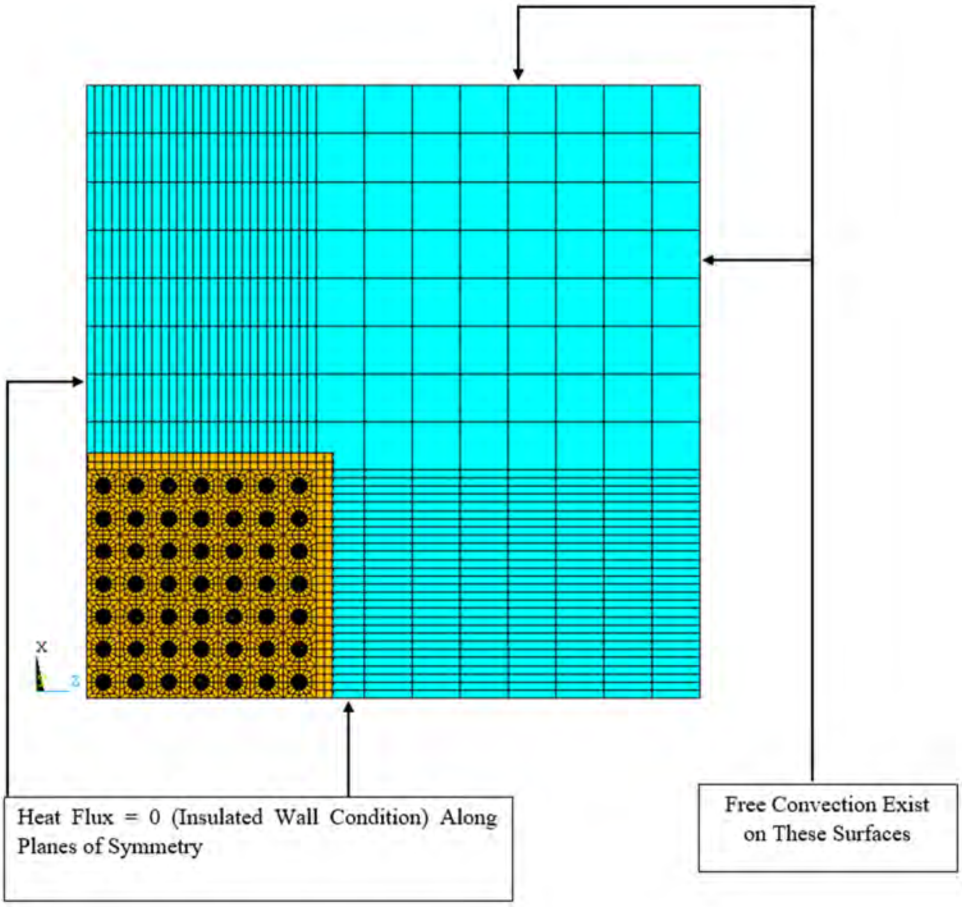

(a) Top View

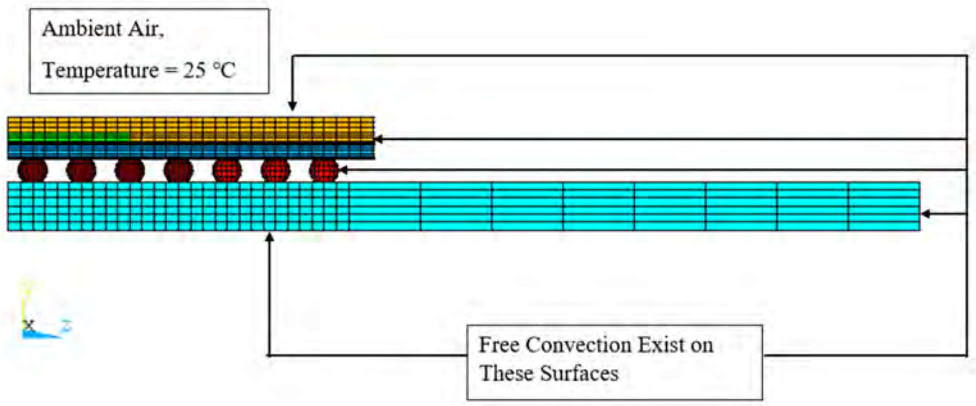

(b) Front View

Figure 3.6 Boundary Conditions for Transient Heat Transfer Analysis

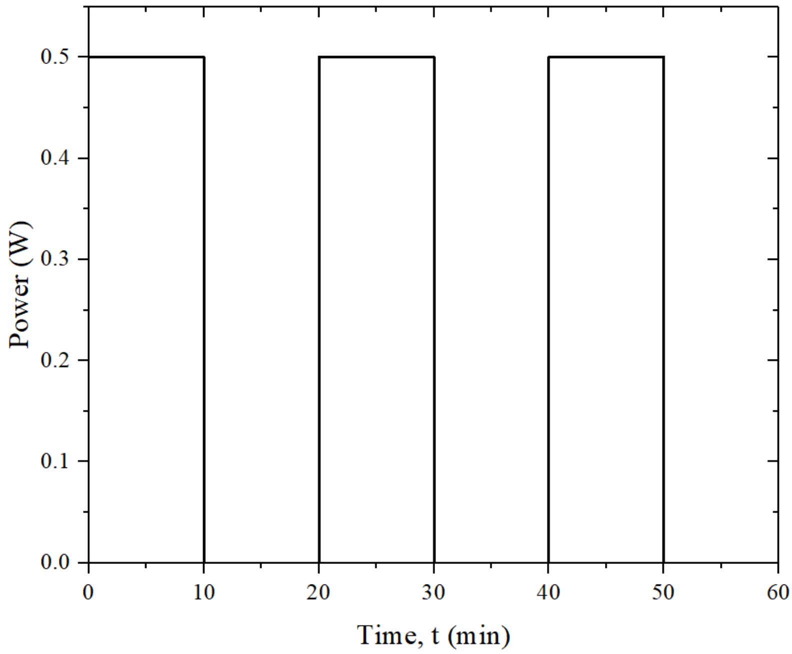

Figure 3.7 Square Wave Input Power

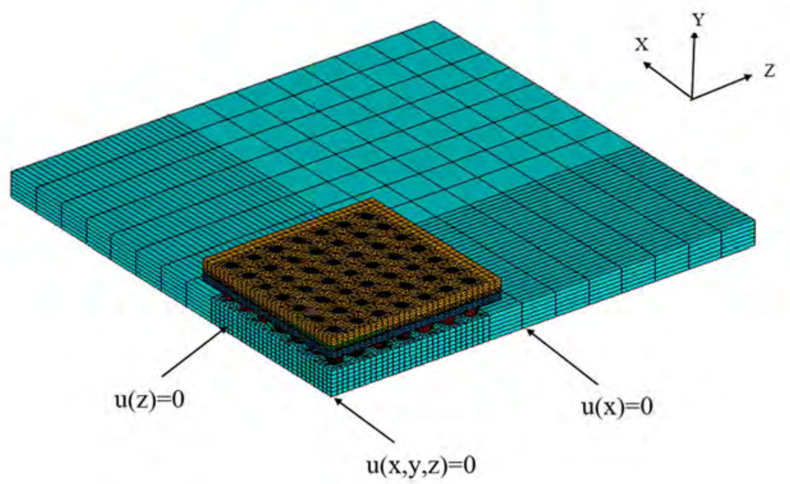

Figure 3.8 Boundary Conditions for Structural Analysis

3.5 Mechanical Bend Cycling Analysis

Mechanical cycling of PBGA component has been simulated in this study. The temperature of the package remains fixed in this analysis. The load and boundary conditions for the mechanical cycling test are shown in Figure 3.9. The same boundary conditions that have been used in structural part of the power cycling case are also used in mechanical cycling case. The displacement controlled bend load is applied sinusoidally at the outermost corner node with an amplitude of 0.125 mm following skipor et al. [63]. At first, the simulation is performed for a bend frequency of 1 Hz. Figure 3.10 shows the loading profile of the mechanical cycling simulation with 1 Hz load frequency. After three cycles, stresses, strains, and accumulated plastic work are extracted through post processing. Plastic work per unit volume (ΔW) is then calculated to use with the life prediction models to predict the number of cycles to failure. This process has been repeated for other frequencies (i.e. 3 Hz and 5 Hz). Effect of solder aging for 0 to 365 days at 100 °C on the mechanical cycling life has also been investigated in this study. Finally, the silver percentage is varied (1~4%) to identify the effects of its variation on the mechanical cycling life of the PBGA package.

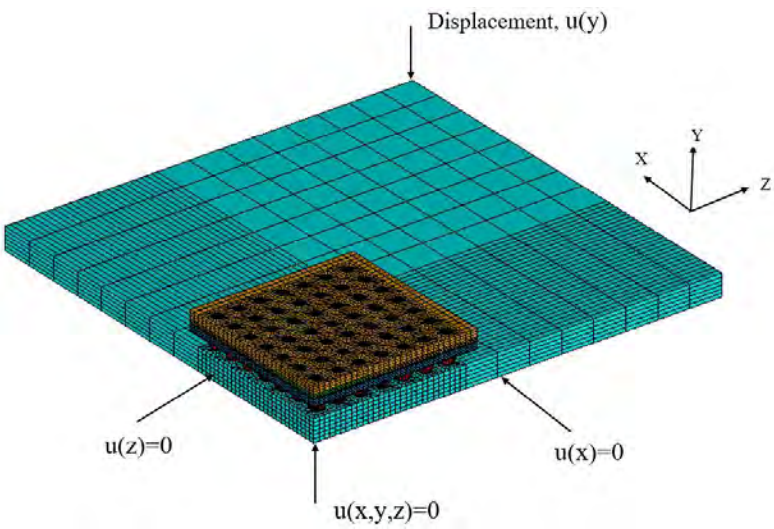

Figure 3.9 Boundary Conditions for Mechanical Bend Cycle Analysis

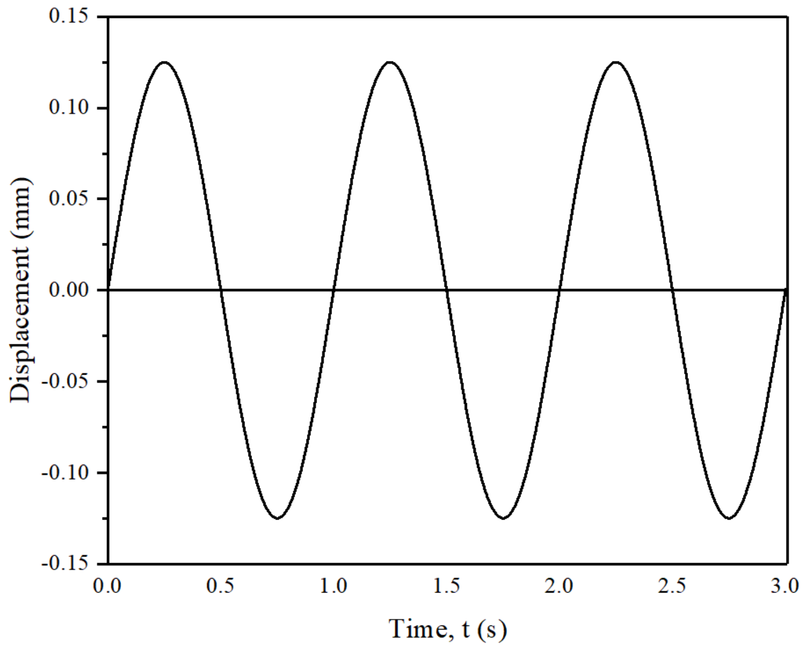

Figure 3.10 Applied Sinusoidal Displacement Load Profile for Bend Cycle Analysis

3.6 Mechanical Properties of Different Package Components

The PBGA package under study has different parts which are made of different materials and have different functions. In this study, the PCB and substrate have been used as orthotropic materials. The silicon die has been considered as linear elastic isotropic material. Also, the solder mask and copper materials have been modeled as linear elastic materials. Die attach material has been considered as linear elastic isotropic material and the CTE of die attach material has been considered as temperature-dependent (due to glass transition effect) which is shown in Figure 3.11. The molding compound or encapsulant has been considered as linear elastic material. The thermomechanical properties of these materials are extracted from literature and other resources [25], [71-74] and are tabulated in Table 3.1 and 3.2.

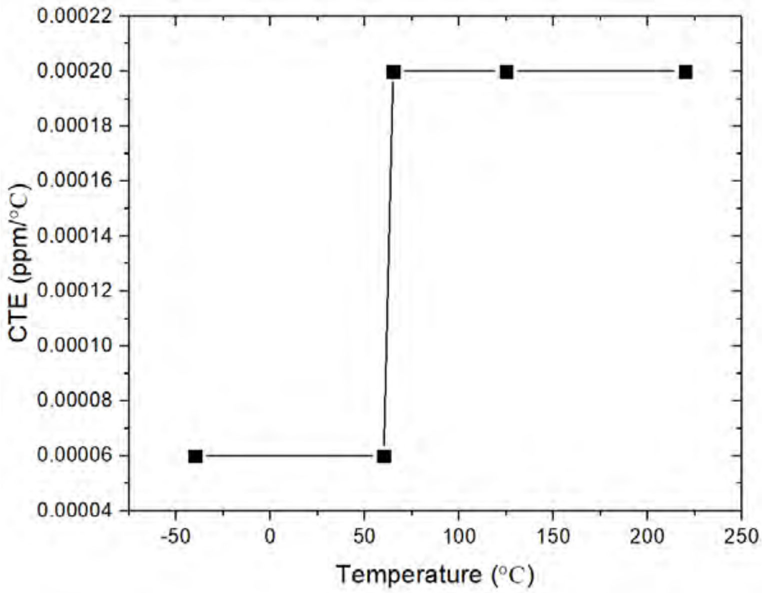

Figure 3.11 Temperature Dependent CTE of Die Attach Material

Table 3.1 Thermal Properties of the Package Components

Material Name	Density (kg/m^3)	Thermal Conductivity (W/m.k)	Specific Heat (J/kg.k)
PCB (FR-4)	1230	0.35	1260
Solder Mask	1995	0.2	1190
SAC105	7320	60	224
SAC205	7350	58.7	228
SAC305	7380	58.0	232
SAC405	7440	62	236
BT- Laminate Substrate	1995	3	1190
Die Attach Material	3500	2	674
Silicon Die	2400	98.9	790
Molding Compound	1880	0.75	920
Copper Pad	8900	389	385

Table 3.2 Mechanical Properties of the Package Components

Material Name	Elastic Modulus (GPa)		Poisson's Ratio	CTE (ppm/°C)
PCB (FR-4)	E_x =16.90 E_y = 7.44 E_z = 16.90	G_{xy} = 3.33 G_{xz} = 7.62 G^{yz} = 3.33	PR_{xy} = 0.39 PR_{xz} = 0.11 PR_{yz} = 0.39	CTE_x = 14.5 CTE_y = 67.2 CTE_z = 14.5
Solder mask	3.1		0.3	16.3
SAC105, SAC205, SAC305, SAC405	Viscoplastic Material (Anand Model is used)			
BT- Laminate Substrate	E_x =17.90 E_y =7.84 E_z = 17.90	G_{xy} = 2.82 G_{xz} = 8.06 G_{yz} = 2.82	PR_{xy} = 0.39 PR_{xz} = 0.11 PR_{yz} = 0.39	CTE_x = 12.4 CTE_y = 57.0 CTE_z = 12.4
Die Attach Material	1.5		0.35	Temperature dependent
Silicon die	169		0.28	2.54
Molding Compound	15.8		0.3	15.5
Copper Pad	117		0.38	17

In this study, the solder balls have been modeled as viscoplastic material with the Anand model [80]. The Anand model uses a scalar internal variable "s" to represent the isotropic resistance to plastic flow offered by the internal state of the material. It unifies the creep and rate-independent plastic behavior of the solder by making use of a stress equation, a flow equation, and an evolution equation. The model needs no explicit yield condition and no loading/unloading criterion. The model is already included in ANSYS.

For the one-dimensional case (uniaxial loading), the stress equation is given by

$$\sigma = cs \; ; \; c < 1 \tag{3.1}$$

where s is the internal variable and c is a function of strain rate and temperature expressed as

$$c=c\left(\dot{\varepsilon}_p,T\right)=\frac{1}{\xi}\sinh^{-1}\left\{\left[\frac{\dot{\varepsilon}_p}{A}\, e^{\left(\frac{Q}{RT}\right)}\right]^m\right\} \tag{3.2}$$

where $\dot{\varepsilon}_p$ is the plastic strain rate, A is the pre-exponential factor, ξ is the multiplier of stress, m is the strain rate sensitivity, Q is the activation energy, R is the universal gas constant, and T is the absolute temperature. By substitution of Eq. (3.2) into Eq. (3.1), the reformatted stress equation becomes:

$$\sigma=\frac{s}{\xi}\sinh^{-1}\left\{\left[\frac{\dot{\varepsilon}_p}{A}\, e^{\left(\frac{Q}{RT}\right)}\right]^m\right\} \tag{3.3}$$

Rearranging Eq. (3.3) and solving for the strain rate yields the flow equation of the Anand model:

$$\dot{\varepsilon}_p=Ae^{-\left(\frac{Q}{RT}\right)}\left[\sinh\left(\xi\frac{\sigma}{s}\right)\right]^{\frac{1}{m}} \tag{3.4}$$

The differential form of the evolution equation for the internal variable s is assumed to be of the form

$$\dot{s}=h(\sigma,s,T)\dot{\varepsilon}_p$$

$$\dot{s}=\left[h_o\left(1-\frac{s}{s^*}\right)^a \operatorname{sign}\left(1-\frac{s}{s^*}\right)\right]\dot{\varepsilon}_p;\ a>1 \tag{3.5}$$

here, the term h(σ, s, T) is associated with the dynamic hardening and recovery processes. Parameter h_o is the hardening constant, a is the strain rate sensitivity of the hardening process, and the term s* is expressed as

$$s^*=\hat{s}\left[\frac{\dot{\varepsilon}_p}{A}\, e^{\left(\frac{Q}{RT}\right)}\right]^n \tag{3.6}$$

where ŝ is a coefficient and n is the strain rate sensitivity of the saturation value of the deformation resistance. Equation (3.6) can be integrated to yield the final version of the evolution equation for the internal variable s:

$$s = \hat{s}\left[\frac{\dot{\varepsilon}_p}{A}\, e^{\left(\frac{Q}{RT}\right)}\right]^n - \left[\left(\hat{s}\left[\frac{\dot{\varepsilon}_p}{A}\, e^{\left(\frac{Q}{RT}\right)}\right]^n - s_o\right)^{(1-a)} + (a-1)\left\{(h_o)\left(\hat{s}\left[\frac{\dot{\varepsilon}_p}{A}\, e^{\left(\frac{Q}{RT}\right)}\right]^n\right)^{-a}\right\}\varepsilon_p\right]^{\frac{1}{1-a}} \quad (3.7)$$

$$s = s(\dot{\varepsilon}_p, \varepsilon_p) \quad (3.8)$$

The final equations in the Anand model (1-D) are the stress equation in Eq. (3.3), the flow equation in Eq. (3.4), and the integrated evolution equation in Eq. (3.7). These expressions include 9 material parameters (constants): A, ξ, Q/R, m in Eqs. (3.3, 3. 4); and constants h_o, a, s_o, ŝ, and n in Eq. (3.7).

In the present analysis, four types of Lead-Free solder materials are considered for life prediction. These solder materials are termed as SAC solders. SAC stands for Sn (tin), Ag (silver) and Copper. In the study, SAC 105, SAC 205, SAC 305, and SAC 405 have been used. In SAC 105, the silver percentage is 1.0% and the percentage of copper is 0.5%. The remaining 98.5% of the solder material is tin. Other solder materials are also termed in this way. Increase in silver content increases the modulus of elasticity of SAC materials. Therefore, SAC 105 has a lower modulus of elasticity and SAC 405 has a higher modulus of elasticity. In the study, reflowed SAC solders from no aging up to severe aging conditions of 365 days aging are considered. As reviewed in literature the behavior of the SAC solder alloy change dramatically with aging. So for the better prediction of the package life, the actual properties that evolve with aging is needed. Anand parameters for these SAC solders for aging are shown in Tables 3.3, 3.4, 3.5, and 3.6 [75, 76]. The temperature-dependent elastic modulus with aging is shown in Figure 3.12, 3.13, 3.14, and 3.15 [77]. Also, the temperature-dependent stress-strain curves of solder balls for different SAC with aging and silver percentage are available in the literature [78].

Table 3.3 Variation of Anand Parameters for SAC105 with Aging

Anand Par.	units	0 day aging	180 days aging	365 days aging
s_o	MPa	7.5	2.9	2.89
Q/R	1/K	8850	8850	8850
A	s^{-1}	6900	8250	9000
ξ	-	4	4	4
m	-	0.215	0.16	0.16
h_o	MPa	137500	60000	58750
$\hat{s}$	MPa	25.1	18.9	17.9
n	-	0.0062	0.00115	0.001
a	-	1.96	2.21	2.22

Table 3.4 Variation of Anand Parameters for SAC205 with Aging.

Anand Par.	units	0 day aging	180 days aging	365 days aging
s_o	MPa	16.5	5.2	5
Q/R	1/K	9090	9090	9090
A	s^{-1}	4300	4900	5200
ξ	-	4	4	4
m	-	0.238	0.177	0.177
h_o	MPa	169000	75000	73300
$\hat{s}$	MPa	29	21.6	19.94
n	-	0.0087	0.00145	0.0013
a	-	1.84	2.09	2.1

Table 3.5 Variation of Anand Parameters for SAC305 with Aging

Anand Par.	units	0 day aging	1 day aging	5 days aging	60 days aging	180 days aging	365 days aging
s_o	MPa	21	16.65	13.5	6	5.8	5.4
Q/R	1/K	9320	9320	9320	9320	9320	9320
A	s^{-1}	3501	3776	3960	4095	4110	4210
ξ	-	4	4	4	4	4	4
m	-	0.25	0.226	0.21	0.18	0.18	0.18
h_o	MPa	180000	151000	135050	89682	77540	73708
$\hat{s}$	MPa	30.2	27.7	26	22.3	21.9	21.4
n	-	0.01	0.0058	0.003	0.0011	0.00098	0.001
a	-	1.78	1.91	1.98	2.03	2.05	2.06

Table 3.6 Variation of Anand Parameters for SAC405 with Aging

Anand Par.	units	0 day aging	180 days aging	365 days aging
s_o	MPa	23.65	6.2	6.14
Q/R	1/K	9580	9580	9580
A	s^{-1}	3175	3725	3800
ξ	-	4	4	4
m	-	0.263	0.184	0.184
h_o	MPa	183000	80000	79840
$\hat{s}$	MPa	31.3	22.2	23
n	-	0.011	0.0018	0.0014
a	-	1.77	2.04	2.05

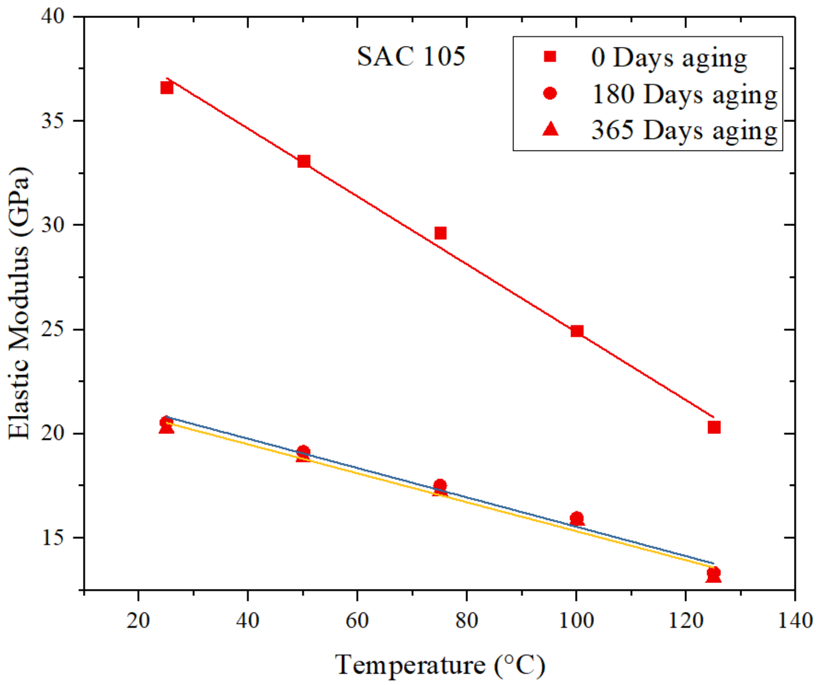

Figure 3.12 Temperature Dependent Elastic Modulus of SAC105 with Aging [77]

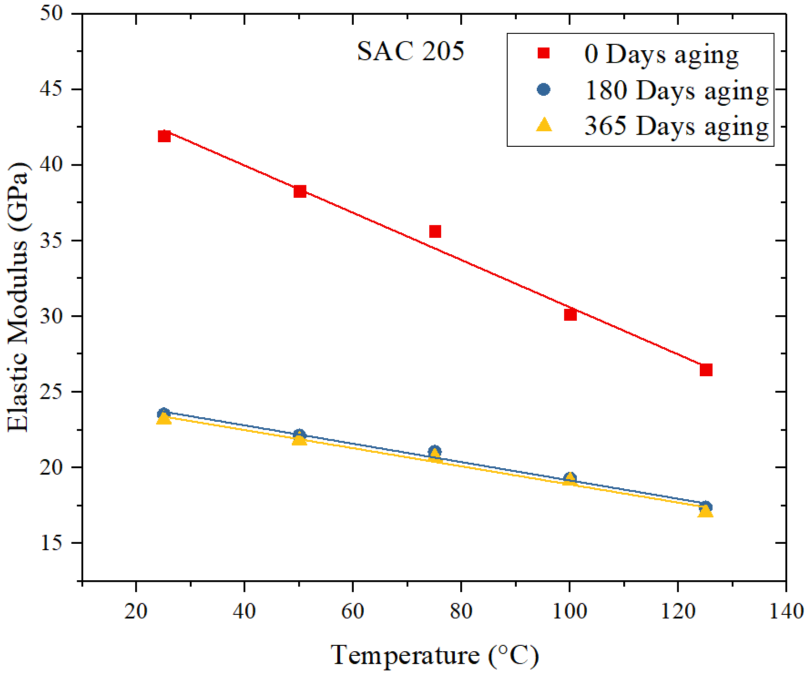

Figure 3.13 Temperature Dependent Elastic Modulus of SAC205 with Aging [77]

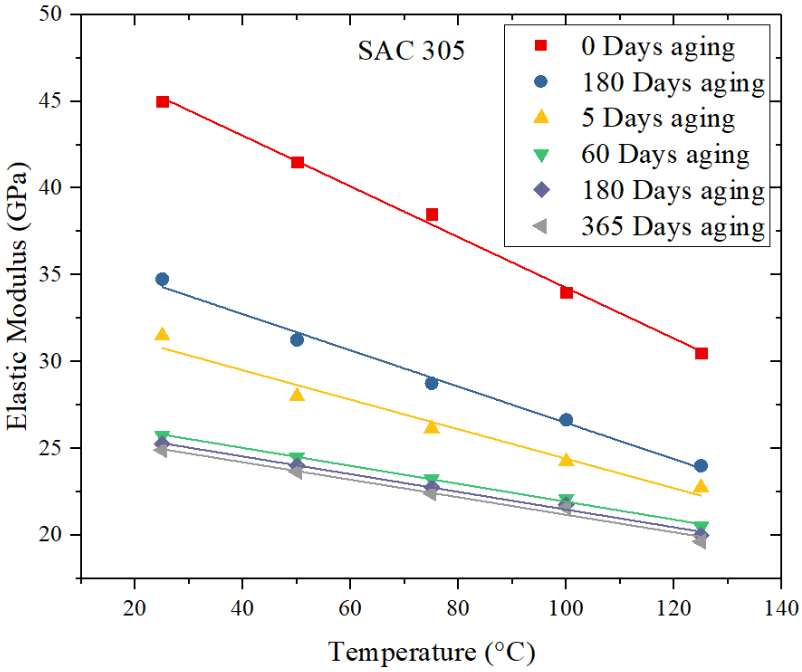

Figure 3.14 Temperature Dependent Elastic Modulus of SAC305 with Aging [77]

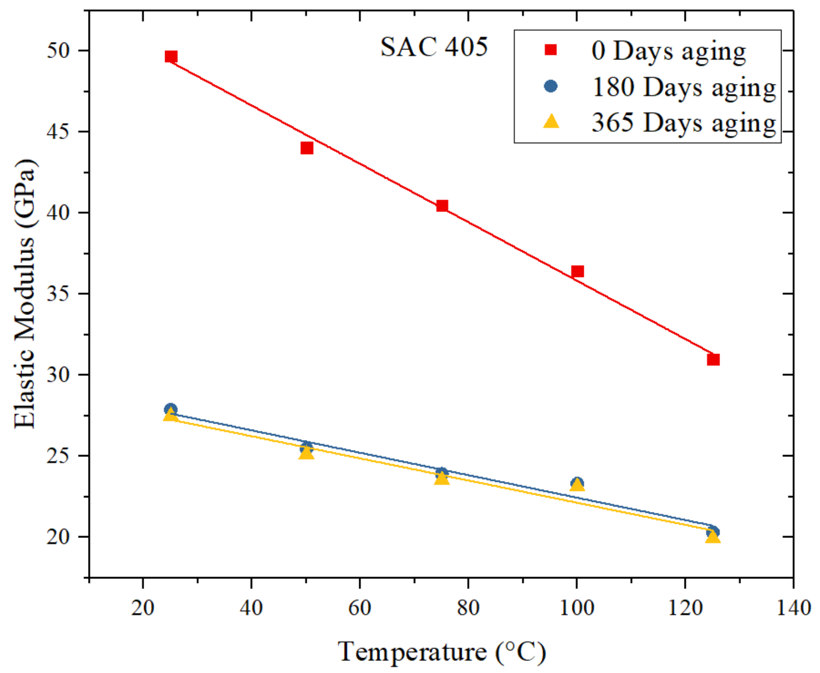

Figure 3.15 Temperature Dependent Elastic Modulus of SAC405 with Aging [77]

3.7 Solder Fatigue Life Prediction Model

Several finite elements based analysis methodologies have been proposed which predict solder joint fatigue life. Of all these methodologies, Darveaux [21] seems to be the most popular due to the ease in its implementation. Darveaux methodology links laboratory measurements of low-cycle fatigue crack initiation and crack growth rates to the inelastic work of the solder. It is a strain energy-based approach, where the work term consists of time-dependent creep and time-independent plasticity. This inelastic behavior is captured in ANSYS using Anand's constitutive model. The modeling methodology utilizes finite element analysis to calculate the viscoplastic strain energy density accumulated per cycle during thermal or power cycling. The strain energy density is then utilized with crack growth data to calculate the number of cycles to initiate a crack, and the number of cycles for the crack to propagate across a solder joints diameter. Darveaux's methodology has been previously presented in the successful analyses of various electronic assemblies from multiple industry sources.

In Darveaux energy dissipation based models for life prediction in solder joints subjected to cyclic loading consists of separate power-law type relations for estimating crack initiation and crack growth rate in solder joints:

$$N_i = K_1 (\Delta W)^{K_2} \tag{3.9}$$

$$\frac{da}{dN} = K_3 (\Delta W)^{K_4} \tag{3.10}$$

where, N_i is the number cycles to crack initiation, da/dN is the crack growth rate (assumed constant) occurring after crack initiation, ΔW is the energy dissipation per cycle in the solder sample (e.g. critical solder ball), and K_1, K_2, K_3, and K_4 are material constants. Once the crack location and path are known in the solder joint, the number of cycles to failure can be estimated using:

$$N_f = N_i + \frac{a_c}{\left[\frac{da}{dN}\right]} \tag{3.11}$$

where, N_f is the number of cycles to failure, a_c is the length of the fully developed crack at failure/fracture, and N_i and da/dN are calculated from ΔW using Eqs. (3.9-3.10). The values of these constants are prone to change with aging. The values of these constants for SAC305 are tabulated in table 3.7 from Motalab et al [42].

Table 3.7 Failure Model Material Constant for SAC305

Aging Time (Days)	K_1 (Cycles/MPa^{K_2})	K_2	K_3 (m/Cycles-MPa^{K_4})	K_4
0	37.97	-2.80	1.4×10^{-6}	1.16
180	1.413	-3.13	2.2×10^{-6}	2.10
365	1.413	-3.16	3.6×10^{-6}	2.40

CHAPTER 4

Results and Discussion

4.1 Introduction

In this chapter, the results of the FE-analysis of a Lead-Free PBGA package under power cycling and mechanical bend cycling has been presented and discussed. This chapter has two major parts. The first part consists of the results of power cycling analysis which includes the transient heat transfer analysis followed by a static structural analysis. The transient heat transfer analysis has been performed for three different input power ranging from 0.4 W to 0.6 W. The second part consists of the mechanical bend cycle analysis. The mechanical bend cycle has been performed at three different test temperatures of 25, 75, and 125 °C and three different loading frequency of 1Hz, 3 Hz and 5 Hz.

4.2 Grid Independency Test

To make the results of the simulation more stable, the sensitivity of the mesh generated has been tested as shown in Figure 4.1. In this test, the results of the power cycling analysis for SAC305 at no aging condition and 0.5 W input power is plotted against no. of element to find the stable mesh. The element number is varied from around 210000 ~ 240000 by varying the number of element layer in the solder neck region. Solder neck region is considered here because the maximum inelastic energy dissipation occurs in this region and thus it is critical for the analysis. From this test, it can be seen that the results of the power cycling analysis varied with the element layer number at the solder neck region. But after a certain number of layers, the results become stable and do not change significantly and it was three layers in the neck region with 241060 element. A Similar test has been performed for mechanical cycling mesh sensitivity and the final stable mesh is used. But in case of mechanical bend cycle, the number of element layer of the solder ball on PCB side is critical and so meshed finely.

The coarse and finely meshed solder ball used in both analysis are shown in Figure 4.2.

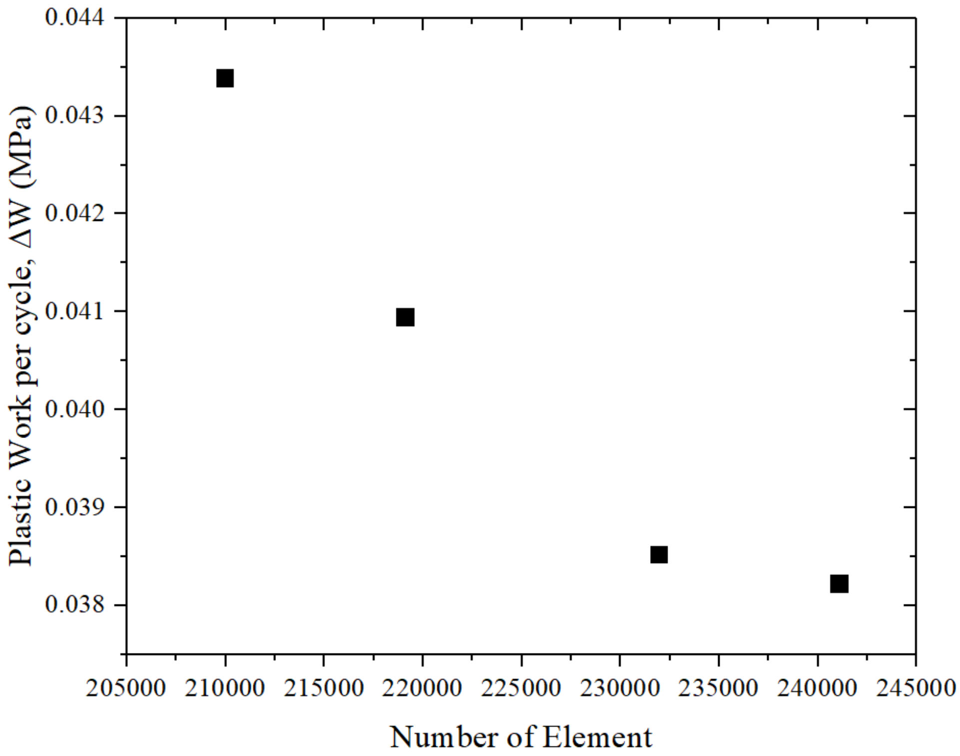

Figure 4.1 Convergence of ΔW with Number of Element

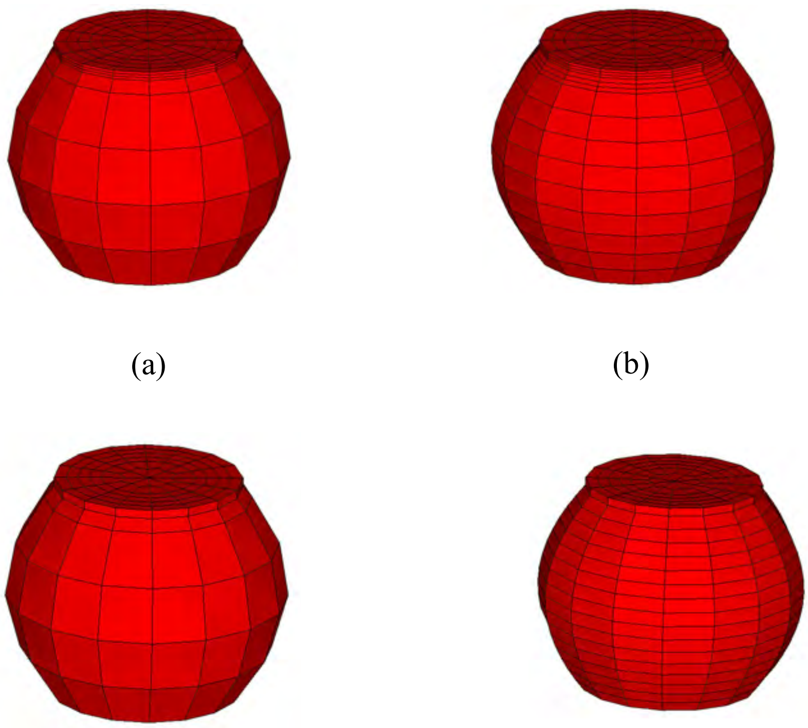

(a) (b)

(c) (d)

Figure 4.2 Coarse and Fine Mesh for Power Cycling ((a) and (b)) and Mechanical Cycling ((c) and (d)).

4.3 Power Cycling Analysis

4.3.1 Thermal Analysis

To know the accurate temperature distribution among the various component of the package, a transient heat transfer analysis has been performed. In this analysis, the silicon die is the only source for heat generation and all other components are regarded as a heat dissipater. Determination of the actual temperature distribution is very important because the response of the package components under thermal/power cycle is governed by the coefficient of thermal expansion of the components. And for different temperature distribution, the thermal expansion will be different which will lead to different results. In Figure 4.3(a) and 4.3(b), the contour plot of the temperature distribution for the entire package has been shown for power level of 0.5 W. It depicts how the temperature varies among the various components. The maximum temperature occurs at the die center which is 110.18 °C and it decreases with the distance from the die. The minimum temperature is found as 27.02 °C at the PCB corner edge at the farthest distance from the die. In Figure 4.4, the contour plot of temperature distribution for the solder ball layer is shown. It can be seen that the maximum temperature in the solder ball (at the center of the package) is slightly less than the die maximum temperature. The temperature distribution obtained in this step is recorded for subsequent use in the structural analysis.

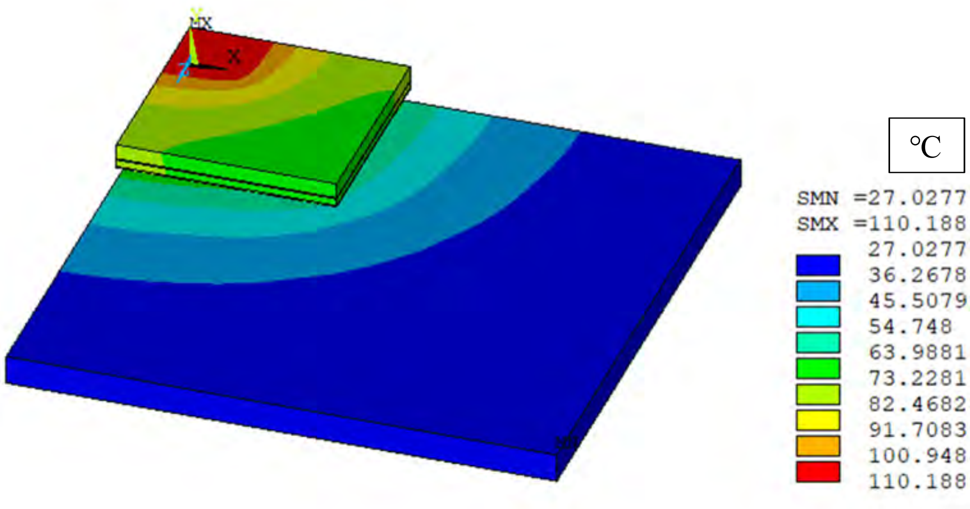

(a)

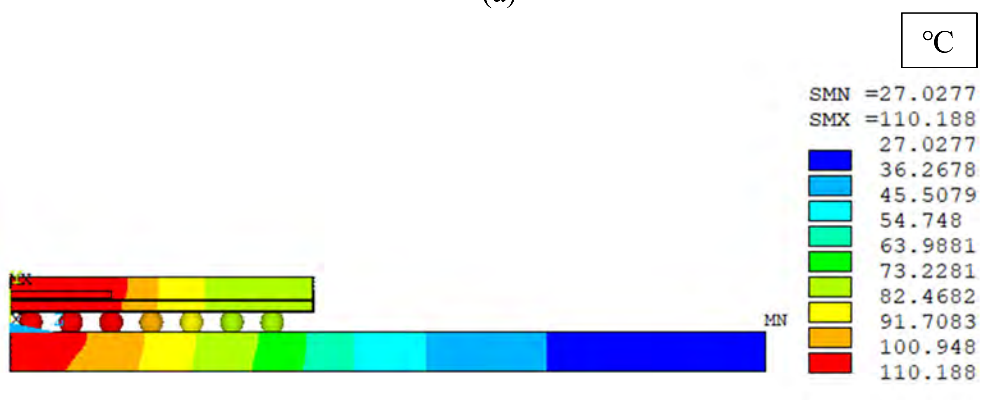

(b)

Figure 4.3 Contour Plot of the Temperature Distribution of the Package (a) Isometric View (b) Front View

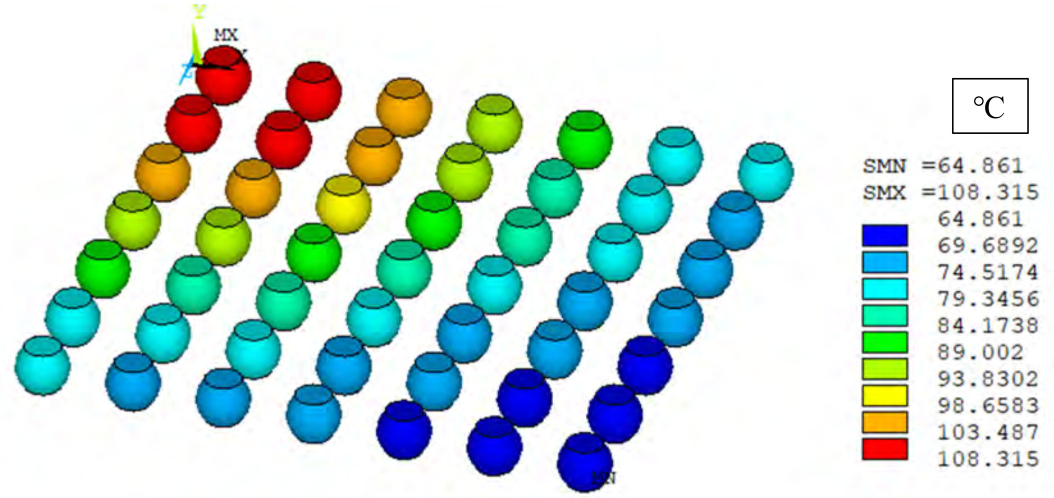

Figure 4.4 Contour Plot of the Temperature Distribution of the Solder Ball Array (Isometric View)

4.3.1.1 Effects of Input Power on Temperature Variation

If the die input power is increased the temperature should also increase which is shown in Figure 4.5. The increase in temperature with power has been observed linear. In Figures 4.6(a) and 4.6(b), the variation of temperature with input power is shown where the maximum and minimum temperatures of the die and solder ball with time are plotted.

From the plot, it is evident that the difference between the maximum and minimum temperatures of the die is not significant, while in case of the solder ball, the difference is significant. This is because the die is the heat source, so the temperature is quite uniform whereas heat is conducted to the solder ball through various package components and thus the temperature variation becomes large. This is also true for other package components. This variation in the temperature difference also causes the variation in temperature gradient for the die and other components.

Eventually, the thermal expansion of the die is almost uniform but in case of other package components, the expansion is not uniform, which is different from the thermal cycling case. In case of thermal cycling, the thermal expansion of each component is uniform due to the uniform temperature distribution but it is different for different components. This is the reason why the results in power cycling and thermal cycling differ.

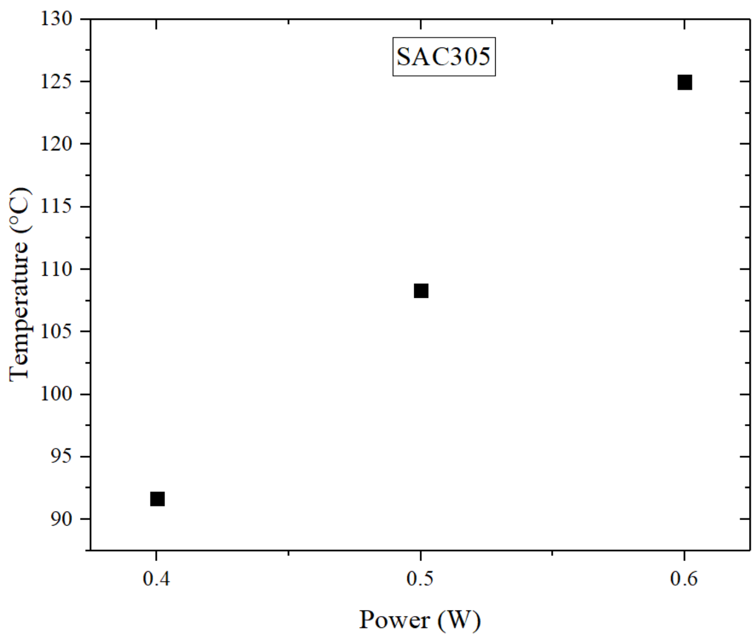

Figure 4.5 Variation of Die Maximum Temperature for Various Input Power for PBGA Package with SAC305 Solder

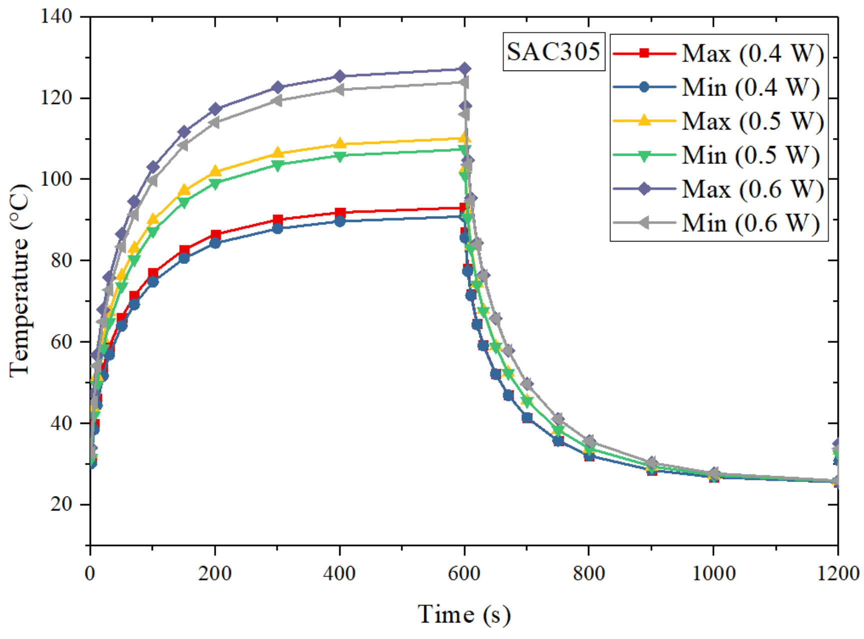

(a)

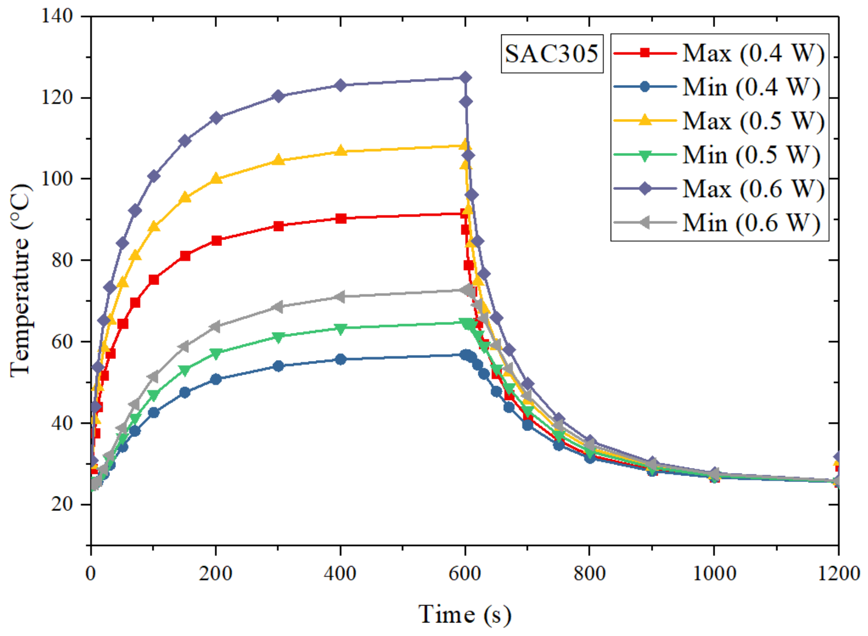

(b)

Figure 4.6 Variation of Maximum and Minimum Temperatures with Time for Different Input Powers for SAC305 solder (1st Cycle) (a) Die Center (b) Solder Ball at the Center of the Package

4.3.1.2 Effects of Silver Percentage on Temperature Variation

In this analysis, four different SAC solders have been used where the silver percentage is varied from 1% to 4%. The thermal conductivity of these alloys are not different. So the temperature distribution of the package with different SAC alloys should not be much different also. In Figure 4.7, the maximum and minimum temperatures of solder ball with time are plotted for different SAC alloys for 0.5 W input power. The graph shows that the temperature distribution is almost same for various silver percentage.

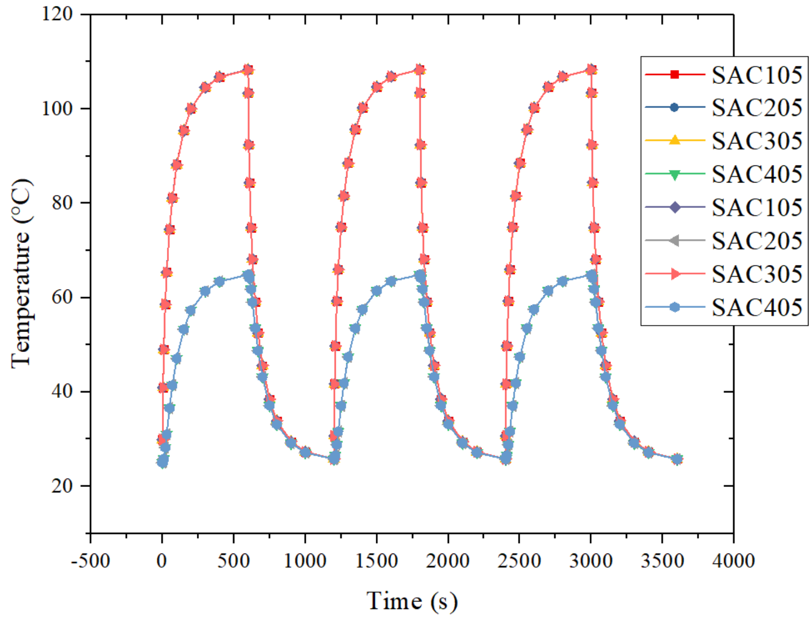

Figure 4.7 Variation of Solder Ball Maximum and Minimum Temperatures with Time for Different SAC Materials

4.3.2 Structural Analysis

4.3.2.1 Location of Critical Solder Ball

In Figure 4.8, the contour plot of the accumulated plastic work for the solder balls are shown for SAC305 solder where the location of the maximum plastic energy dissipating solder ball is found in the second row and second column position from the package center (upper left corner). Stress is generated in the package due to the mismatch of the coefficient of thermal expansion of the components. In case of thermal or power cycling, the location of the critical solder ball occurs under the die edge. This phenomenon can be explained by the die shadow effect. A die shadow effect is caused by higher shear stress on the solder joints under the die due to the coefficient of thermal expansion (CTE) mismatch between the die and the substrate on which the package is surface mounted. According to this die shadow effects, the solder ball under the die shadow which is at the longest distance from the center of the package, should be the critical solder ball. However, the critical solder ball in the present analysis is found to be the second solder ball along the diagonal from the center instead of the third solder ball. This is because the die shadow effect on the third solder ball is not fully sensed due to the half-covering of this solder ball by the die (Figure 3.4). So the critical location of the solder ball found in the analysis is justified. After finding the location of the critical solder ball in the ball grid array, the location of the crack initiation is analyzed.

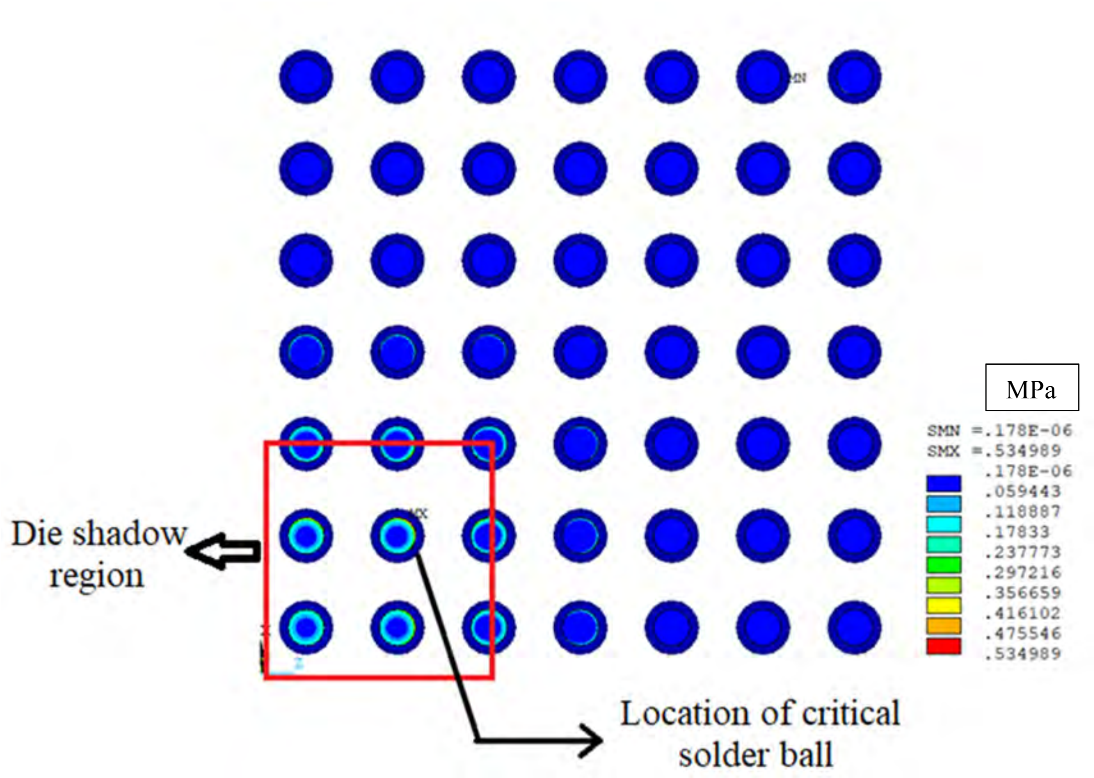

Figure 4.8 Contour Plot of PLWK of SAC305 Solder Ball Array after 3rd Cycle

It can be seen from the contour plot of the plastic work of the critical solder ball in Figure 4.9(a) and 4.9(b) that the location of crack initiation should occur in the package side and in the solder neck region.

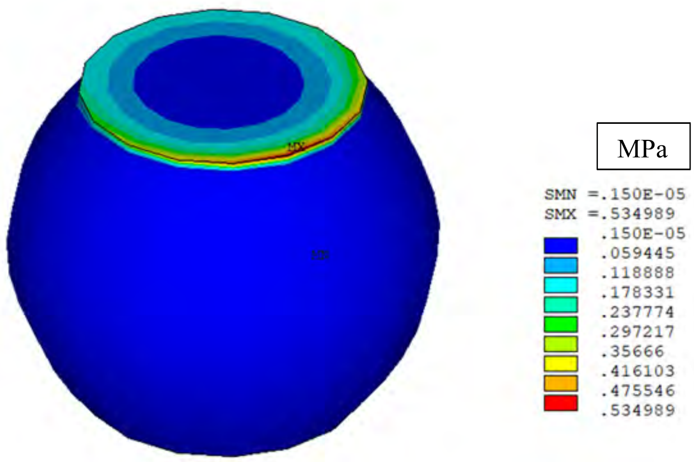

(a)

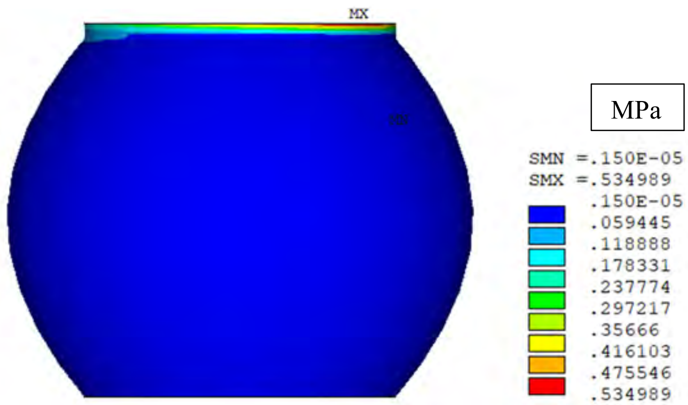

(b)

Figure 4.9 Contour Plot of PLWK of the Critical Solder Ball (a) Isometric View (b) Front View

4.3.2.2 Effect of Silver Percentage

4.3.2.2.1 Variation of von-Mises Stress

The thermally induced stresses in the solder joints are due to the mismatches among the coefficient of thermal expansion of the various bonded materials that constitute the electronic packaging assembly. The contour plot of equivalent (von-Mises) stress for the critical solder ball is shown in Figure 4.8 where maximum stress occurs at the solder neck region. In Figure 4.11, the variation of the maximum von-Mises stress with time for SAC305 non aged solder alloy and 0.5 W input power is shown. This von-Mises stress represents the stress which is responsible for the distortion of the material and related to the failure of the material according to the distortion energy failure theory. In the present analysis, the von-Mises stress is related to the plastic work accumulation such that with the increase of von-Mises stress, plastic work accumulation will also increase. It is evident from Figure 4.11 that the cyclic stresses got stabilized after the first power cycle. The cyclic stress first increases with time when the power is on. After reaching a certain value it decreases with time even in the power-on condition and reaches a minimum value at the end of the power-on cycle. Normally the critical solder joint is in compression when the power is ‘on’ and in tension when the power is ‘off’, which is clearly evident from Figure 4.12 where the maximum normal stress (σ_y) at the critical solder ball location is shown. In solder joints, the highest stress is experienced at the beginning of the power ‘off’ phase and the lowest stress is obtained at the end of the power ‘on’ phase.

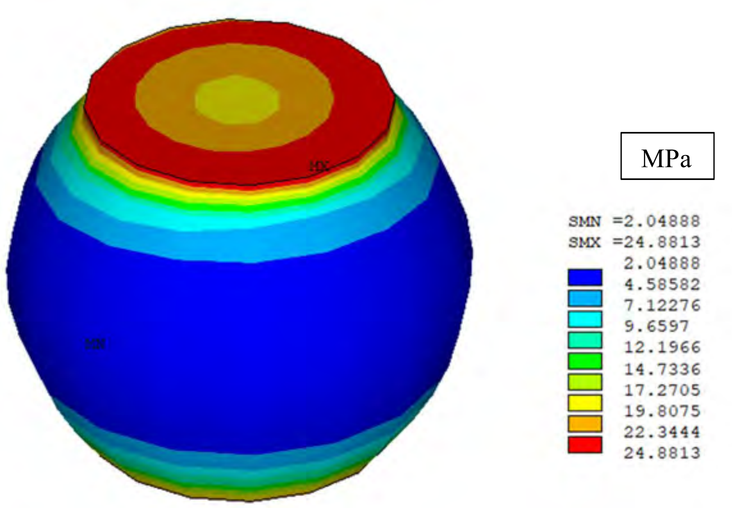

Figure 4.10 Contour Plot of von-Mises Stress Distribution of the Critical Solder Ball at the End of 3rd Cycle for SAC305 Solder and 0.5 W Input Power

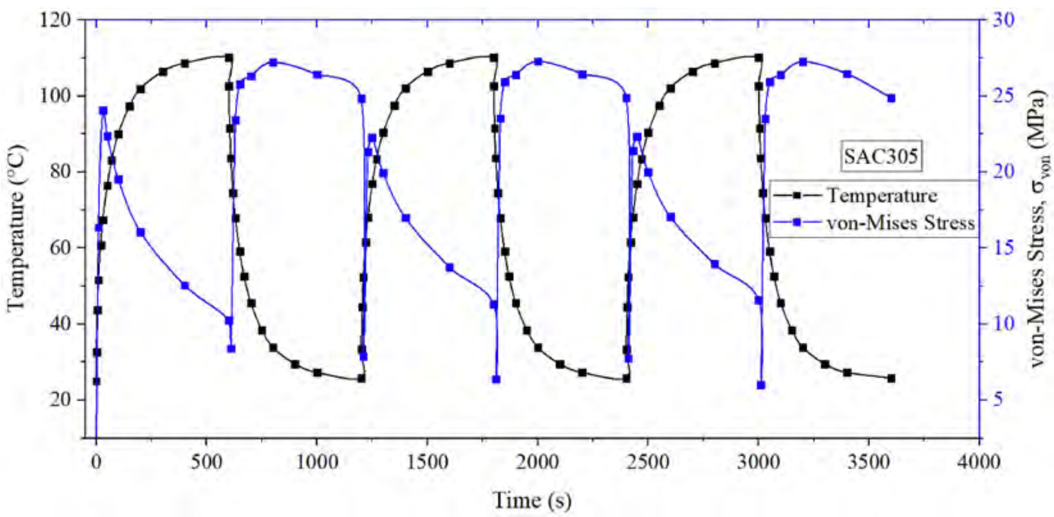

Figure 4.11 Variation of Maximum von-Mises Stress of the Critical Solder Ball Along with Temperature Profile for SAC305 Solder and 0.5 W Input Power

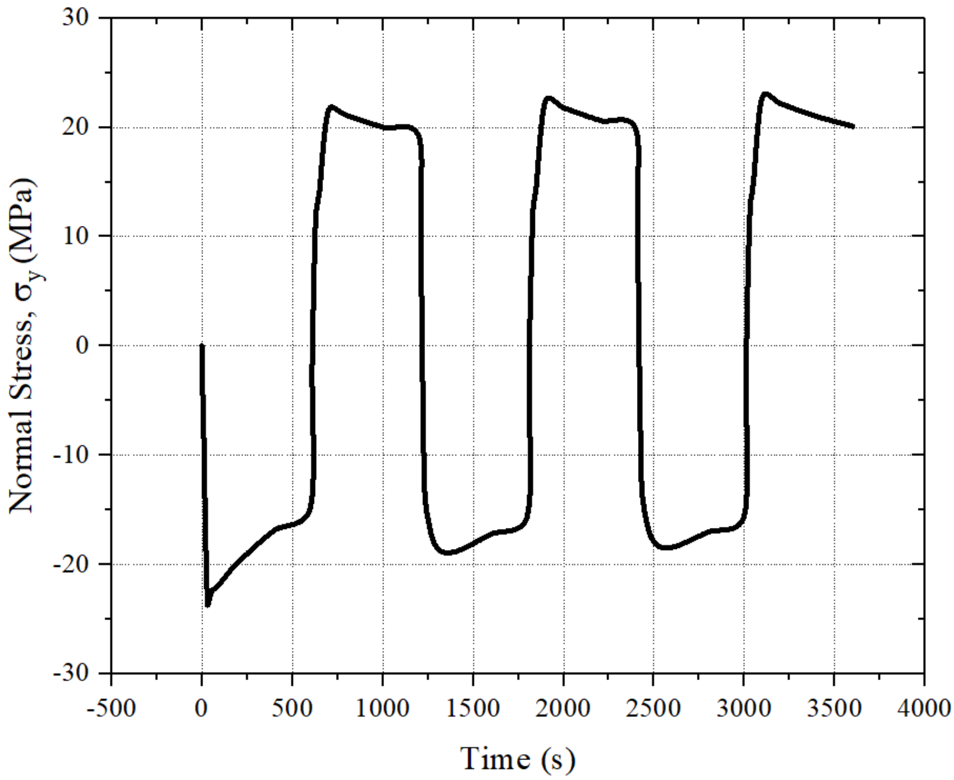

Figure 4.12 Maximum Normal Stress Variation of the Critical Solder Ball with Time for SAC305 Solder

Figure 4.13 shows the variation of the von-Mises stress at the critical solder ball locations for four different SAC alloys. As seen in this figure, the cyclic stress in the solder joint follows similar trend but have differences in magnitude. For the SAC alloy with the highest silver percentage, the induced stress is the highest with a maximum value of 32.01 MPa, while for SAC alloy with 1% silver, the maximum value of the von-Mises stress is found to be 16.22 MPa showing a reduction of 49.32%. It should be noted that these variation in the stress level result from the differences in the solder joint material properties. Reduced silver percentage leads to reduction in the stiffness and hardness, which results in a reduction of the stress in the solder joints.

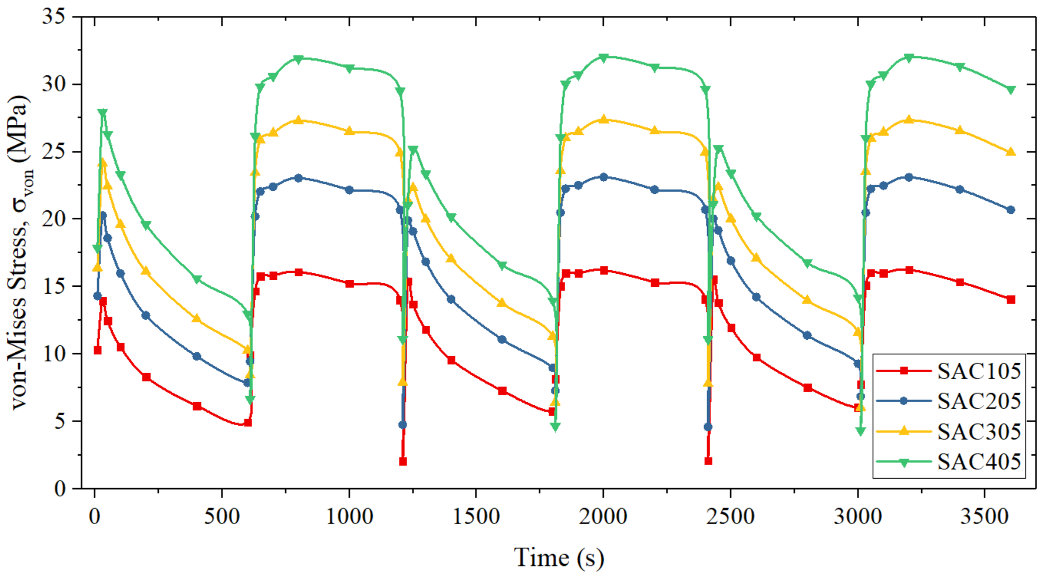

Figure 4.13 Variation of Maximum von-Mises Stress of the Critical Solder Ball with Time for Different SAC Solders at No Aging Condition and 0.5 W Input Power

4.3.2.2.2 Variation of Hysteresis Loop

If the stress and strain data are plotted, there will be a loop due to the plastic deformation which is called the hysteresis loop and the enclosed area of the hysteresis loop represent the plastic work done in a cycle (ΔW). Figure 4.14 shows the von-Mises stress-strain hysteresis curve in the solder joint for three cycles and for SAC305 non aged with 0.5 W input power. The hysteresis curve becomes stable after the second cycle which is evident from the Figure 4.15 where values of ΔW with cycles are plotted.

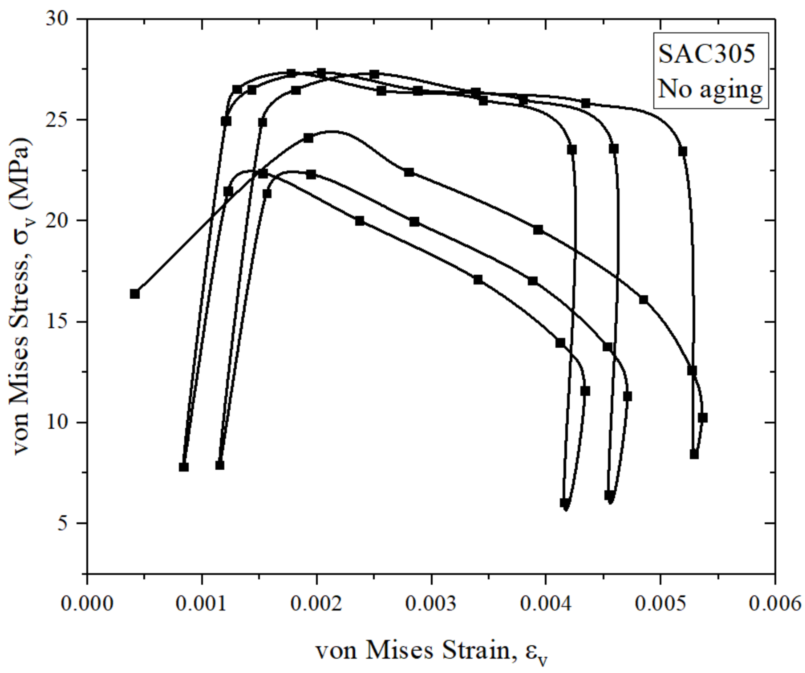

Figure 4.14 Stress-Strain Hysteresis Loop

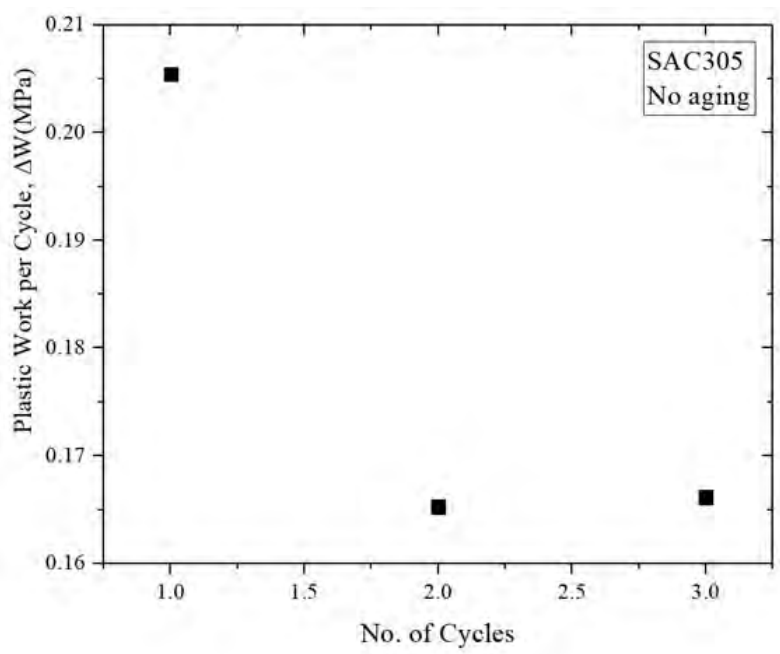

Figure 4.15 Convergence of ΔW with Number of Cycle

The evolution of stress-strain hysteresis curve with silver percentage is shown in Figure 4.16. In this figure, the von-Mises stress-strain hysteresis curves for the critical solder joint for different SAC alloys are plotted (slightly adjusted) for the last cycle only. It is evident that there is a significant difference in the stress-strain range of the hysteresis curves due to the change in silver percentage. The area enclosed by the curve is related to the magnitude of the plastic work per cycle (ΔW). In case of higher silver percentage, both the stress and strain range are higher than the package with lower silver percentage. The enclosed area of the curve also decreases which indicates lesser amount of plastic work per cycle thus higher fatigue life.

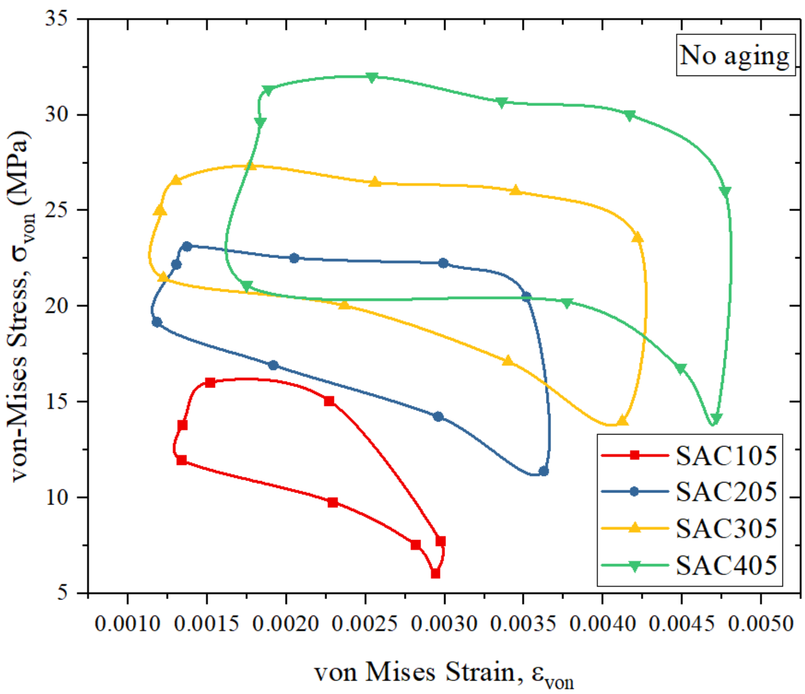

Figure 4.16 von-Mises Stress-Strain Hysteresis Loop for Different SAC Solders at No Aging Condition and 0.5 W Input Power

4.3.2.2.3 Variation of PLWK

A body accumulates plastic work (W_{pl}) when external loads imposed on the body cause inelastic strains in the body. Power cycling of PBGA packages induces plastic deformation and hence plastic work accumulation in the solder joints due to the coefficient of thermal expansion (CTE) mismatches among the different materials comprising the assembly.

The effects of silver percentage on plastic work accumulation is plotted in Figure 4.17. The plastic work increases with the increase of silver percentage which is also evident from the stress-strain curves. It is observed from the figure that the accumulated plastic work (PLWK) increases with time. Moreover, PLWK increases with increasing the silver percentage in solder material. Also, the difference in plastic work accumulation between SAC305 and SAC405 is lesser than that of SAC105 and SAC205 solders. So for higher amount of silver, the curves tend to converge as seen from the figure.

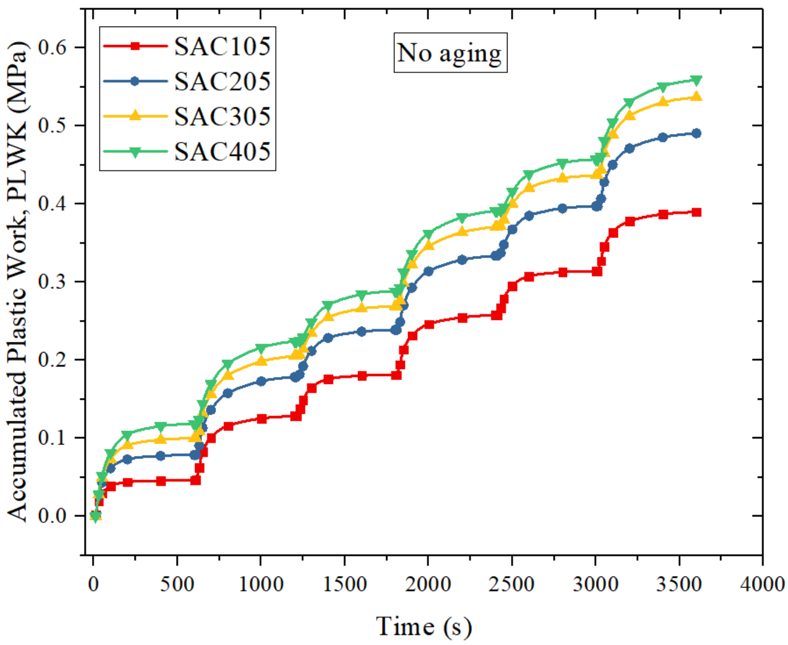

Figure 4.17 Variation of PLWK for Different Silver Percentages of the SAC Solder

4.3.2.2.4 Variation of ΔW

The plastic work dissipated per cycle (ΔW) is the metric parameter to compare the performance of the package under different cases. The value of ΔW was calculated for the last cycle at the critical solder joints using the curves presented in Figure 4.17. To minimize the mesh dependency of the calculated plastic work values in the joints, it is conventional to calculate volume averaged values across a set of N elements along the crack path using the relationship:

$$(W_{pl})_{Averaged} = \frac{\sum_{i=1}^{N}(W_{pl})_i V_i}{\sum_{i=1}^{N} V_i} \qquad 4.1$$

Where $(W_{pl})_i$ and V_i are the elemental values of the accumulated plastic work and volume respectively. In the present analysis, the volume average ΔW is calculated following Park et al. [27].

Variation of silver percentage causes great change in the microstructure of the SAC alloy and its mechanical properties. This change in properties and microstructure also cause change in plastic energy dissipation or ΔW. The effects of silver percentage on ΔW is shown in Figure 4.18 for different input powers. From this figure, it can be seen that at low power levels, the effect of silver percentage on ΔW is not significant. However, for higher power levels, the effect of silver percentage is detrimental for the life of the package as greater amount of ΔW is observed for those cases. Also, the value of ΔW increases more rapidly for higher input power levels. From Figure 4.18, it is observed that for the maximum power level of 0.6 W, the ΔW increases by 46.47% when the silver percentage is changed from 1 to 4%, while this change is about 27.07% for 0.5 W power. So increased power level accelerates the rate of plastic work dissipation per cycle in the solder joint.

From the above discussion, it can be concluded that the silver percentage of the SAC solder alloy has significant effects on the stress distribution, hysteresis loop, plastic work accumulation, and finally on plastic work dissipation per cycle of the solder joint. An increase in silver percentage in the SAC alloy is thus detrimental for the life of the PBGA package in power cycling.

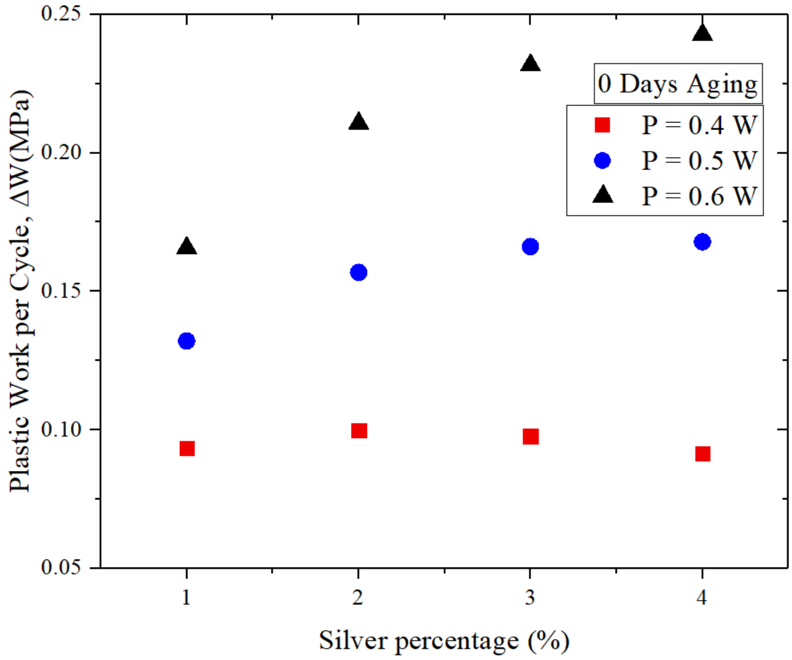

Figure 4.18 Variation of ΔW with Silver Percentage of the SAC Alloy for Different Input Powers and No Aging Condition

4.3.2.3 Effect of Aging

4.3.2.3.1 Variation of von-Mises Stress

Isothermal aging causes great change in the mechanical properties of the solder alloy. This change is also reflected in the stress of the solder alloy. The effect of aging on stress is shown in Figures 4.19. It shows the variation of von-Mises stress of critical solder joint for different prior aging conditions of the PBGA assemblies. As seen from the figure, the cyclic stresses in the solder joint for the no prior aging condition is the highest with a maximum value of 27.36 MPa. For 365 days of prior aging, the maximum value of the predicted von-Mises stress drops to 13.55 MPa showing a reduction of 50.47%. Aging causes reductions in the stiffness and hardness of the solder material, which in turn results in a reduction of the stresses in the solder joints. Moreover, the reduction in stress values is dramatic during first few days of aging and then it changes slowly for longer aging time.

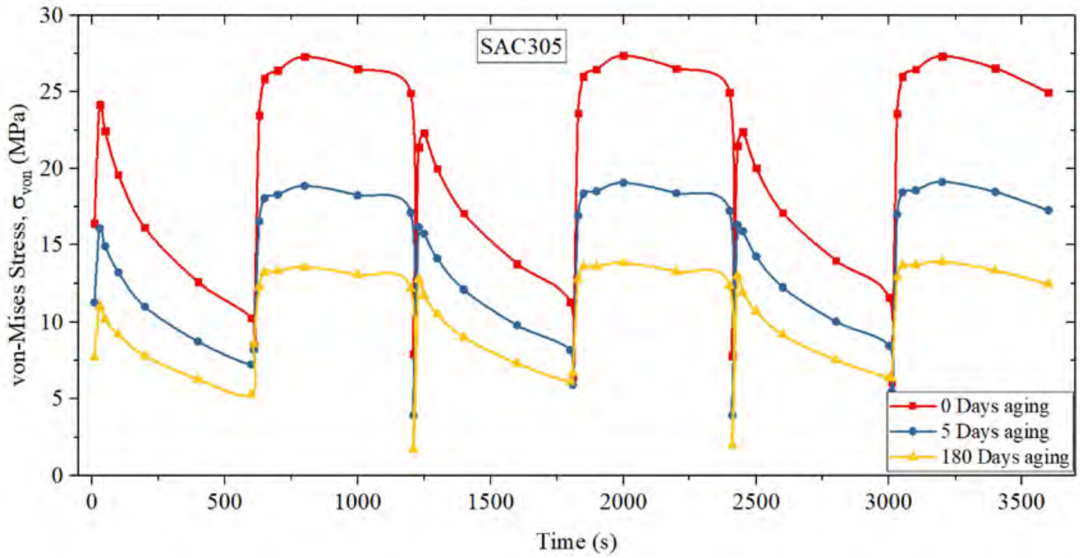

Figure 4.19 Variation of Maximum von-Mises Stress of the Critical Solder Ball with Time for Different Aging Conditions for SAC305 Solder and 0.5 W Input Power

4.3.2.3.2 Variation of Hysteresis Loop

Figure 4.20 shows the von-Mises stress-strain hysteresis curves in the critical solder joint for different aging times for SAC305 solder alloy. All curves show similar trend but have a significant difference in the stress-strain range of the hysteresis loop due to isothermal aging. The stress and strain range as well as the area of the hysteresis loop decrease with aging time. So the loop is the biggest for solder with no prior aging whereas it is the smallest for 365 days of solder aging at 100 °C.

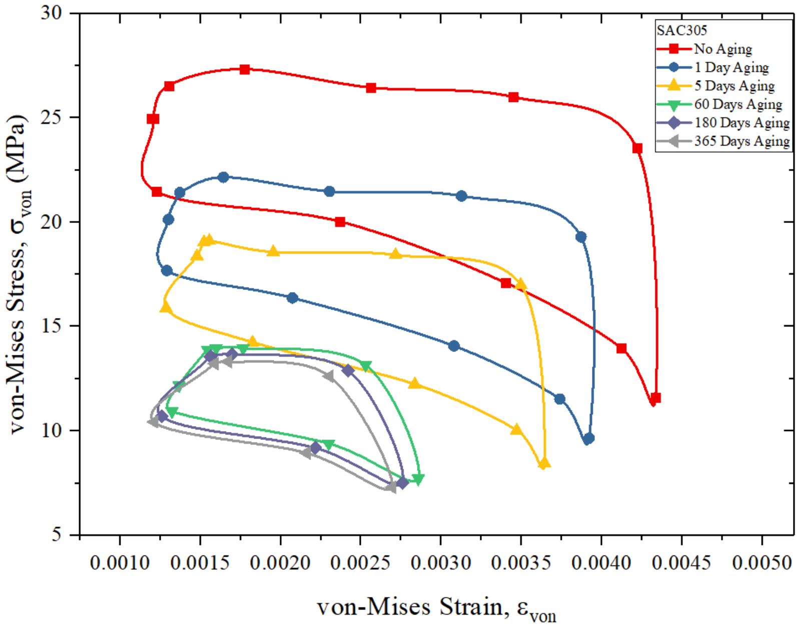

Figure 4.20 von-Mises Stress-Strain Hysteresis Loop for Different Aging Conditions for SAC305 Solder and 0.5 W Input Power

4.3.2.3.3 Variation of PLWK

Figures 4.21 shows the accumulated plastic work (W_{pl}) in the solder joints of the PBGA components, after three complete power cycles for different aging conditions. The figure shows that the highest rate of plastic work accumulation occurs in the non-aged assembly and the smallest PLWK is obtained for solder with 365 days of aging. For the assemblies with prior aging, although the mechanical properties of the solder material are degraded, the shear fatigue ductility increases leading to lesser plastic deformation resulting in lower rates of plastic work accumulation compared to the non-aged configuration.

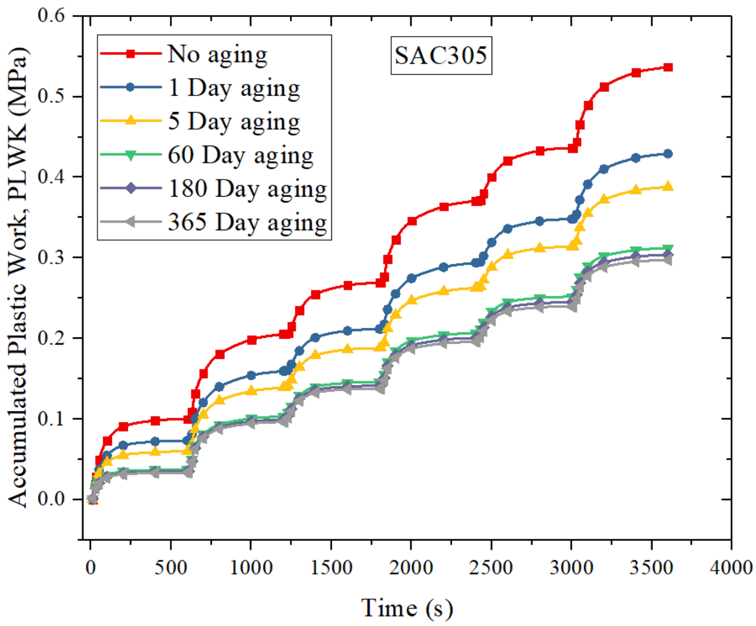

Figure 4.21 Variation of PLWK for Different Aging Conditions for SAC305 Solder

It is also observed that the results for the 60 days, 180 days and 365 days aging cases are relatively close together, revealing the observations that aging causes large changes during the first 60 days of aging, and smaller steady change after that point.

4.3.2.3.4 Variation of ΔW

In Figure 4.22, the effects of isothermal aging on plastic work dissipation per cycle (ΔW) is shown for SAC305 for different input powers. Six different aging times of 0, 1, 5, 60, 180 and 365 days at 100 °C are considered. The figure shows ΔW reduces as aging time increases. In most of the thermal cycling analysis, ΔW increases with aging time, however, the reverse case was also reported in some literature [45]. These difference may be due to the different temperature distribution of package in thermal and power cycling cases. Package warpage and degree of shear deformation depend on the temperature distribution. All these differences lead to the opposite results in thermal and power cycling tests. This trend can be explained in terms of deformation and strain. The decrease in plastic work may be resulted from lower plastic deformation or strain which is shown in Figure 4.23 for no aging and 365 days of aging conditions. It is observed that amount of plastic strain is higher for non aged solder ball than the ball with 365 days of aging. This is because shear deformation due to CTE mismatch is higher in non aged solder joint, and the aged solder has superior shear fatigue ductility. For this lower plastic deformation with aging, the total deformation should also decrease with aging which is also observed from Figure 4.25. However, the elastic deformation for the aged solder should increase due to the lower stiffness of the aged solder which is also presented in Figure 4.24. It is also evident from Figure 4.22 that the change in ΔW with aging occurs very rapidly with aging up to first 60 days of aging and after that, it changes slowly. When the input power is low that is 0.4 W, ΔW is also low with a value of 0.098 MPa at no aging condition. The highest value of ΔW at 0.6 W input power has been found to be 0.232 MPa. For an input power of 0.6 W, ΔW decreases to 0.133 MPa from no aging to 180 days aging and the reduction is about 42.48 %. For further aging, ΔW is reduced to 0.13 MPa for 365 days of extreme aging and the reduction is 43.77% which is very close to the reduction of 180 days aging. Finally, ΔW drops by 28.74 % and 30 % for 0.4 W input power at 180 days and 365 days of aging. So it is revealed that at low input power, the effects of thermal aging on the change of ΔW is comparatively smaller.

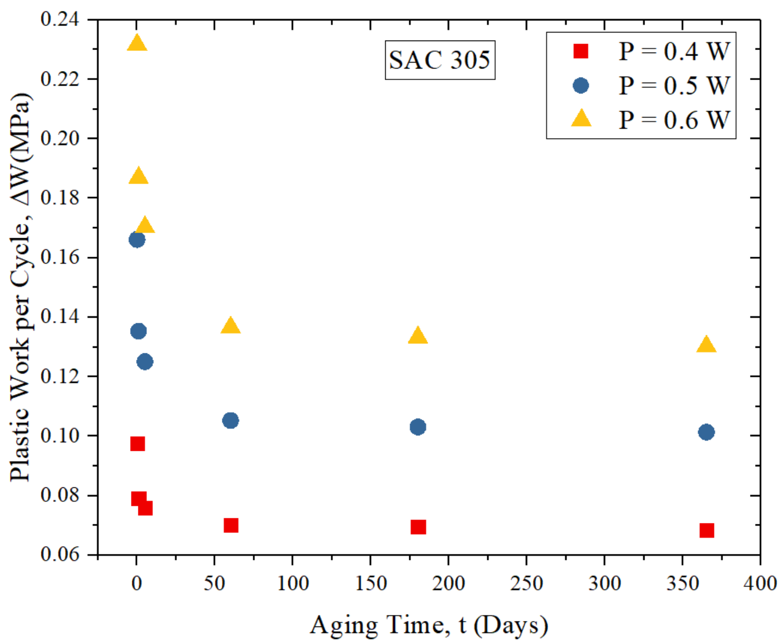

Figure 4.22 Variation of ΔW with Aging Time for SAC305 Solder for Different Input Powers

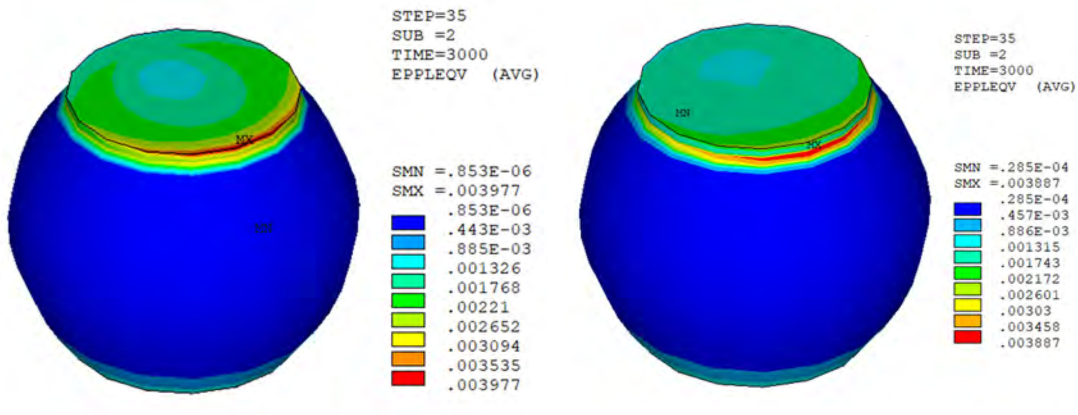

No aging 365 days of aging

Figure 4.23 von-Mises Plastic Strain of the Critical Solder Ball for SAC305 Alloy and 0.5 W Input Power

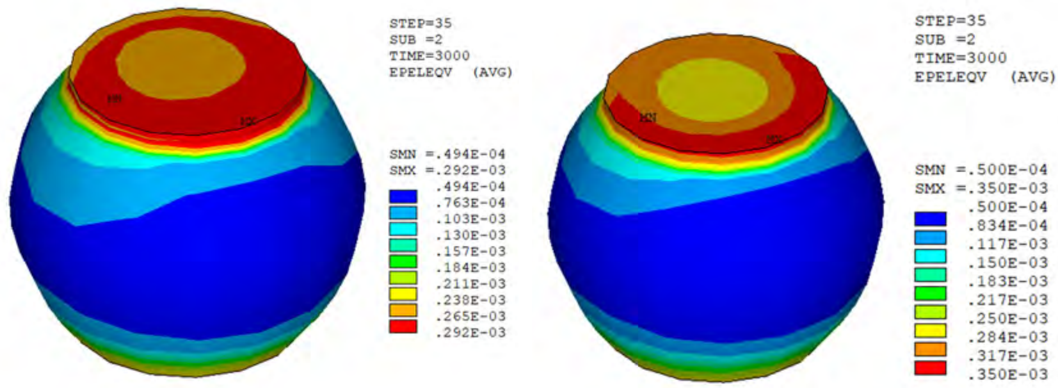

No aging 365 days of aging

Figure 4.24 von-Mises Elastic Strain of the Critical Solder Ball for SAC305 Alloy and 0.5 W Input Power

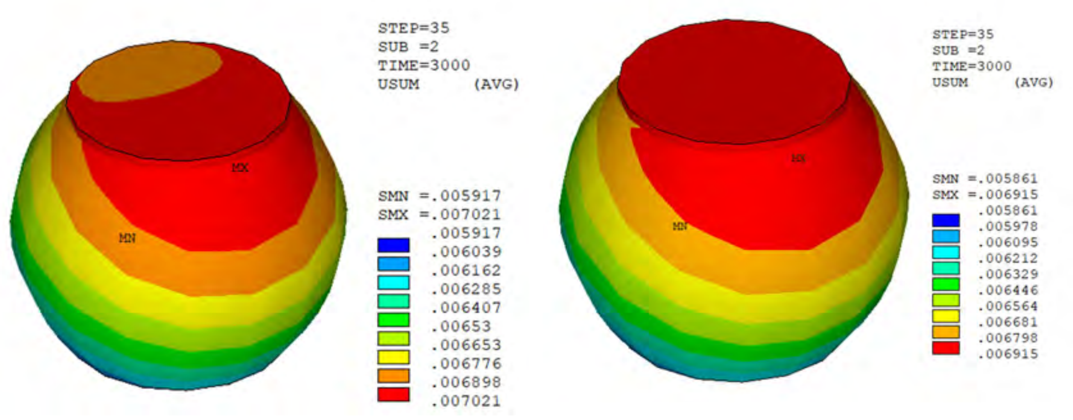

No aging 365 days of aging

Figure 4.25 Total Deformation of the Critical Solder Ball for SAC305 Alloy and 0.5 W Input Power

In Figures 4.26(a)-4.26(c), the effects of aging on ΔW for different SAC alloy packages for input powers of 0.4 W, 0.5 W, and 0.6 W are shown respectively. From Figure 4.26(a) it can be seen that the effect of thermal aging is similar for all the SAC alloys that is ΔW is decreased with increasing the aging time. The decrease in ΔW for SAC105 is around 44.3 % at 365 days of aging but it is only 22.1 % for SAC405. So solder balls with lower silver percentages are more sensitive to aging. Similarly, effects of aging on ΔW for different SAC alloys for power levels of 0.5 W and 0.6 W are shown in Figures 4.26(b)-(c). Similar results are also obtained in these power levels also.

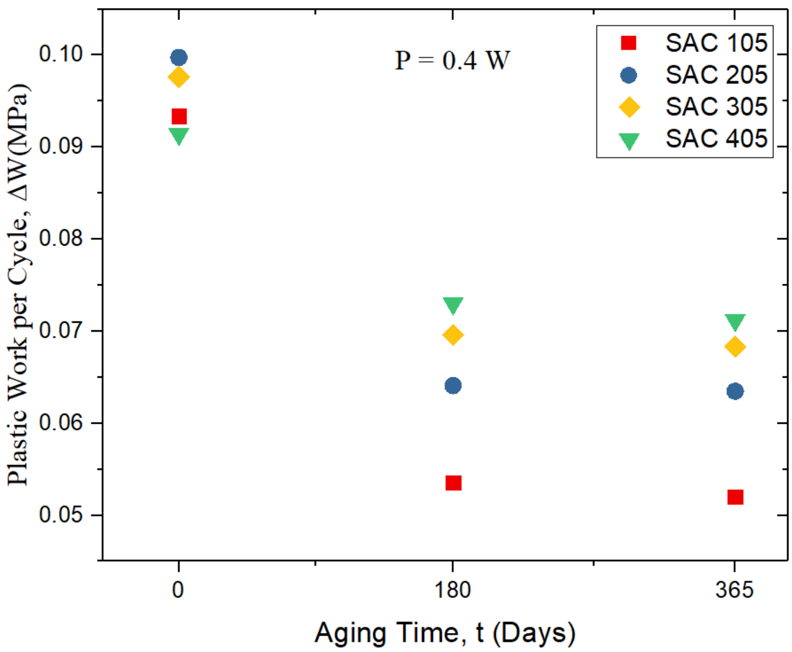
P = 0.4 W
SAC 105
SAC 205
SAC 305
SAC 405
Plastic Work per Cycle, ΔW(MPa)
0.10
0.09
0.08
0.07
0.06
0.05
0
180
365
Aging Time, t (Days)

(a)

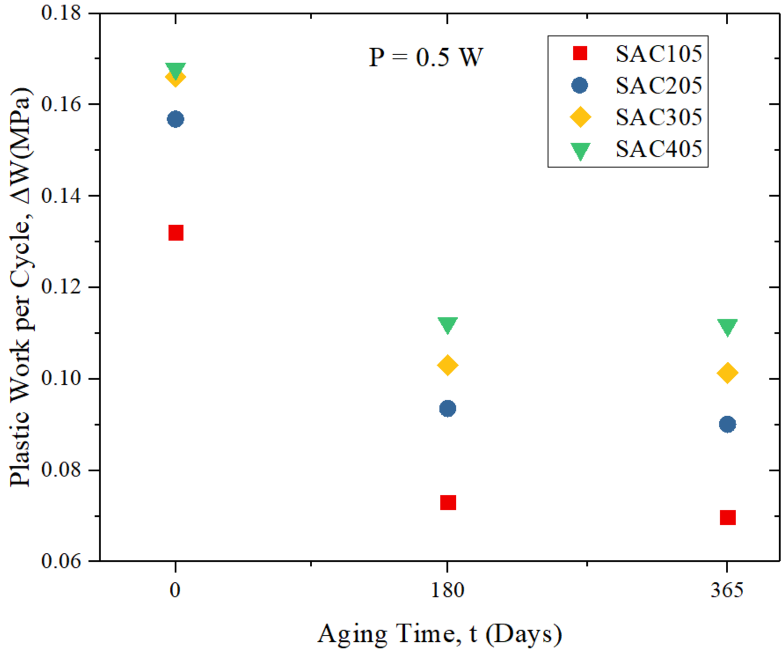
P = 0.5 W
SAC105
SAC205
SAC305
SAC405
Plastic Work per Cycle, ΔW(MPa)
0.18
0.16
0.14
0.12
0.10
0.08
0.06
0
180
365
Aging Time, t (Days)

(b)

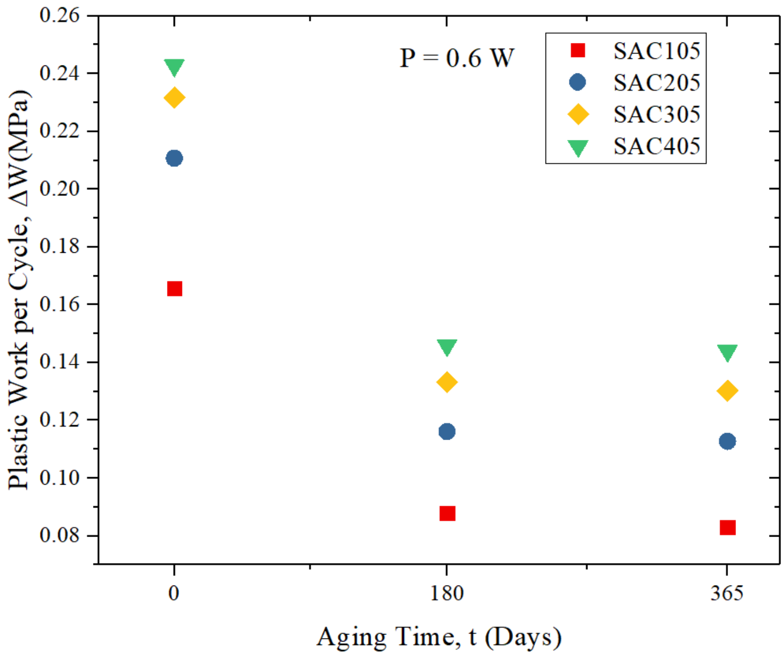

(c)

Figure 4.26 Variation of ΔW with Aging Time for Different SAC Solders for (a) 0.4 (b) 0.5, and (c) 0.6 W Input Powers

So from the above discussion, it can be said that ΔW decreases with aging for all SAC alloys and this declination is highest for SAC105 and lowest for SAC405. Also, the drop in ΔW increases with the input power levels for all SAC alloys. Interestingly, the level of reduction tend to converge to a point for all the SAC alloys with the increase of power level.

Another thing to be noted from Figure 4.27(a)-4.27(d), where the variation of ΔW is plotted for different aging times at different constant silver percentage that the slope of the change in ΔW becomes stepper for higher silver percentage for all aging conditions.

In conclusion, it can be stated that aging has significant effect on the stress distribution, hysteresis loop, plastic work accumulation, and finally on plastic work dissipation per cycle. Aging improves the power cycling life of the PBGA package by decreasing ΔW for all SAC alloys considered and for all three input powers.

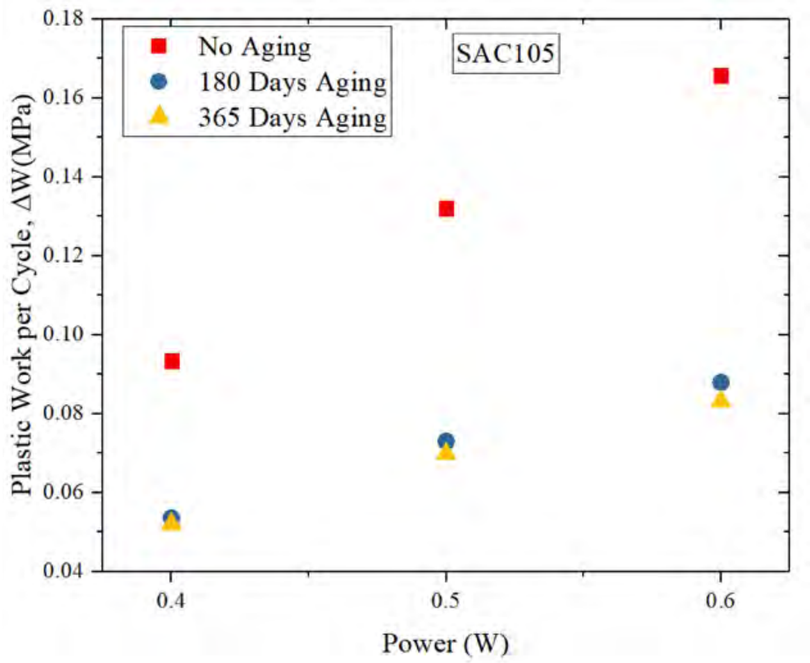
No Aging
180 Days Aging
365 Days Aging
SAC105
Plastic Work per Cycle, ΔW(MPa)
0.18
0.16
0.14
0.12
0.10
0.08
0.06
0.04
0.4
0.5
0.6
Power (W)

(a)

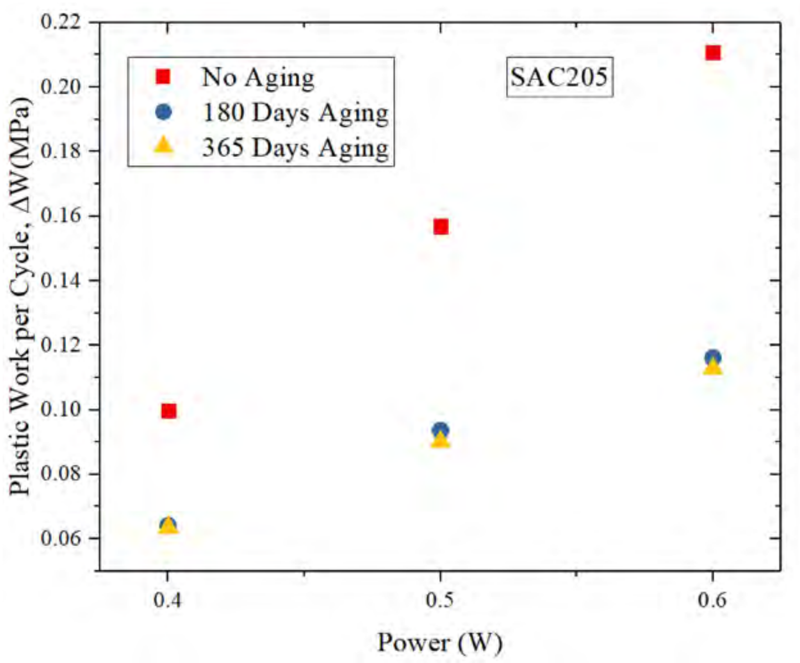
No Aging
180 Days Aging
365 Days Aging
SAC205
Plastic Work per Cycle, ΔW(MPa)
0.22
0.20
0.18
0.16
0.14
0.12
0.10
0.08
0.06
0.4
0.5
0.6
Power (W)

(b)

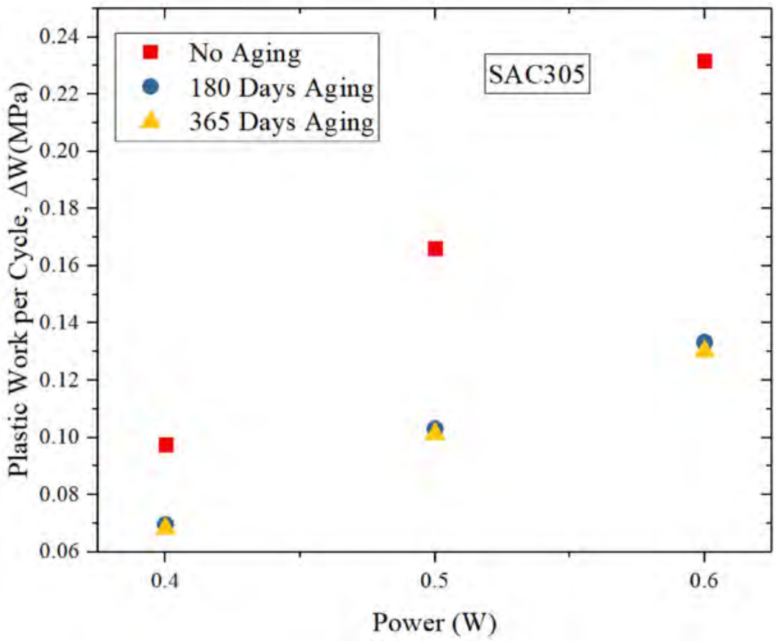

(c)

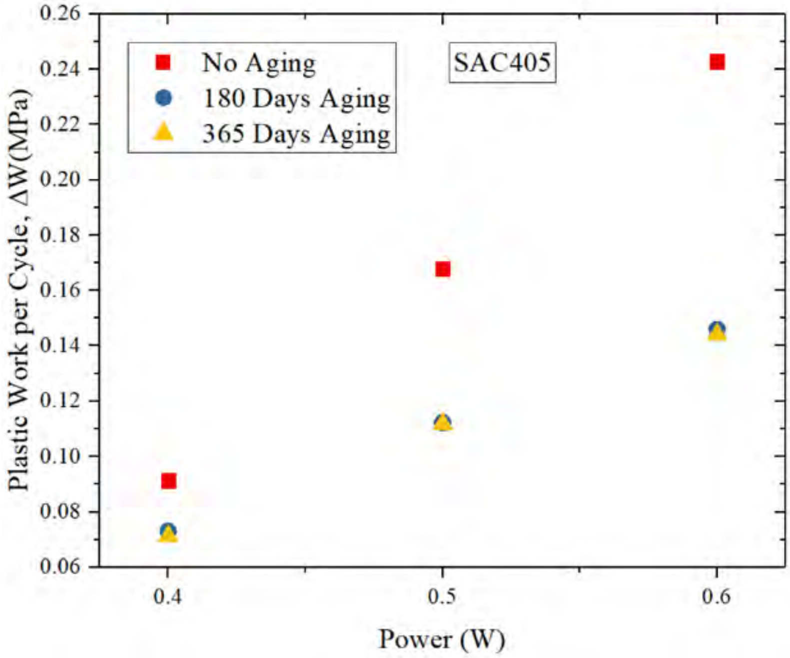

(d)

Figure 4.27 Variation of ΔW with Input Power for (a) SAC105 (b) SAC205 (c) SAC305, and (d) SAC405 Solders and Different Aging Conditions

4.3.2.5 Effect of Aging on Power Cycling Fatigue Life of PBGA Package

The power cycling fatigue life of the PBGA package has been calculated using darauvex approach with the constants of life predictions extracted from motalab et al. [42]. Due to the unavailability of the constants for other SAC alloys, only the life of SAC305 has been calculated at three aging conditions of 0, 180, and 365 days aging. The characteristic life of the PBGA package for these aging conditions is shown in Figure 4.28. Power cycling life of the PBGA packages also increases with aging for all input power levels. However, the increase in life is different for different power level. For low input power, the increase in life for a small decrease in ΔW is magnified to a great extent. This is because ΔW and life prediction models follow an exponential relation. So a small change in ΔW results in a big change in life for a lower value of ΔW. But for a higher value of ΔW, the change in life with ΔW has not been exaggerated so much. The life of the package has been increased as much as 2.56 times for an input power of 0.4 W from no aging to 365 days severe aging. The improvement of life for other input powers are 3.59 times and 4 times for 0.5 W and 0.6 W input power respectively.

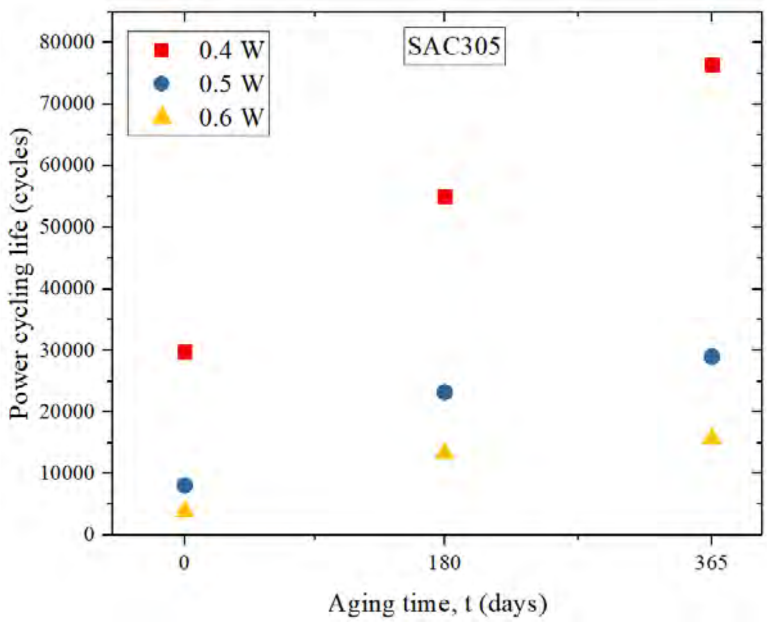

Figure 4.28 Characteristic Life Variation with Aging for Different Input Powers for SAC305 Solder

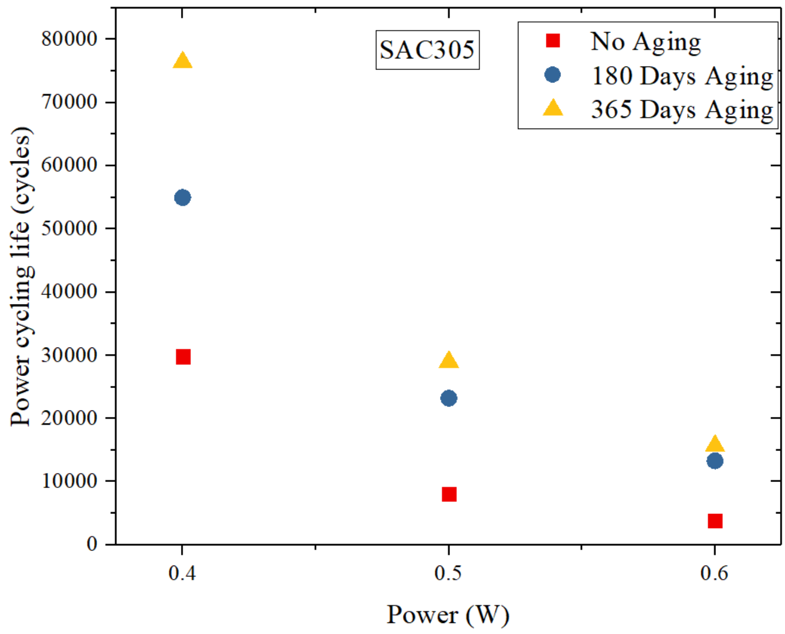

Figure 4.29 Characteristic Life Variation of the SAC305 Solder with Various Input Powers and Different Aging Condition

Another thing to be noticed from Figure 4.29, where the life is plotted with the varying input power that although ΔW increases linearly with increasing power level but the life is not so due to the logarithmic relation between ΔW and life predicting model. It follows a nonlinear decreasing trend with increasing power level and tends to become flat which provoke that the severity of input power slows down at higher power level and no aging condition.

In summary, the effect of isothermal aging of the SAC solder alloy, silver percentage of the SAC solder alloy and input power of the die on solder joint life of a PBGA microprocessor package under power cycling have been investigated through finite element analysis. The results show that ΔW decreases with aging time for all SAC alloys. Also, for the same aging time, package with lower silver content has the lowest value of ΔW. Finally, the higher the input power the higher the value of ΔW for the same aging time and silver percentage.

4.4 Mechanical Bend Cycling

In the subsequent sections, the results of mechanical bend cycle have been presented and discussed. The mechanical bend cycle analysis has been performed following the same protocol as power cycling except that the applied load is structural where a displacement load with a sinusoidal profile rather than thermal temperature load has been applied. The applied load induces stress which causes plastic deformation. Due to this plastic deformation, inelastic energy dissipation occurs in the solder ball that causes crack initiation and propagation with further cycles and finally the solder ball fails. The main parameter for this failure, that is plastic work per cycle (ΔW), along with stress, accumulated plastic work (PLWK), and stress-strain hysteresis loop have been compared for different cases that are analyzed.

4.4.1 Location of Critical Solder Ball

The location of the critical solder ball is the solder ball that has the maximum plastic work. In Figure 4.30 the contour plot of plastic work per volume is shown for SAC305 package at room temperature at a frequency of 1 Hz with no aging condition. From the figure, it can be seen that the maximum plastic work per volume occurs at the outermost corner solder joint which is in conformity to the experimental work available in the literature [63]. This is due to the fact that the deformation in this solder joint is the highest than any other solder joint.

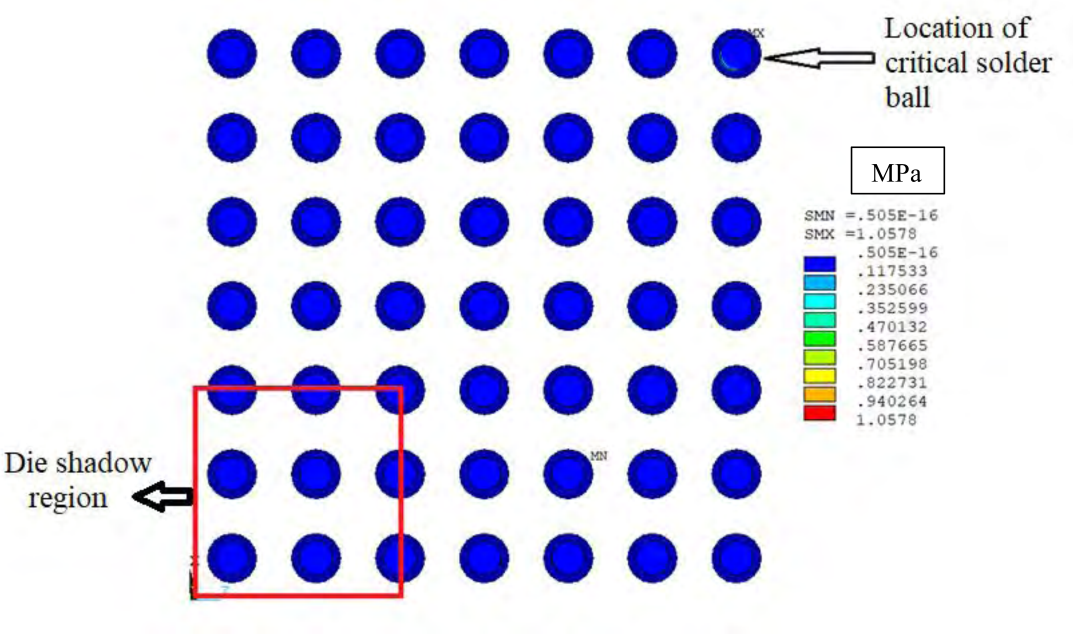

Figure 4.30 Contour Plot of PLWK of Full Solder Ball Array for SAC305 Solder at Room Temperature and Frequency of 1 Hz

In Figure 4.31, the critical solder joint is shown separately to show the location of crack initiation. From this Figure, the location of crack initiation is found to be on the PCB side of the joint where maximum plastic work accumulation occurs and this conforms to the experimental results.

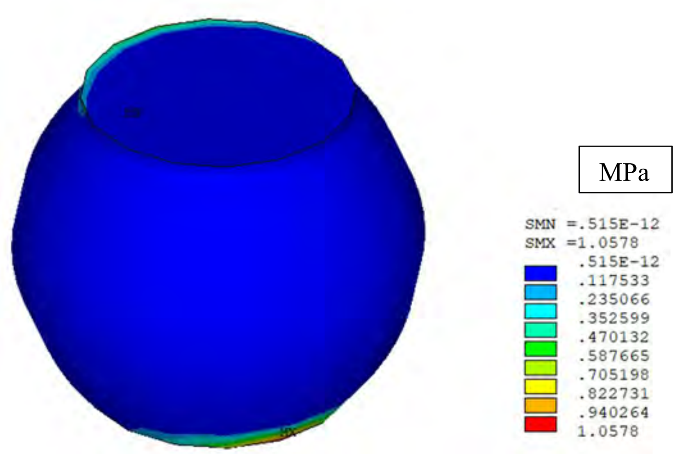

(a)

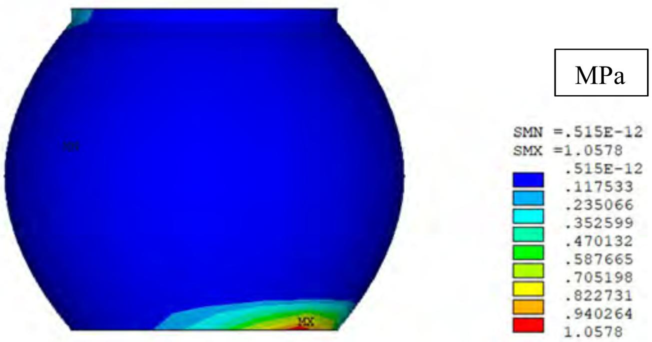

(b)

Figure 4.31 Contour Plot of PLWK of the Critical Solder Ball for SAC305 at Room Temperature and Frequency of 1 Hz (a) Isometric View (b) Front View

4.4.2 Effect of Silver Percentage

4.4.2.1 Variation of von-Mises Stress

Figure 5.32 shows the contour plot of the von-Mises stress of the critical solder joint where the maximum stress is seen to be on the PCB side of the solder. The bending induced stress profile on the solder joint is shown in Figure 5.33 where the von-Mises stress is plotted with the load profile. It can be seen from the figure that the stress increased when the displacement increased in both direction and decreases during unloading. Also, the PCB side of the solder joint is in compression when the displacement is positive (upward) and in tension when the displacement is negative (downward).

In Figure 4.34, the effect of silver percentage on von-Mises stress is shown. The figure shows a decrease in stress value with reduced silver percentage due to the lower stiffness although the variation pattern is similar.

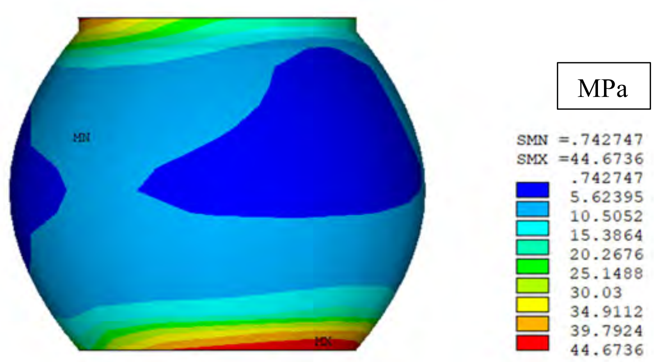

(a)

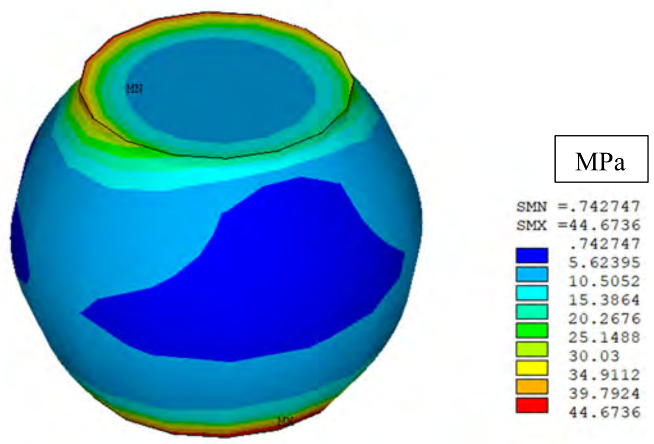

(b)

Figure 4.32 Contour Plot of von-Mises Stress of the Critical Solder Ball for SAC305 for no Aging at Room Temperature and Frequency of 1 Hz (a) Front View (b) Isometric View

In Figure 4.34, the von-Mises stress for different SAC alloys are plotted where the maximum stress value is found to be 57.66 MPa for 4% silver SAC alloy and the minimum stress value is found to be 31.45 MPa for 1% silver SAC alloy showing a reduction of 45.45% in stress as we go from 4 to 1% of silver.

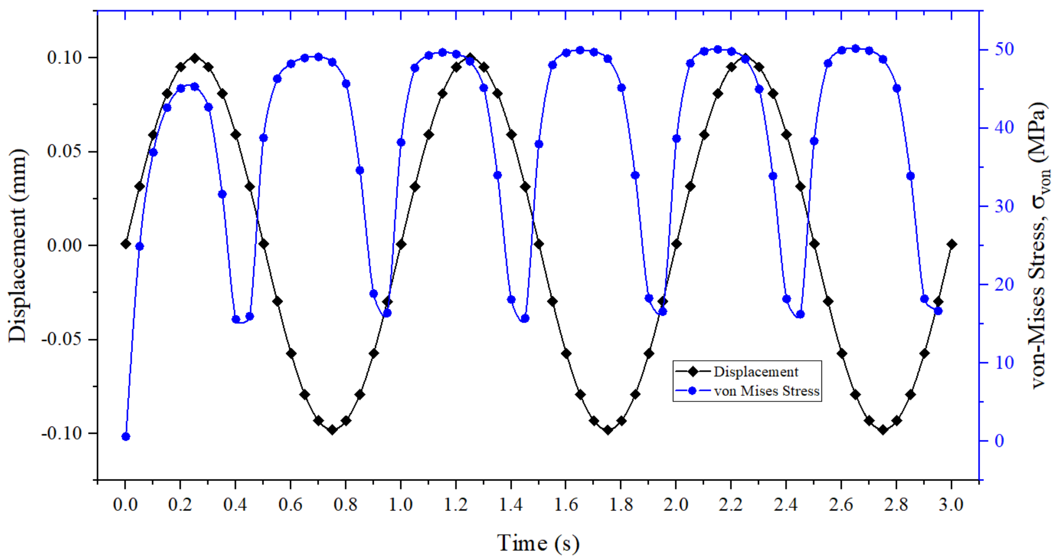

Figure 4.33 Variation of von-Mises Stress of the Critical Solder Ball with Time Along with the Displacement Profile for SAC305 Solder at Room Temperature and Frequency of 1 Hz

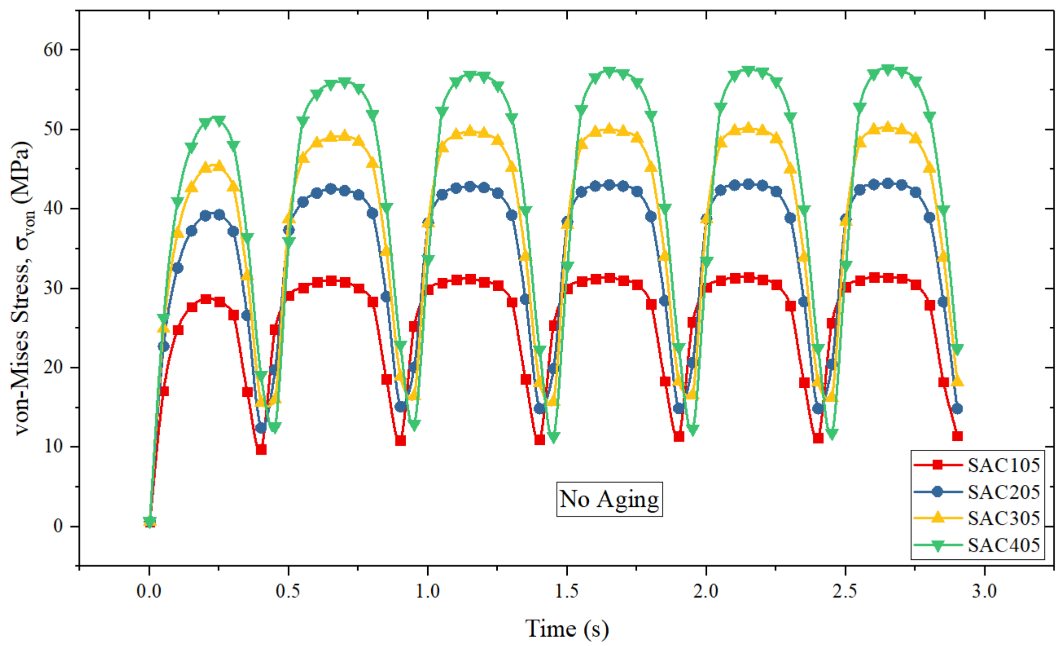

Figure 4.34 Variation of Maximum von-Mises Stress of the Critical Solder Ball with Time for Different Percentage of Silver in the Solder Joint at Room Temperature at Frequency of 1 Hz and No Aging Condition

4.4.2.2 Variation of Hysteresis Loop

If the stress and strain data are plotted, there will be a loop due to the plastic deformation which is called the hysteresis loop and the enclosed area of the hysteresis loop represent the plastic work done in a cycle. The plastic work has different component. Both normal stress and shear stress contribute to the total plastic work accumulation of the solder joint. As a representative, only the normal stress-strain data are presented and discussed here. In Figure 4.35, the normal stress-strain data for three loading cycles are plotted for SAC305 solder for no aging at room temperature and 1 Hz frequency. From the figure, it can be seen that the loop becomes stable after two cycles of loading. In Figure 4.36, the effect of silver percentage on the stress-strain hysteresis loop is shown. Here, the hysteresis loop is shown for the final loading cycle only.

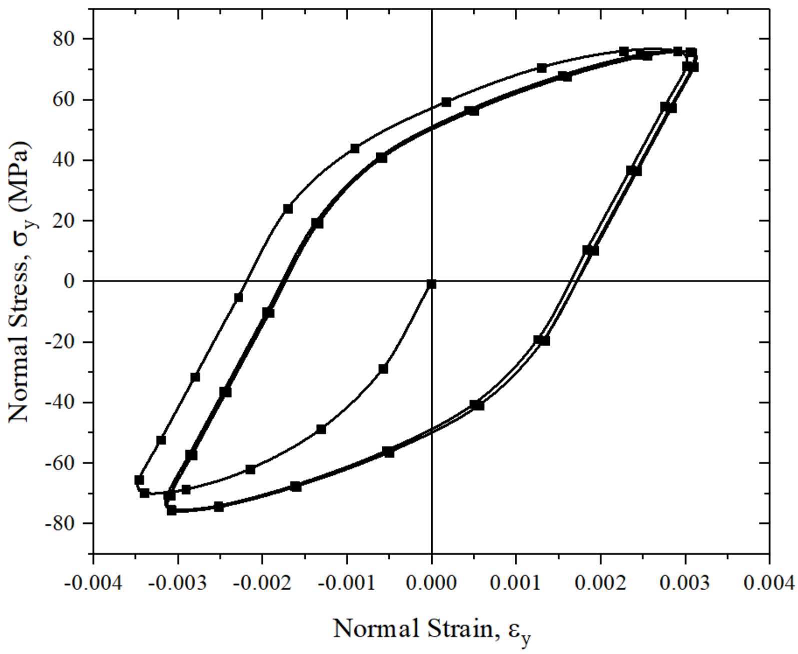

Figure 4.35 Stress-Strain Hysteresis Loop for Three Loading Cycles for SAC305 Solder for No Aging Condition at Room Temperature and 1 Hz Frequency

The figure depicts that the hysteresis loop is rotating from a vertical position to a horizontal position with reduced silver percentage causing a decrease in stress range and an increase in strain range. However, the decrease in stress value is more offset by the increase in strain due to the higher plastic deformation. The area of the loop, as well as the plastic work per cycle, also increases with lowering Ag%.

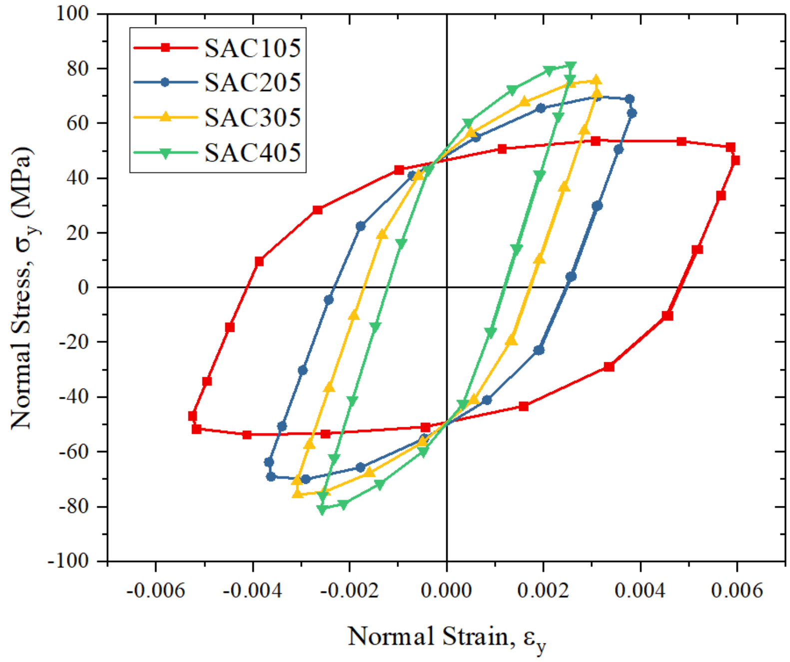

Figure 4.36 Stress-Strain Hysteresis Loop after 3rd Cycle Loading for Different SAC Solder for No Aging Condition at Room Temperature and 1 Hz Frequency

4.4.2.3 Variation of PLWK

Due to the plastic deformation that arises from the loading, plastic work is done on the solder ball and continuous dissipation of inelastic energy occur. This plastic work per volume (PLWK) is plotted in Figure 4.37 with load profile. The figure shows that plastic work accumulation occurs during the cyclic. Also, there is no accumulation of plastic work during unloading time. In Figure 4.38, the effect of silver percentage on plastic work accumulation is shown. It is evident from this figure that the plastic work accumulation increases with reduced silver percentage although the variation pattern is similar for different SAC alloys. This is because the plastic deformation increases with decreased silver percentage due to the decrease in strength, stiffness and deformation resistance of the solder material.

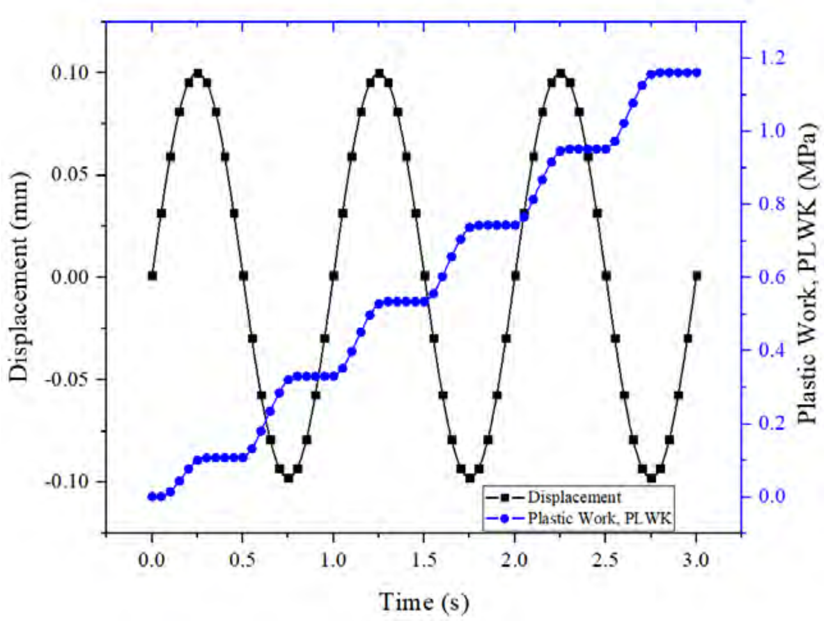

Figure 4.37 Variation of PLWK of the Critical Solder Joint with Time along with the Load Profile for SAC305 at Room Temperature at Frequency of 1 Hz and No Aging Condition

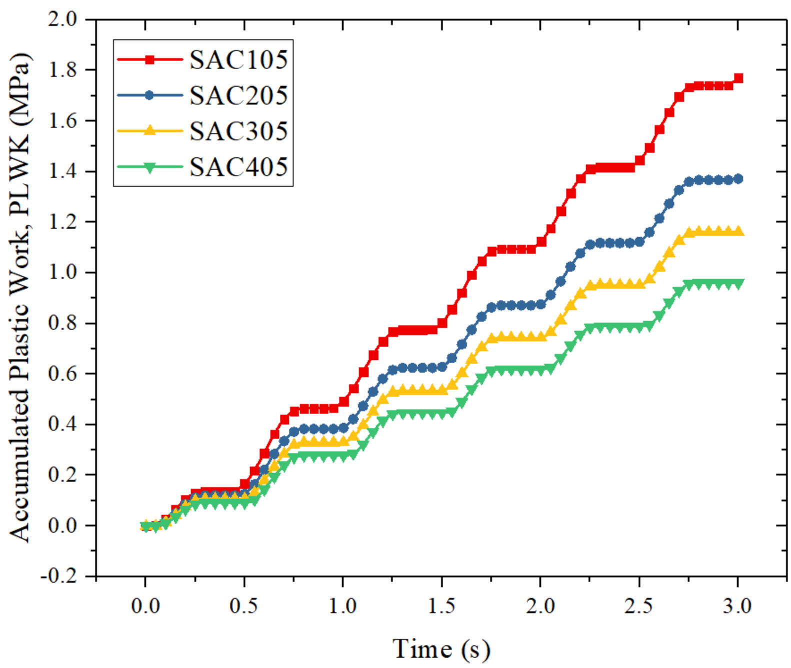

Figure 4.38 Variation of PLWK of the Critical Solder Joint with Time for Different SAC Solder at Room Temperature at Frequency of 1 Hz and No Aging Condition

4.4.2.4 Variation of ΔW

The accumulated plastic work per cycle that is ΔW is the main parameter for damage analysis in the solder joint. The solder joint with highest ΔW is the critical solder joint and the location of highest ΔW is the critical location where crack initiate and propagate to failure. The ΔW of the critical solder joint at the critical location has been calculated for various cases to show the effects of those cases. The higher the ΔW value the lower the life of the solder joint. In order to do the calculation of ΔW, a volume average technique has been used as recommended by [79] where the outer solder ring elements are used as the representative volume.

In Figure 4.39, the variation of ΔW with silver percentage has been shown for three different testing temperature and no aging condition at 1 Hz frequency to show the effect of silver percentage on ΔW. From the figure, ΔW decreases as much as 71.5 % for a change in silver percentage from 1 to 4 at 25 °C temperature. The reductions are 56.15 % and 43.87 % for 75 and 125 °C testing temperatures respectively. This reduction in ΔW occurs because the higher temperature causes a degradation in the stiffness and strength of the solder material which slows down further reduction of ΔW at higher temperature.

In Figure 4.40, the effect of silver percentage on ΔW for different loading frequency is shown for no aging and room temperature conditions. The figure also shows a similar trend as in Figure 4.39 and higher frequency reduces the value of ΔW further due to the higher loading rate. The decrease in ΔW for 1 Hz frequency is about 71.5% as one goes from 1 % silver to 4% silver, whereas, the decrease in ΔW for 5 Hz frequency is about 76.2% for the same silver variation. This suggests that the frequency has a small influence on the effect of silver percentage on ΔW. It is also depicted that this improvement with frequency will tend to cease after some point.

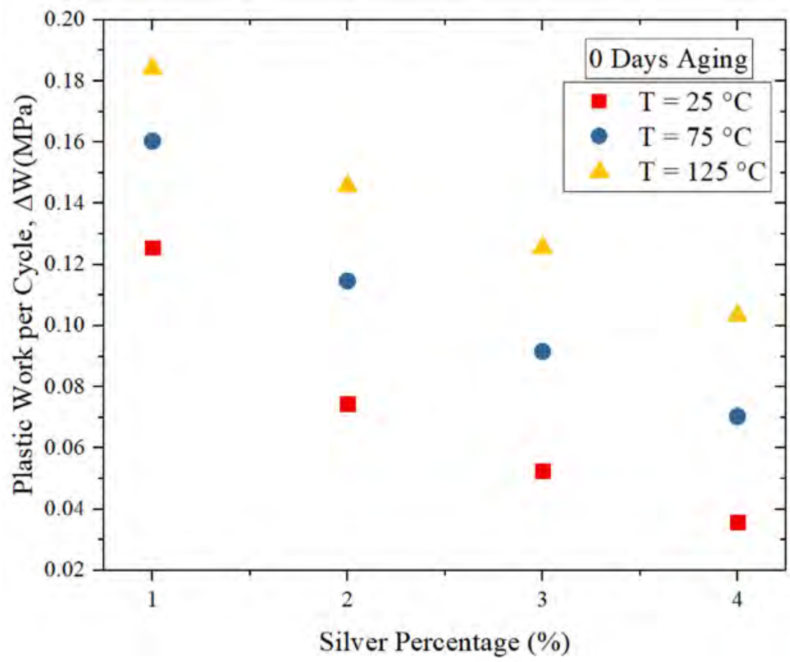

Figure 4.39 Variation of ΔW with Silver Percentage of the Solder Material for Different Testing Temperature at No Aging Condition and 1 Hz Frequency

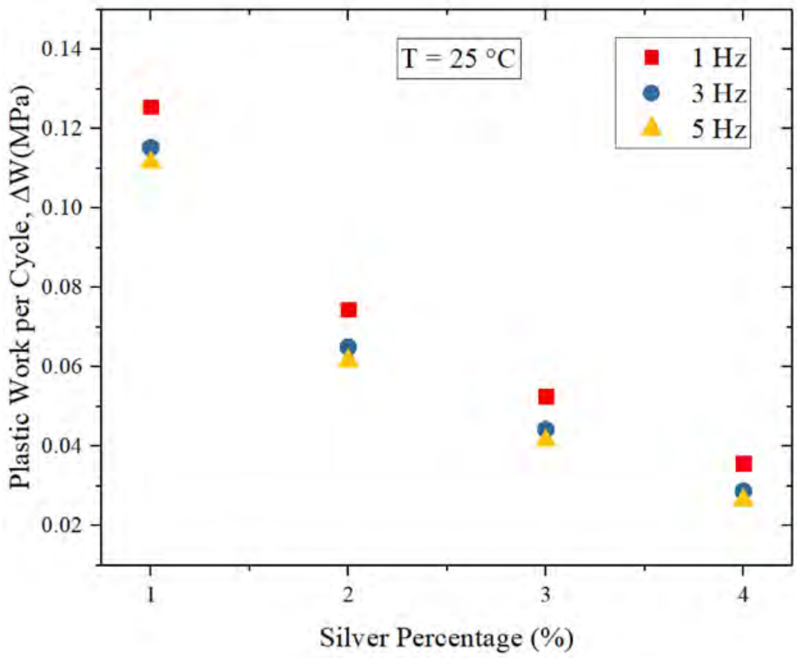

Figure 4.40 Variation of ΔW with Silver Percentage of the Solder Material for Different Loading Frequency at No Aging and Room Temperature Conditions

From the above discussion, it can be asserted that silver percentage of the SAC solder alloy has significant effect on the stress distribution, hysteresis loop, plastic work accumulation, and finally on ΔW in mechanical bend cycle. An increase in silver percentage in the SAC alloy is beneficial for the mechanical cycle life of the PBGA package due to the decrease in ΔW.

4.4.3 Effect of Aging

4.4.3.1 Variation of von-Mises Stress

In Figure 4.41, the effect of aging on von-Mises stress are shown for three mechanical cycles. The figure shows a similar trend as in power cycling case for different aging time and the stress value decreases with aging time due to the lower stiffness. In this figure, the von-Mises stress for SAC305 alloy is shown for different aging time where the maximum stress value is found to be 50.19 MPa for no aging condition and the minimum stress value is found to be 23.51 MPa for 365 days of aging showing a reduction of 53.16%.

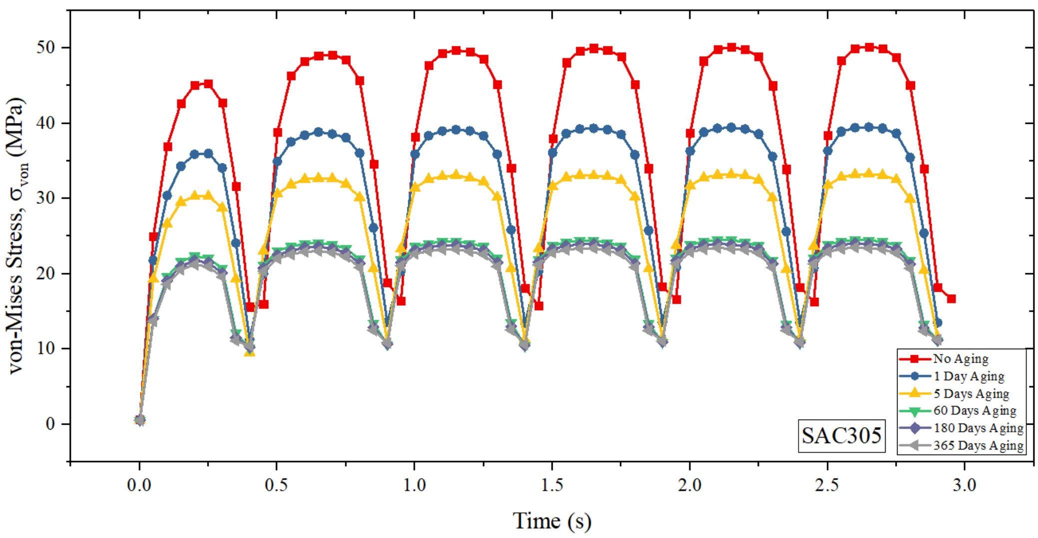

Figure 4.41 Variation of Maximum von-Mises Stress of the Critical Solder Ball with Time for Different Aging Times for SAC305 Solder at Room Temperature and Frequency of 1 Hz

4.4.3.2 Variation of Hysteresis Loop

In Figure 4.42, the effect of aging on the stress-strain hysteresis loop is shown. The figure shows that the hysteresis loop is rotating from a vertical position to a horizontal position with increasing aging time causing a decrease in stress range and an increase in strain range. However, the decrease in stress value is more offset by the increase in strain due to the higher plastic deformation of the solder with aging. The area of the loop, as well as the plastic work per cycle, also increases with increasing time.

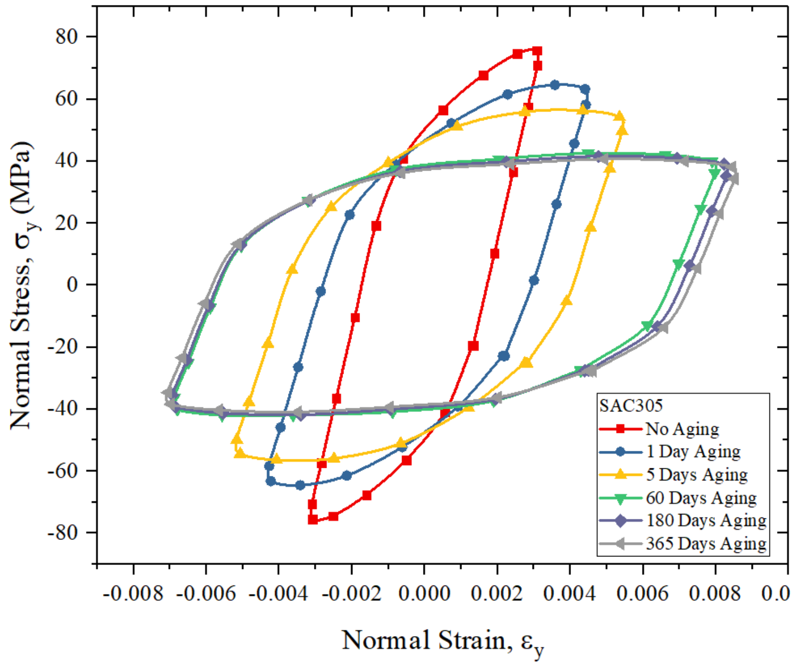

Figure 4.42 Stress-Strain Hysteresis Loop after the 3rd Cycle of Loading for Different Aging Times for SAC305 Solder at Room Temperature and 1 Hz Frequency

4.4.3.3 Variation of PLWK

In Figure 4.43, the effect of aging on plastic work accumulation is shown. From this figure, it is clear that the plastic work accumulation increases with increasing aging time although the variation pattern is similar. This is because, the plastic deformation increases due to the decrease in strength and deformation resistance of the solder joint for higher aging time.

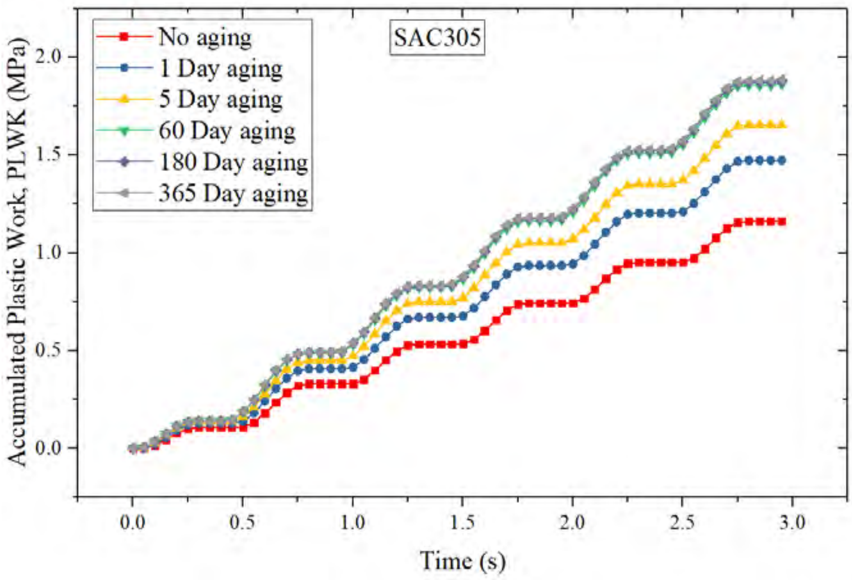

Figure 4.43 Variation of PLWK of the Critical Solder Joint with Time for Different Aging Times for SAC305 Solder at Room Temperature and Frequency of 1 Hz

4.4.3.4 Variation of ΔW

To show the effect of aging on ΔW, the variation of ΔW with aging time is plotted in Figure 4.44 for SAC305 solder joint for different testing temperature and 1 Hz frequency. The variation follows a similar trend as in power cycling for different testing temperatures. However, the figure shows a detrimental effect of aging on the life of solder joint by increasing the value of ΔW. The value of ΔW increases with the increase of aging time due to the degradation of structural properties with aging. Also, a huge change in ΔW occurs just within 60 days of aging. For instance, the change in ΔW from no aging to 365 days of aging is around 196.88% at room temperature whereas the change in ΔW from no aging to 60 days of aging is about 184.9% at room temperature. On the other hand, the change in ΔW from no aging to 365 days of aging is around 63.15% at 125 °C temperature whereas the change in ΔW from no aging to 60 days of aging is about 59.83% at 125 C temperature. In Figures 4.45(a), 4.45(b), and 4.45(c), the effects of aging are plotted for different SAC solder materials at different constant testing temperatures. In Figure 4.45(a), ΔW increases by 60.6% for SAC105 solder joint from no aging to 365 days of aging at room temperature, whereas ΔW increases from no aging to 365 days of aging for SAC405 at room temperature by

303.69%. In Figure 4.45(c), ΔW increases by 16.5% for SAC105 solder joint from no aging to 365 days of aging at 125 °C temperature, whereas ΔW increases from no aging to 365 days of aging for SAC405 at 125 °C temperature by 86%. So, it can be stated that the effect of aging at room temperature is more prominent than at higher temperatures. This is because of the tendency to reach a saturation value of ΔW at a higher temperature and higher aging time.

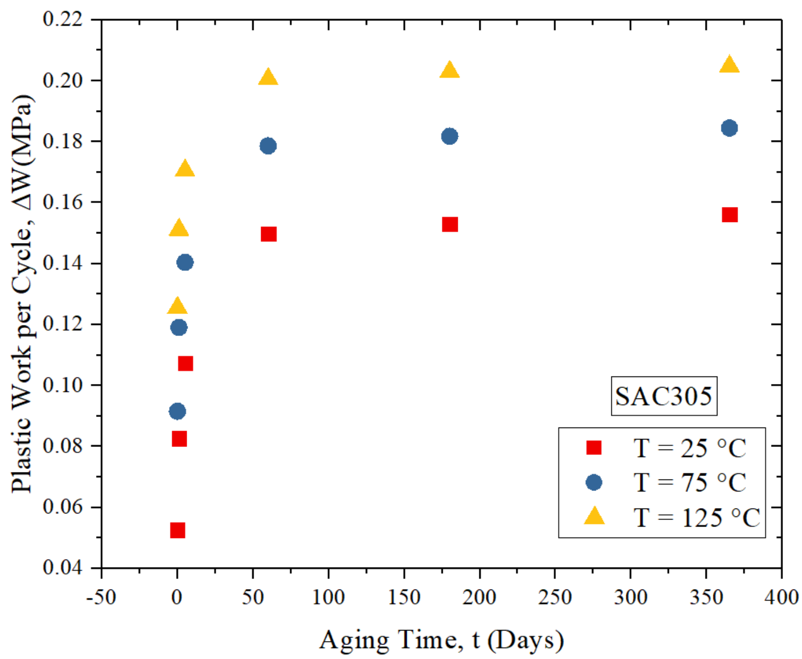

Figure 4.44 Variation of ΔW with Aging Time for SAC305 Solder at Different Testing Temperature and 1 Hz Frequency

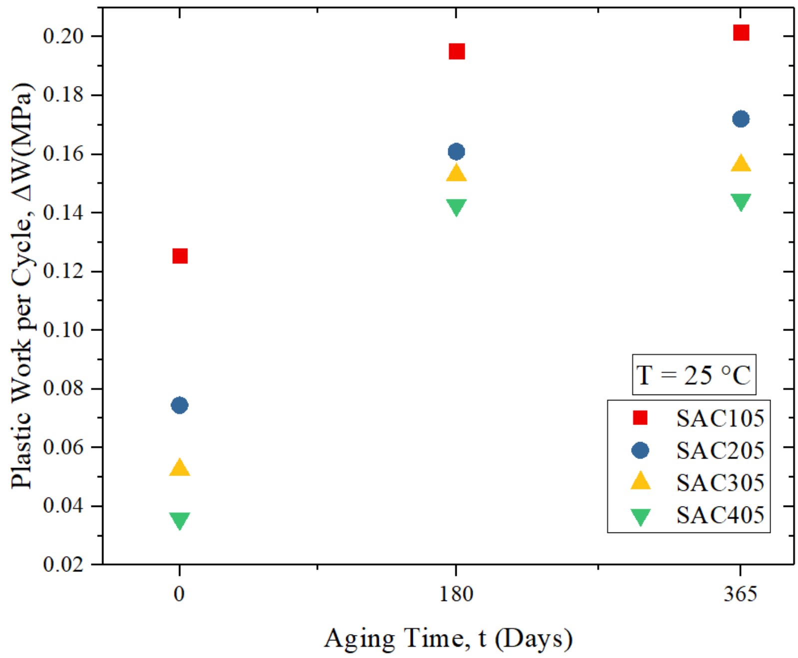

Plastic Work per Cycle, ΔW(MPa)
0.20
0.18
0.16
0.14
0.12
0.10
0.08
0.06
0.04
0.02
0
180
365
Aging Time, t (Days)
T = 25 °C
SAC105
SAC205
SAC305
SAC405

(a)

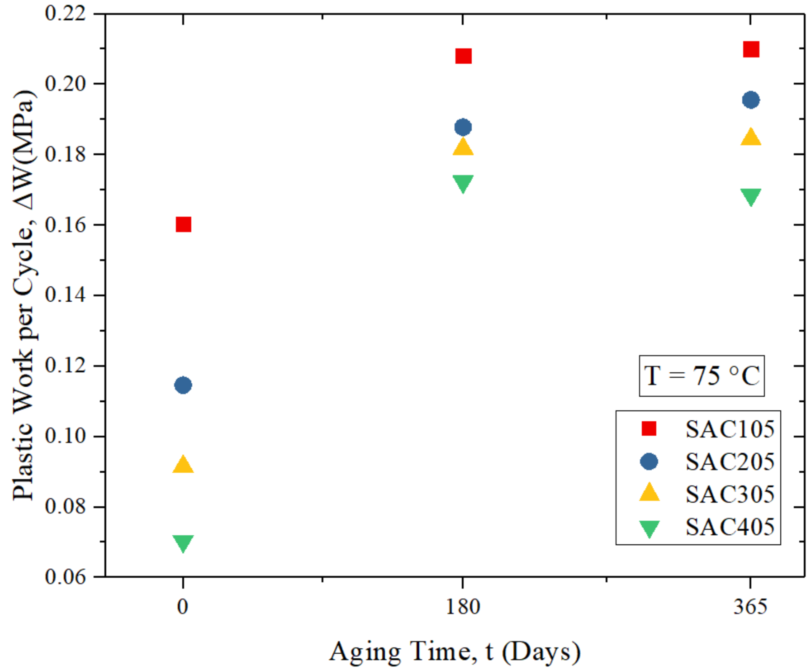

Plastic Work per Cycle, ΔW(MPa)
0.22
0.20
0.18
0.16
0.14
0.12
0.10
0.08
0.06
0
180
365
Aging Time, t (Days)
T = 75 °C
SAC105
SAC205
SAC305
SAC405

(b)

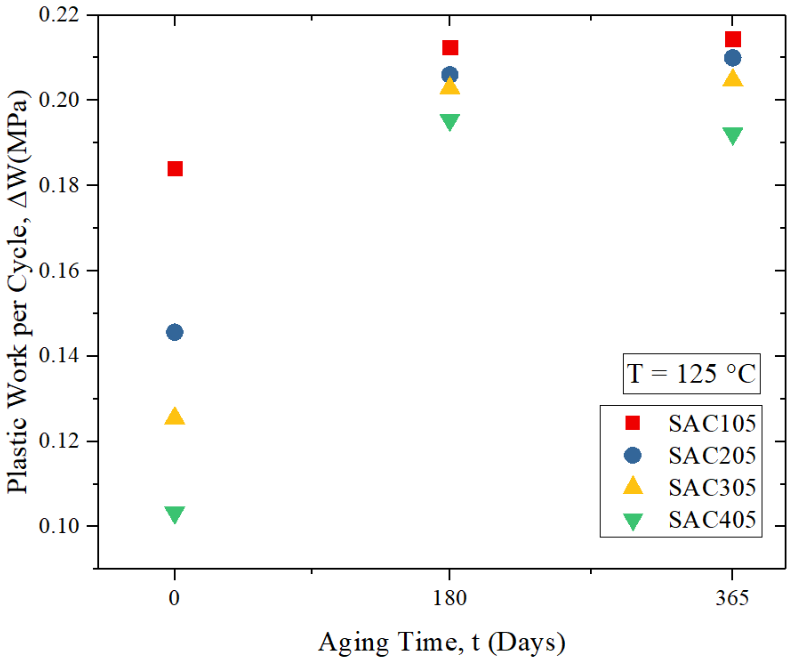

(c)

Figure 4.45 Variation of ΔW with Aging Time for Different SAC Solders at (a) 25 (b) 75, and (c) 125 °C Temperatures and 1 Hz Frequency

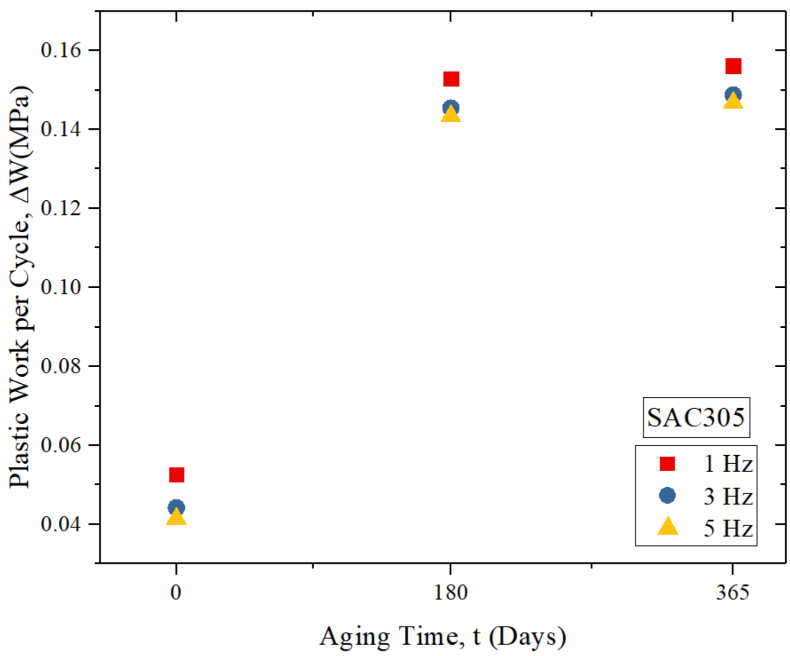

Figure 4.46 Variation of ΔW with Aging Time for Different Loading Frequencies for SAC305 Solder and Room Temperature

Finally, in Figure 4.46, the effect of aging on ΔW is shown for different loading frequency for SAC305 solder joint at room temperature where the change in ΔW from no aging to 365 days of aging is around 196.88% at 1 Hz while, it is around 254.15% for 5 Hz loading frequency.

These analyses reveal that aging has a detrimental effect for all SAC solder type at all testing temperature and all testing frequency but at different degree with a slight deviation for SAC405 at 75 and 125 °C testing temperatures. At these temperatures, ΔW decreases slightly from 180 days aging to 365 days aging. This is because of the fact that the value of the coefficient for deformation resistance saturation value is slightly higher for 365 days of aging than 180 days of aging. Also, after severe aging (365 days of aging) further change in ΔW due to aging can be considered negligible.

In conclusion, it can be said that aging affects the stress distribution, hysteresis loop, plastic work accumulation, and finally on plastic work dissipation per cycle to a great extent. Aging deteriorate the mechanical bend cycle life of the PBGA package by increasing ΔW for all SAC alloys, loading frequency, and testing temperatures.

4.4.4 Effect of Temperature

4.4.4.1 Variation of von-Mises Stress

In Figure 4.47, the effect of temperature on von-Mises stress is shown which also shows a similar trend as previous. The higher the temperature, the lower the stress due to the lower stiffness at higher temperature. In this figure, the von-Mises stress for SAC305 alloy is shown for different testing temperature at no aging and 1 Hz loading frequency. The maximum stress value is found to be 50.19 MPa for room temperature condition and the minimum stress value is found to be 31.81 MPa for 125 C testing temperature showing a reduction of 36.62% in stress.

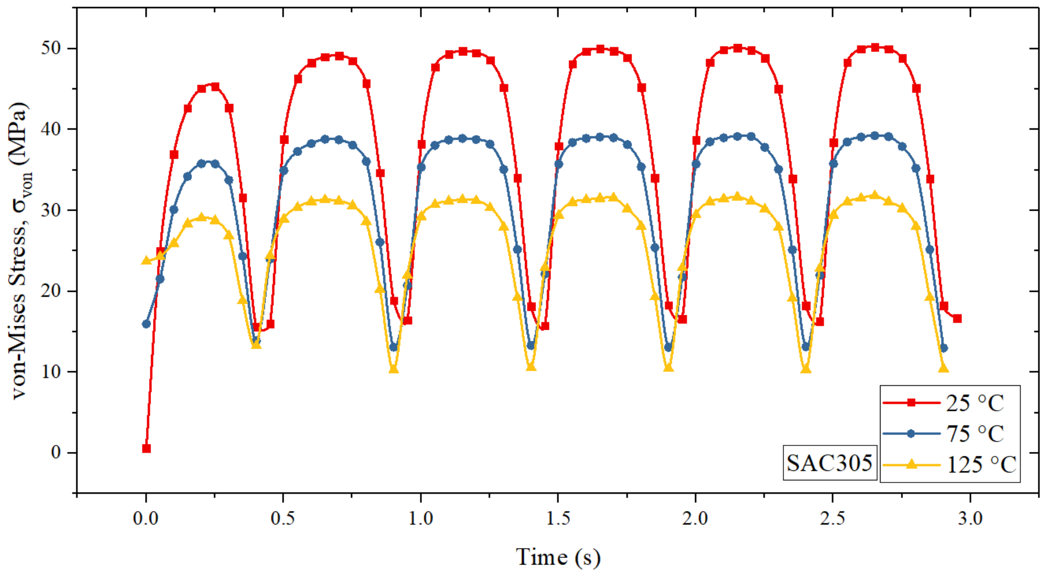

Figure 4.47 Variation of Maximum von-Mises Stress of the Critical Solder Ball with Time for Different Testing Temperatures for SAC305 Solder at No Aging Condition and Frequency of 1 Hz

4.4.4.2 Variation of Hysteresis Loop

In Figure 4.48, the effect of temperature on the stress-strain hysteresis loop is shown. It can be seen from the figure that the hysteresis loop is rotating from a vertical position to a horizontal position with increased temperature causing a decrease in stress range and an increase in strain range. But the decrease in stress range is more offset by the increase in strain range due to the higher plastic deformation of the solder with increased temperature. The area of the loop, as well as the plastic work per cycle, also increases with increasing temperatures.

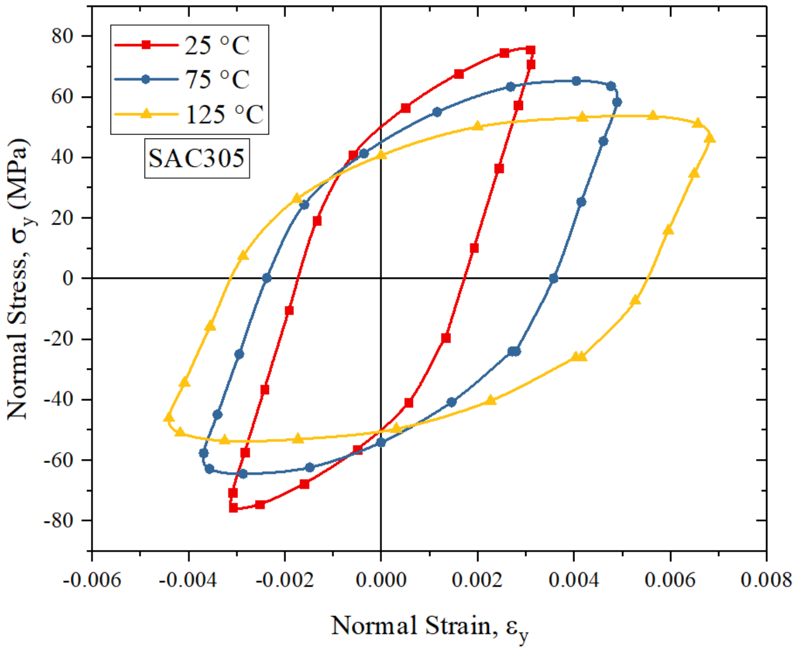

Figure 4.48 Stress-Strain Hysteresis Loop after the 3rd Cycle of Loading for Different Testing Temperatures for SAC Solder at No Aging Condition And 1 Hz Frequency

4.4.4.3 Variation of PLWK

In Figure 4.49, the effect of temperature on plastic work accumulation is shown. From this figure, it is evident that the plastic work accumulation increases with temperature while the variation pattern is similar. This is because the plastic deformation increases with temperature due to the decrease in stiffness of the solder material.

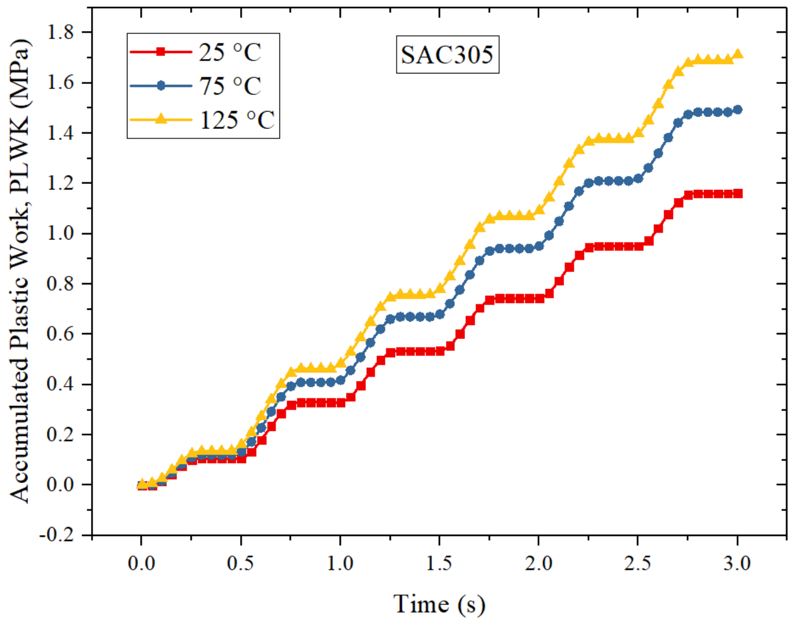

Figure 4.49 Variation of PLWK of the Critical Solder Joint with Time for Different Testing Temperatures for SAC305 Solder at Frequency of 1 Hz and No Aging Condition

4.4.4.4 Variation of ΔW

Structural properties of the solder joint depend largely on the operating temperature. This change in properties results in the change of the ΔW values as well as in the life of the solder joint. To show the effect of temperature on ΔW, Figures from 4.50 to 4.51 are plotted where the variation of ΔW with temperature are shown from different angle of views. From Figures 4.50(a) to 4.50(c), the effect of temperature on ΔW has been plotted for different SAC solder joints at different constant aging time conditions. From these figures, it can be seen that the higher the testing temperature, the higher the value of ΔW, meaning acceleration in failure. It is also depicted from these figures that the change in ΔW with temperature at a constant aging time increases with the increase of silver percentage of the SAC solder alloy. For instance, the increase in ΔW for SAC105 solder from 25 °C to 125 °C temperature change is 46.7 %, whereas it is 188.82 % for SAC405 solder alloy at no aging condition.

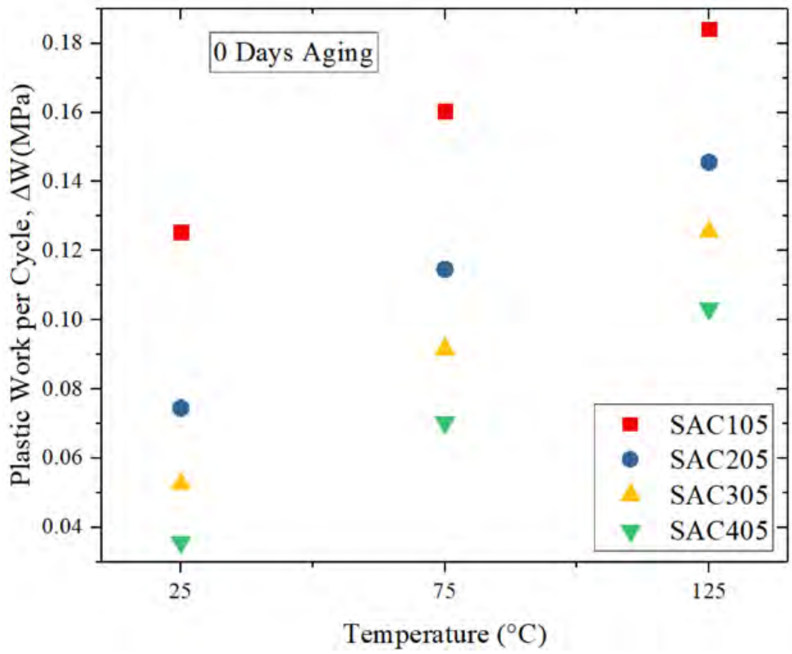
0 Days Aging
Plastic Work per Cycle, ΔW(MPa)
0.18
0.16
0.14
0.12
0.10
0.08
0.06
0.04
SAC105
SAC205
SAC305
SAC405
25
75
125
Temperature (°C)

(a)

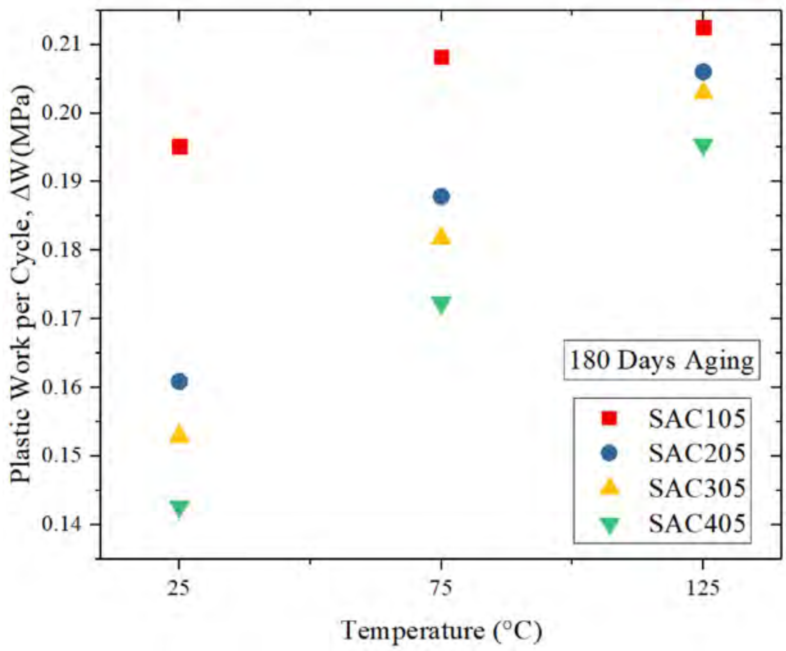
Plastic Work per Cycle, ΔW(MPa)
0.21
0.20
0.19
0.18
0.17
0.16
0.15
0.14
180 Days Aging
SAC105
SAC205
SAC305
SAC405
25
75
125
Temperature (°C)

(b)

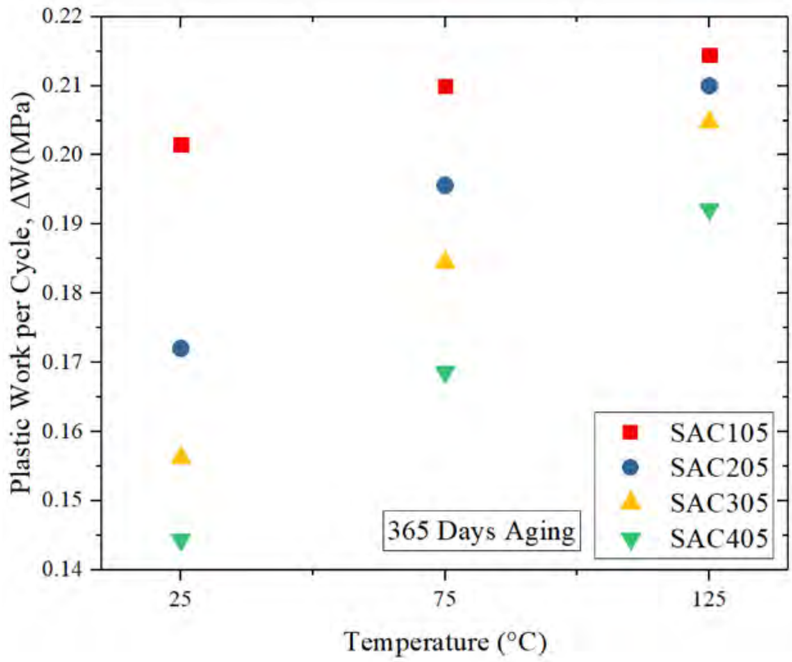

(c)

Figure 4.50 Variation of ΔW with Temperature for Different SAC Solders at (a) No Aging (b) 180 Days Aging, and (c) 365 Days Aging Conditions and 1 Hz Frequency

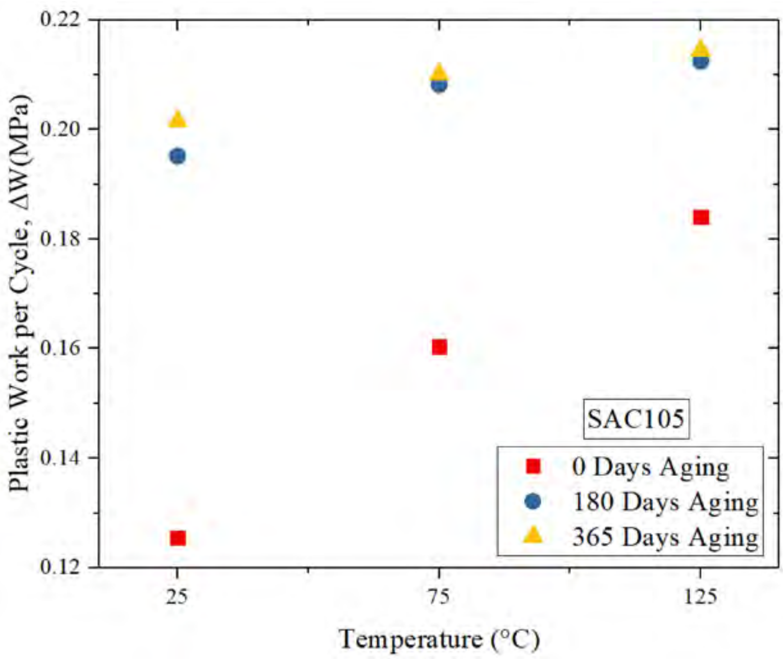

(a)

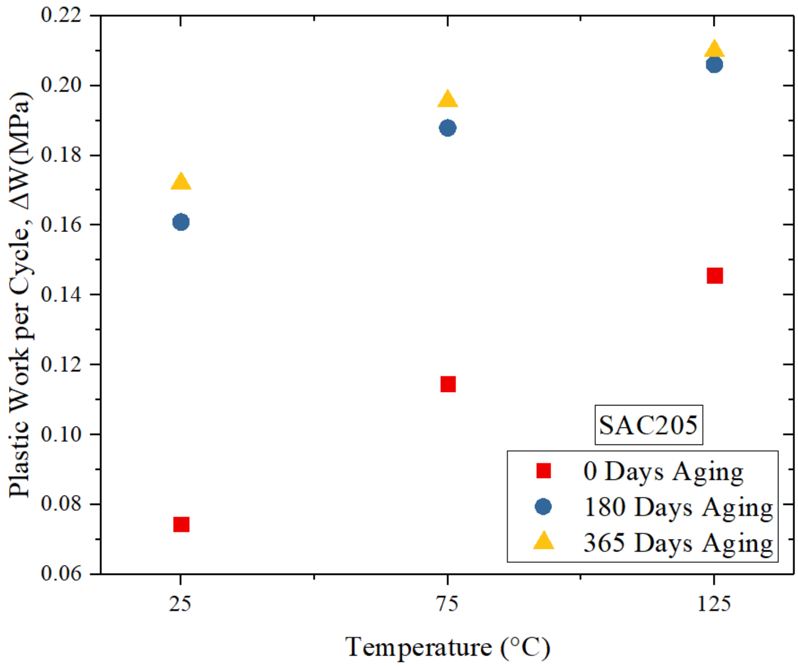
0.22
0.20
0.18
0.16
0.14
0.12
0.10
0.08
0.06
Plastic Work per Cycle, ΔW(MPa)
25
75
125
Temperature (°C)
SAC205
0 Days Aging
180 Days Aging
365 Days Aging

(b)

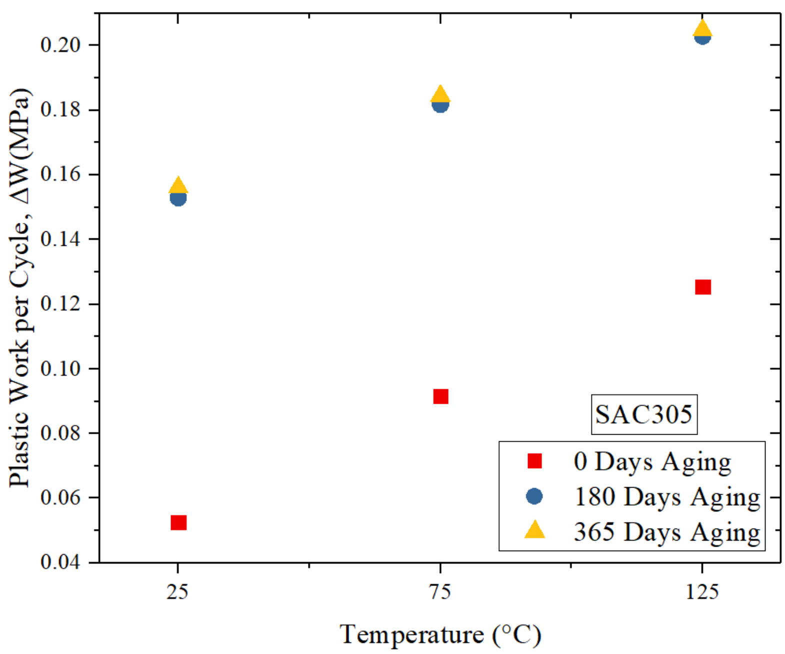
0.20
0.18
0.16
0.14
0.12
0.10
0.08
0.06
0.04
Plastic Work per Cycle, ΔW(MPa)
25
75
125
Temperature (°C)
SAC305
0 Days Aging
180 Days Aging
365 Days Aging

(c)

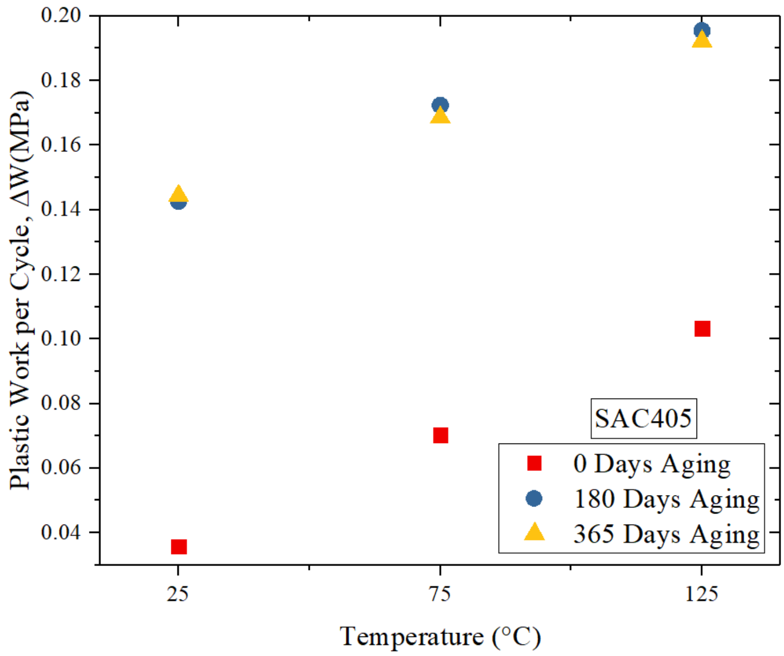

(d)

Figure 4.51 Variation of ΔW with Temperature for Different Aging Times for (a) SAC105 (b) SAC205 (c) SAC305 (d) SAC405 Solders and 1 Hz Frequency

From Figure 4.51(a) to Figure 4.51(d), the effect of temperature on ΔW has been plotted for different aging time at constant silver percent solder alloy. From these figures, it is very clear that the change in ΔW at no aging condition is higher than other aging times for all SAC alloys. For instance, the change in ΔW for SAC105 solder alloy at no aging condition is about 46.7 %, whereas it is only 6.4 % for 365 days of aging.

It can be concluded that temperature also has a substantial effect on the stress distribution, hysteresis loop, plastic work accumulation, and finally on plastic work dissipation per cycle. Temperature declines the mechanical bend cycle life of the PBGA package by increasing ΔW for all SAC alloys and aging condition.

4.4.5 Effect of Frequency

4.4.5.1 Variation of von-Mises Stress

In Figure 4.52, the effect of frequency on von-Mises stress is shown. The figure shows a slight increase in stress value with frequency due to the higher loading rate. In this figure, the von-Mises stress for SAC305 alloy is shown for different loading frequency and the maximum stress value is found to be 54.25 MPa for 5 Hz loading frequency and the minimum stress value is found to be 50.19 MPa for 1 Hz showing a reduction of only 7.48% in stress.

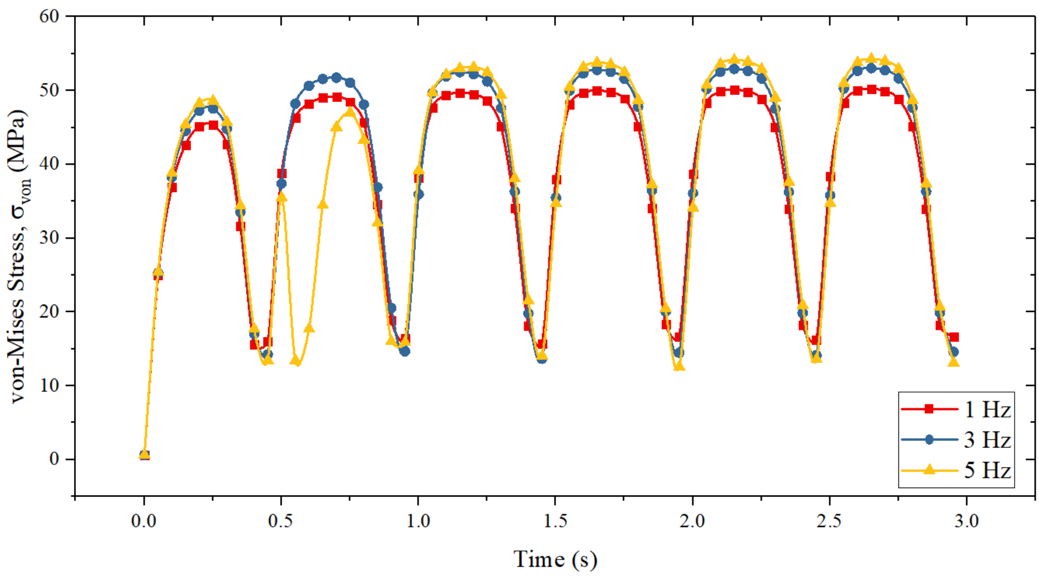

Figure 4.52 Variation of Maximum von-Mises Stress of the Critical Solder Ball with Time for Different Loading Frequencies for SAC305 Solder at Room Temperature and No Aging Condition

4.4.5.2 Variation of Hysteresis Loop

In Figure 4.53, the effect of loading frequency on the stress-strain hysteresis loop is shown. It can be portrayed from the figure that the hysteresis loop rotates slightly from a vertical position to a horizontal position with decreased loading frequency causing a slight decrease in stress range and an increase in strain range. But the decrease in stress range is somewhat more offset by the increase in strain range due to the higher plastic deformation of the solder ball with decreased loading frequency. The area of the loop, as well as the plastic work per cycle, also decreases with the increase in loading frequency.

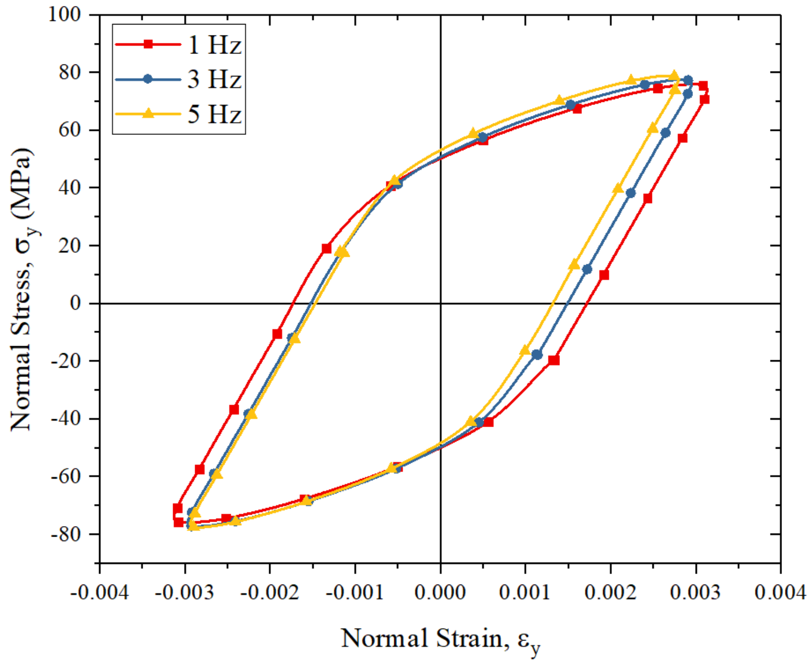

Figure 4.53 Stress-Strain Hysteresis Loop after the 3rd Cycle of Loading for Different Loading Frequencies for SAC Solder at Room Temperature and No Aging Conditions

4.4.5.3 Variation of PLWK

In Figure 4.54, the effect of loading frequency on plastic work accumulation is shown. In this figure, it can be seen that the plastic work accumulation decreases with increasing loading frequency and follow a similar trend for all loading frequencies. This is because the plastic deformation decreases with increasing loading frequency due to the improved strength at higher loading rate.

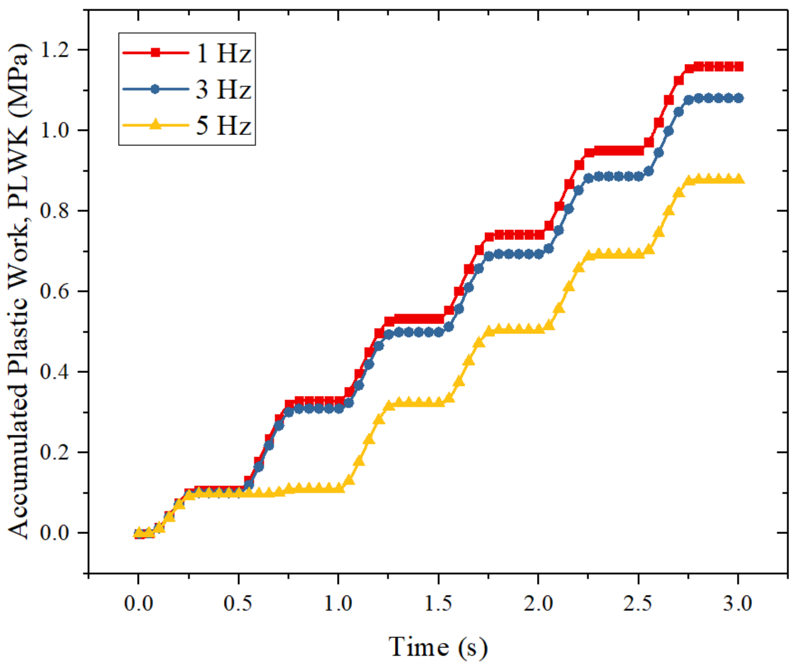

Figure 4.54 Variation of PLWK of the Critical Solder Joint with Time for Different Loading Frequencies for SAC305 Solder at Room Temperature and No Aging Conditions

4.4.5.4 Variation of ΔW

Finally, the effect of frequency on ΔW is shown in Figure 4.55 for different SAC alloys at no aging condition and room temperature. The variation dictates that with the increase in loading frequency, ΔW also decreases leading to a positive effect on solder joint life for all SAC alloys. The decrease in ΔW for SAC105 is about 11% from 1 Hz to 5 Hz loading frequency change, but this decrease in ΔW increases by 25.77 for SAC405 solder for the same change in loading frequency.

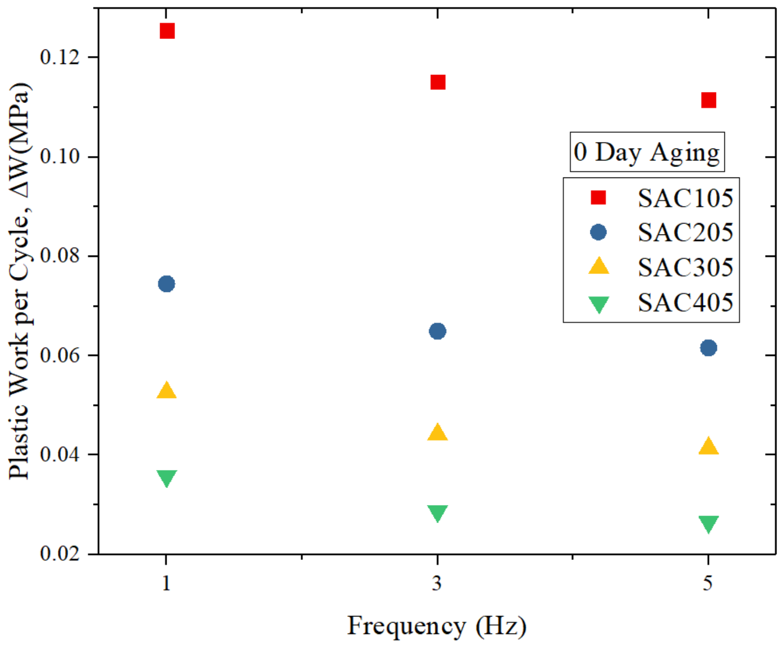

Figure 4.55 Variation of ΔW with Frequency for Different SAC Solders at Room Temperature and No Aging Conditions

From the above discussion, it is evident that effect of loading frequency on the stress distribution, hysteresis loop, plastic work accumulation, and finally on plastic work dissipation per cycle is not so prominent like the other cases. Although, higher loading frequency is slightly beneficial to the mechanical bend cycle life of the PBGA package.

In summary, the effects of isothermal aging of the SAC solder alloy, silver percentage of the SAC solder alloy, testing temperature and loading frequency on the solder joint life of a PBGA microprocessor package have been investigated through finite element analysis. From the results, it can be concluded that the PBGA package with lower silver percentage, aged for higher time, operated at a higher temperature and low frequency has the highest value of ΔW as well as the lowest bend fatigue life. Also, the effect of frequency on ΔW is lower compared to other cases.

4.5 Numerical Validation

The finite element results found in the analysis are compared with the experimental results that are available in the literature. At first, the temperature distribution of the package is compared in Figure 4.56 where the maximum and minimum temperature of the package of finite element analysis results are plotted against the experimental results [25]. The trend of the results conform to each other. Secondly, the location of the critical solder ball in power cycle and mechanical bend cycle is also in good agreement with the result found in the literature [25], [63].

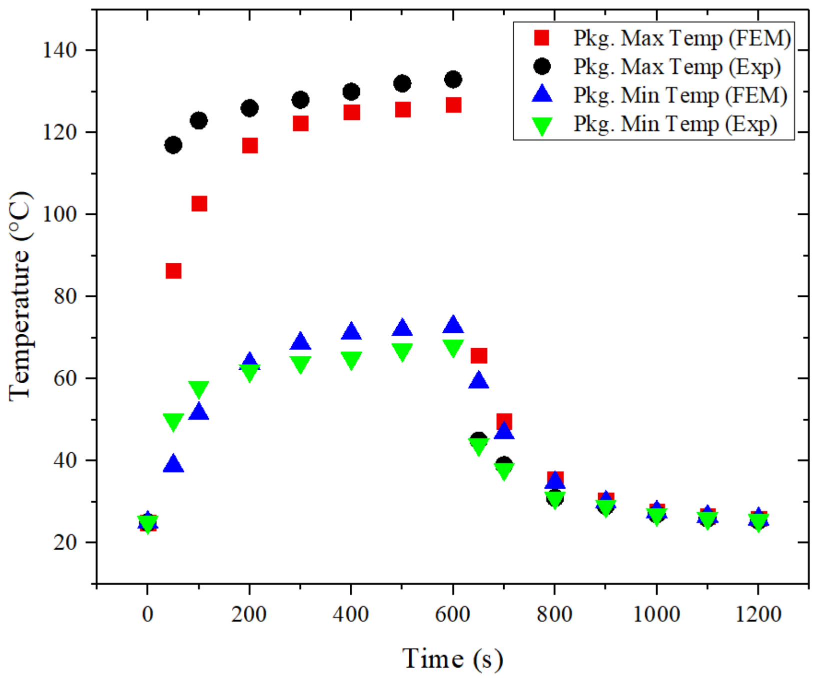

Figure 4.56 Comparison of Experimental [25] and Finite Element Result of the Variation of Package Maximum and Minimum Temperatures with Time for SAC305 Solder and 0.6 W Input Power (1st Cycle)

Moreover, the location of crack initiation in power cycling is compared with the experimental results [25] in Figure 4.57. They are found to be in consistence with each other. Furthermore, the normal stress distribution of the critical solder ball is plotted with the experimental results [25] in Figure 4.58 and shows a similar match.

Finally, the location of crack initiation in mechanical bend cycling is compared with the experimental results [63] in Figure 4.59 and are in good agreement.

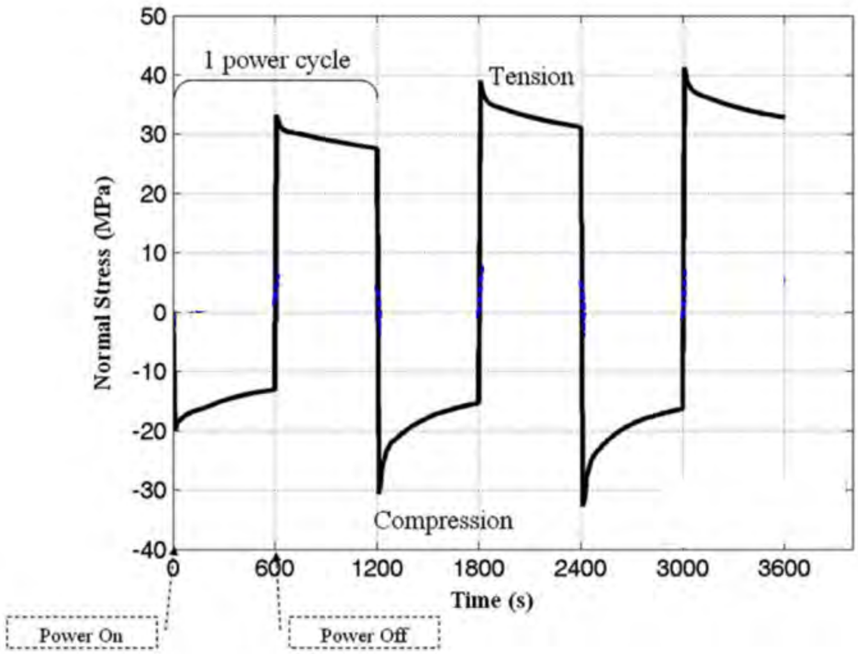

(a)

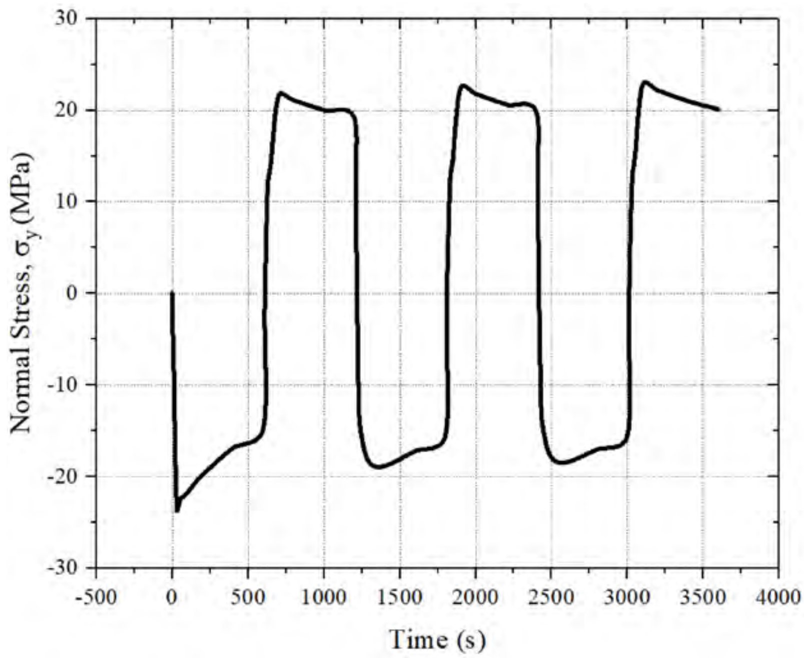

(b)

Figure 4.57 Comparison of Maximum Normal Stress Variation of the Critical Solder Ball with Time (a) Li et al. [25] (b) Finite Element Result

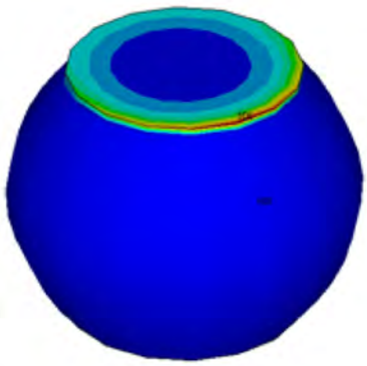

(a)

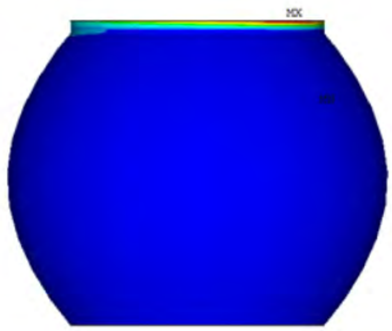

(b)

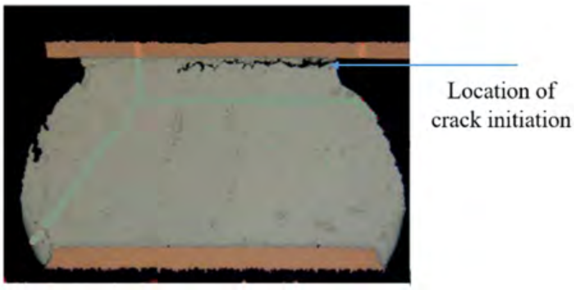

(c)

Figure 4.58 Comparison of the Location of Crack Initiation in the Critical Solder Joint (a) and (b) Finite Element Results (c) Li et al. [25]

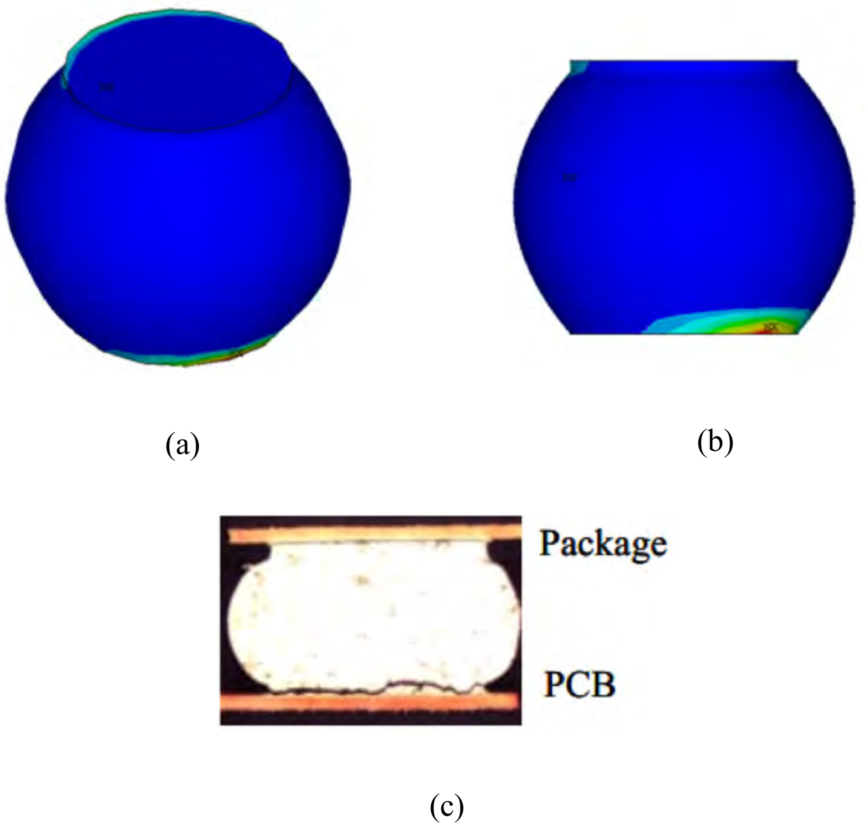

Figure 4.59 Comparison of the Location of Crack Initiation in the Critical Solder Joint (a) and (b) Finite Element Results (c) Skipor et al. [63]

CHAPTER 5

Conclusions

5.1 Summary of the Finite Element Analysis Results

In this thesis, a 3D model of PBGA microprocessor package has been built to simulate the investigation under power and mechanical cycling by finite element method. The effects of solder aging on the power and mechanical cycling have been investigated. It is also investigated how the variation of silver percentage in SAC alloys affects the power and mechanical cycling life. To investigate these, solder joints are considered to be prior aged for various aging times (0 to 365 days at 100 °C) and the silver percentage in solder is also varied from 1 to 4%, which is available in most of the commercially available packages. In power cycling, three different power levels have been used (0.4, 0.5, 0.6 W) and in mechanical cycling, the simulations are performed for three frequencies (1, 3, 5 Hz) and at three testing temperatures (25, 75, 125 °C). The main conclusions of this research are as follows:

- A 3-D finite element model of the 196 I/O PBGA microprocessor component has been developed in commercial software ANSYS for the analysis of power and mechanical bend cycle.
- The power cycling (upto three cycles) simulations are carried out in two steps. Firstly a transient heat transfer analysis is performed to identify the temperature distribution in the package, and then in the second step the structural analysis is performed by using the obtained temperature distribution as FE load.
- The transient thermal analysis shows that a non uniform temperature distribution exists among the various components of the package which is different than the thermal cycle case. The maximum temperature takes place in

the die center and the minimum temperature appears at the outermost corner of the package.

- The temperature distributions of the solder ball as well as the package do not vary significantly with the variation of Ag% in SAC solder.
- In power cycling, the location of the critical solder ball has been found to be the second solder ball along the diagonal direction from the center of the package, which is the die shadow solder ball whereas the location of the critical solder ball has been found to be the outermost corner ball in case of mechanical bend cycling analysis.
- The location of crack initiation in power cycling has been found to be in the copper-SAC alloy interface and on the package side, while in case of mechanical bend cycle, it is found to be in the bulk solder and on PCB side.
- The effect of variation of silver percentage on plastic energy dissipation per cycle is different for power cycling and bend cycling analysis. Increasing the silver percentage in solder increases the plastic energy dissipation resulting in the decrease in power cycling fatigue life whereas in mechanical cycling, increasing silver percentage decreases the plastic energy dissipation resulting an increase in fatigue life.
- Thermal aging of the solder alloy also has opposite effects in power and mechanical cycling. With the increment of aging time, the plastic energy dissipation reduces in power cycling resulting in the increase of power cycling fatigue life. However, in case of bend cycle, the plastic energy dissipation increases with aging time leading to the reduced fatigue life of solder joints.
- With the increase of input power in power cycle, the temperature of the package also increases that accelerates the plastic energy dissipation, resulting in poor fatigue life. On the other hand, with the increase of testing temperature in bend

cycle, the plastic energy dissipation also increases that accelerates the fatigue failure of the solder joint.

- In power cycling, the SAC105 solder joint with longest aging time (365 days) and smallest input power has the lowest plastic energy accumulation and the highest fatigue life, whereas in mechanical bend cycle, SAC405 solder ball with no aging of solder, high loading frequency and tested at low temperature has the lowest plastic energy accumulation and highest fatigue life.
- Based on the above discussion, it is revealed that both aging and variation of Ag% have opposite impact in the power and mechanical cycling life. So a tradeoff is required depending on the type of application of the electronic components. The package designers might get benefitted from the results presented in this thesis.

5.2 Limitations

- Due to the unavailability of life prediction model constants for SAC 105, SAC 205 and SAC 405 materials, analyses have been performed based on plastic energy dissipation per cycle (ΔW) in power cycle, for these solder materials.
- Due to the unavailability of life prediction model constants for SACN05 alloys, analyses have been performed based on plastic energy dissipation per cycle (ΔW) only in mechanical bend cycle.

5.3 Recommendations for Future Works

- The effect of package geometry and materials properties of the various package components on power cycle and mechanical bend cycle fatigue life can be investigated for the optimization of these parameters.
- For more accurate results, it is important to include correct material behavior in ANSYS. Although the behavior of solder material has been considered as temperature dependent, temperature dependent full stress-strain curves also need to be included for other materials. Once these data will be available, the analysis can be done for better results.
- Aging of solder alloy alone has been considered in the analysis. But the aging of other components can be considered for more accurate and realistic results.
- For more accurate life prediction of PBGA package, some experimental analysis can be made for the specific package. Fitting constants for life prediction model can be determined by performing power and bend cycling experiments with this package.
- The ambient temperature in power cycle is held constant which is not true. So the effect of ambient temperature should be incorporated in power cycling to have a more accurate temperature distribution of the package to get more realistic results.
- The combined effect of power and bend cycle can be investigated for more accurate life prediction of the package.

References

[1] Electronic Packaging Technologies, <http://www.doe.carleton.ca/~tjs/10-Packaging>

[2] Vianco, P. T., "Development of Alternatives to Lead-Bearing Solders," Proceedings of the Technical Program on Surface Mount International, San Jose, CA, 1993.

[3] Hwang, J. S., Implementing Lead-Free Electronics, McGraw-Hill, New York, 2005.

[4] Lee, N. C., "Getting Ready for Lead-free Solders," Soldering & Surface Mount Technology, Vol. 9, pp. 65-69, 1997.

[5] Glazer, J., "Metallurgy of Low Temperature Pb-Free Solders For Electronic Assembly," International Materials Reviews, Vol. 40, pp. 65-93, 1995.

[6] Wiese, S., Schubert, A., Walter, H., Dukek, R., Feustel, F., Meusel, E., and Michel, B., "Constitutive Behavior of Lead-free Solders vs. Lead-containing Solders - Experiments on Bulk Specimens and Flip-Chip Joints," Proceeding of the 51st Electronic Components and Technology Conference, pp. 890-902, 2001.

[7] McCabe, R. J., and Fine, M. E., "Athermal And Thermally Activated Plastic Flow in Low Melting Temperature Solders At Small Stresses," Scripta Materialia, vol. 39, pp. 189-195, 1998.

[8] Lau, J. H., "Solder Joint Reliability of Flip Chip and Plastic Ball Grid Array Assemblies under Thermal, Mechanical, and Vibrational Conditions," IEEE Transactions on Components, Packaging, and Manufacturing Technology, Part B: Advanced Packaging, vol. 19, pp. 728-735, 1996.

[9] Hertzberg, R. W., Vinci, R. P., and Hertzberg, J. L., Deformation and Fracture Mechanics of Engineering Materials, 4th edition, John Wiley & Sons Inc, 1996.

[10] E606-92, Standard Practice for Strain-Controlled Fatigue Testing, Annual Book of ASTM Standards, Vol. 3, 2004.

[11] Mustafa, M., Roberts, J. C., Suhling, J. C., Lall, P., “The Effects of Aging of the Cyclic Stress-Strain and Fatigue Behaviors of Lead Free Solders,” Proceedings of InterPACK 2013, pp. 1-12, 2013.

[12] Che, F.X. and Pang, J.H., “Thermal Fatigue Reliability Analysis for PBGA with Sn-3.8 Ag-0.7 Cu Solder Joints,” Proceedings of the 6th Electronics Packaging Technology Conference (EPTC 2004), IEEE, pp. 787-792, December 2004.

[13] George, E., Das, D., Osterman, M. and Pecht, M., “Thermal Cycling Reliability of Lead-Free Solders (SAC305 And Sn3. 5Ag) for High-Temperature Applications,” IEEE Transactions on Device and Materials Reliability, Vol. 11, pp. 328-338, 2011.

[14] Zhao, Y., Basaran, C., Cartwright, A. and Dishongh, T., “Thermomechanical Behavior of Micron Scale Solder Joints: An Experimental Observation,” Journal of the Mechanical Behavior of Materials, Vol. 10, pp.135-146, 1999.

[15] Tsai, M.Y., Hsu, C.J. and Wang, C.O. , “Investigation of Thermomechanical Behaviors of Flip Chip BGA Packages during Manufacturing Process And Thermal Cycling,” IEEE Transactions on Components and Packaging Technologies, Vol. 27, pp. 568-576, 2004.

[16] Qi, Y., Lam, R., Ghorbani, H.R., Snugovsky, P. and Spelt, J.K., “Temperature Profile Effects In Accelerated Thermal Cycling of SnPb And Pb-Free Solder Joints,” Journal of Microelectronics Reliability, Vol. 46, pp. 574-588, 2006.

[17] Lau, C.S., Abdullah, M.Z., Mujeebu, M.A. and Yusop, N.M.D., “Finite Element Analysis on the Effect of Solder Joint Geometry for the Reliability of Ball Grid Array Assembly with Flexible and Rigid PCBs,” Journal of Engineering Science and Technology, Vol. 9, pp. 47-63, 2014.

[18] Motalab, M., Shakil, A.S., Rahman, T. and Suhling, J.C., “Variation of Thermal Cycling Life Prediction of PBGA Microprocessor Components with Substrate Properties,” Journal of Emerging Trends in Engineering and Applied Sciences (JETEAS), Vol. 6, pp. 371-376, 2015.

[19] Lee, S.W. and Lau, J.H., “Effect of Chip Dimension and Substrate Thickness on the Solder Joint Reliability of Plastic Ball Grid Array Packages,” Circuit World, Vol. 23, pp. 16-19, 1997.

[20] Han, B., Chopra, M., Park, S., Li, L. and Verma, K., “Effect of Substrate CTE on Solder Ball Reliability of Flip Chip Ball Grid Array Package Assembly,” Journal of Surface Mount Technology, Vol. 9, pp. 25-34, 1996.

[21] Darveaux, R., “Effect of Simulation Methodology on Solder Joint Crack Growth Correlation,” Proceedings of the 50th Electronic Components and Technology Conference, pp.1048-1058, 2000.

[22] Popp, D.H., Mawer, A. and Presas, G., “Flip Chip PBGA Solder Joint Reliability: Power Cycling versus Thermal Cycling,” Motorola Semiconductor Products Sector, Austin, TX, 2005.

[23] Ham, S.J., Cho, M.S. and Lee, S.B., “Thermal Deformations of CSP Assembly During Temperature Cycling and Power Cycling,” International Symposium on Electronic Materials and Packaging, pp. 350-357, 2000.

[24] Rodgers, B., Punch, J. and Jarvis, J., “Finite Element Modelling of A BGA Package Subjected to Thermal and Power Cycling,” Eighth Intersociety Conference on Thermal and Thermomechanical Phenomena in Electronic Systems, pp. 993-1000, 2002.

[25] Li, J., Karppinen, J., Laurila, T. and Kivilahti, J.K., “Reliability of Lead-Free Solder Interconnections in Thermal and Power Cycling Tests,” IEEE Transactions on Components and Packaging Technologies, Vol. 32, pp. 302-308, 2009.

[26] Laurila, T., Mattila, T., Vuorinen, V., Karppinen, J., Li, J., Sippola, M. and Kivilahti, “Evolution of Microstructure and Failure Mechanism of Lead-Free Solder Interconnections in Power Cycling and Thermal Shock Tests,” Microelectronics Reliability, Vol. 47, pp. 1135-1144, 2007.

[27] Park, S.B. and Ahmed, I.Z., “Shorter Field Life in Power Cycling for Organic Packages,” Journal of Electronic Packaging, Vol. 129, pp.28-34, 2007.

[28] Kariya, Y., Hosoi, T., Terashima, S., Tanaka, M. and Otsuka, M., "Effect of Silver Content on the Shear Fatigue Properties of Sn-Ag-Cu Flip-Chip Interconnects," Journal of electronic materials, Vol. 33, pp. 321-328, 2004.

[29] Kang, S.K., Lauro, P., Shih, D.Y., Henderson, D.W., Gosselin, T., Bartelo, J., Cain, S.R., Goldsmith, C., Puttlitz, K.J. and Hwang, T.K., "Evaluation of Thermal Fatigue Life and Failure Mechanisms of Sn-Ag-Cu Solder Joints with Reduced Ag Contents," Proceedings of the 54th Electronic Components and Technology Conference, Vol. 1, pp. 661-667, 2004.

[30] Henshall, G., Bath, J., Sethuraman, S., Geiger, D., Syed, A., Lee, M.J., Newman, K., Hu, L., Kim, D.H., Xie, W. and Eagar, W., "Comparison of Thermal Fatigue Performance of SAC105 (Sn-1.0 Ag-0.5 Cu), Sn-3.5 Ag, And SAC305 (Sn-3.0 Ag-0.5 Cu) BGA Components with SAC305 Solder Paste," Proceedings of IPC APEX, 2009.

[31] Zhang, X. and Lee, S.R., "Critical issues in computational modeling and fatigue life analysis for PBGA solder joints," The International journal of microcircuits and electronic packaging, Vol. 21, pp. 253-261, 1998.

[32] Xiao, Q., Bailey, H. J., and Armstrong, W. D., "Aging Effects on Microstructure and Tensile Property of Sn3. 9Ag0. 6Cu Solder Alloy," Journal of Electronic Packaging, Vol. 126, p. 208, 2004.

[33] Ding, Y., Wang, C., Tian, Y., and Li, M., "Influence of Aging Treatment on Deformation Behavior of 96.5Sn3.5Ag Lead Free Solder Alloy During In Situ Tensile Tests," Journal of Alloys and Compounds, Vol. 428, pp. 274–285, 2007.

[34] Ma, H., Suhling, J. C., Lall, P., and Bozack, M. J., "Reliability of the Aging Lead Free Solder Joint," Proceedings of the 56th Electronic Components and Technology Conference, pp. 849-864, 2006.

[35] Zhang, Y., Cai, Z., Suhling, J. C., Lall, P., and Bozack, M. J., "The Effects of Aging Temperature on SAC Solder Joint Material Behavior and Reliability," Proceedings of the 58th Electronic Components and Technology Conference, pp. 99-112, 2008.

[36] Z Cai., Zhang, Y., Suhling, J. C., Lall P., Johnson, R. W., and Bozack, M. J., “Reduction of Lead Free Solder Aging Effects Using Doped SAC Alloys,” Proceedings of the 60th Electronic Components and Technology Conference, pp.1493-1511, 2010.

[37] Basit, M.M., Motalab, M., Suhling, J.C. and Lall, P., “The Effects of Aging on the Anand Viscoplastic Constitutive Model for SAC305 Solder,” IEEE 14th Intersociety Conference on Thermal and Thermomechanical Phenomena in Electronic Systems (ITherm), pp. 112-126, 2014.

[38] Mustafa, M., Cai, Z., Suhling, J. C., and Lall, P., “The Effects of Aging on The cyclic Stress-Strain Behavior and Hysteresis Loop Evolution of Lead Free Solders,” Proceedings of the 61th Electronic Components and Technology Conference, pp. 927-939, 2011.

[39] Kim, D. G., Kim, J. W., and Jung S. B., “Effect of Aging Conditions on Interfacial Reaction and Mechanical Joint Strength between Sn–3.0Ag–0.5Cu Solder and Ni–P UBM,” Materials Science and Engineering B, Vol. 121, pp. 204–210, 2005.

[40] Coyle, R. J., Solan, P. P., Serafino, A. J., and Gahr, S. A., “The Influence of Room Temperature Aging on Ball Shear Strength and Microstructure of Area Array Solder Balls,” Proceedings of the 50th Electronic Components and Technology Conference, pp. 160-169, 2000.

[41] Lee, T. K., Ma, H., Liu, K. C., and Xue, J., “Impact of Isothermal Aging on Long- Term Reliability of Fine-Pitch Ball Grid Array Packages with Sn-Ag-Cu Solder Interconnects: Surface Finish Effects,” Journal of Electronic Materials, Vol. 39, pp. 2564-2573, 2010.

[42] Motalab, M., Mustafa, M., Suhling, J. C., Zhang, J., Evans, J. L., Bozack, M. J., Lall, P., “Correlation of Reliability Models Including Aging Effects with Thermal Cycling Reliability Data,” Proceedings of the 63rd Electronic Components and Technology Conference, pp. 986-1004, 2013.

[43] Zhang, J., Thirugnanasambandam, S., Evans, J. L., Bozack, M. J., Zhang, Y., Suhling, J. C., "Correlation of Aging Effects on the Creep rate and Reliability in Lead Free Solder Joints," SMTA Journal, Vol. 25(3), pp. 19-28, 2012.

[44] Zhang, T., Evans, J., Mitchell, C., Li, Z. Z., Crandall, E., Ridenour, J., and Xie, F., "Reliability of Lead-Free BGA with SnPb Solder Paste for Harsh Environments," Proceedings SMTA/CAVE Symposium on AIMS Harsh Environment Electronics, 2009.

[45] Smetana, J., Coyle, R., Read, P., Popowich, R., Fleming, D., and Sack, T., "Variations in Thermal Cycling Response of Pb-free Solder Due to Isothermal Preconditioning," Proceedings of SMTAI 2011, pp. 641-654, 2011.

[46] Li, M., Lee, K. Y., Olsen, D. R., Chen, W. T., Tan, B. T. C., and Mhaisalkar, S., "Microstructure, Joint Strength and Failure Mechanisms of SnPb and Pb-Free Solders in BGA Packages," IEEE Transactions on Electronics Packaging Manufacturing, Vol. 25, pp. 185-192, 2002.

[47] Darveaux, R., "Shear Deformation of Lead Free Solder Joints," Proceedings of the 55th Electronic Components and Technology Conference, pp. 882-893, 2005.

[48] Lee, T. K., Zhou, B., and Bieler, T. R., "Impact of Isothermal Aging and Sn Grain Orientation on the Long-Term Reliability of Wafer-Level Chip-Scale Package Sn– Ag–Cu Solder Interconnects," IEEE Transactions on Components, Packaging and Manufacturing Technology, Vol. 2, Issue 3, pp. 496-501, 2012.

[49] Zhang, J., Hai, Z., Thirugnanasambandam, S., Evans, J.L., Bozack, M.J., Zhang, Y. and Suhling, J.C., "Thermal Aging Effects on The Thermal Cycling Reliability of Lead-Free Fine Pitch Packages" IEEE transactions on components, packaging and manufacturing technology, Vol. 3, pp. 1348-1357, 2013.

[50] Ahmed, S., Wu, J., Fu, N., Suhling, J.C. and Lall, P., "Quantification and Modeling of Microstructural Evolution in Lead Free Solders During Long

Term Isothermal Aging," in 2018 IEEE 68th Electronic Components and Technology Conference (ECTC), pp. 162-171, 2018.

[51] Ma, H., Suhling, J. C., Zhang, Y., Lall, P., and Bozack, M. J., "The Influence of Elevated Temperature Aging on Reliability of Lead Free Solder Joints," Proceedings of the 57th Electronic Components and Technology Conference, pp. 653-668, 2007.

[52] Lampe, B. T., "Room Temperature Aging Properties of Some Solder Alloys," Welding Journal, Vol. 55, pp. 330-340, 1976.

[53] Zhang, Y., "The Effects of Aging on the Mechanical Behavior of Lead Free and Mixed Formulation Solder Alloys," Ph.D. Dissertation, Auburn University, 2010.

[54] Zhang, Y., Cai, Z., Suhling, J. C., Lall, P., and Bozack, M. J., "The Effects of SAC Alloy Composition on Aging Resistance and Reliability," Proceedings of the 59th Electronic Components and Technology Conference, pp. 370-389, 2009.

[55] Anderson, I. E., and Harringa, J. L., "Elevated Temperature Aging of Solder Joints Based on Sn-Ag-Cu: Effects on Joint Microstructure and Shear Strength," Journal of Electronic Materials, Vol. 33, pp. 1485-1496, 2004.

[56] Chavali, S., Singh, Y., Kumar, P., Subbarayan, G., Dutta, I., and Edwards, D. R., "Aging Aware Constitutive Models for SnAgCu Solder Alloys," Proceedings of the 61st Electronic Components and Technology Conference, pp.701-705, 2011.

[57] Bansal, A., Lee, T. K., Liu, K.C., and Xue, J., "Effects of Isothermal Aging and In- Situ Current Stress on The Reliability of Lead-Free Solder Joints," Proceedings of the 60th Electronic Components and Technology Conference, pp. 1529-1535, 2010.

[58] Fix, A. R., Nüchter, W., and Wilde, J., "Microstructural Changes of Lead-Free Solder Joints During Long-Term Aging, Thermal Cycling and Vibration Fatigue," Soldering and Surface Mount Technology, Vol. 20, pp. 13-21, 2008.

[59] Lee, S. W. R., Tsui, Y.-K., Hunag, X., and Yan, E. C. C., "Effects of Room Temperature Storage Time on the Shear Strength of PBGA Solder Balls," Proceedings of the 2002 ASME International Mechanical Engineering Congress and Exposition, pp. 1-4, 2002.

[60] Lee, T. K., and Ma, H., "Aging Impact on the Accelerated Thermal Cycling Performance of Lead-Free BGA Solder Joints in Various Stress Conditions," Proceedings of the 62nd Electronic Components and Technology Conference, pp. 477-482, 2012.

[61] Mustafa, M., Roberts, J. C., Suhling, J. C., and Lall, P., "The Effects of Aging on the Fatigue Life of Lead Free Solders," Proceedings of the 64th Electronic Components and Technology Conference, pp. 666-683, Orlando, FL, May 27-30, 2014.

[62] Lall, P., Shantaram, S., Suhling, J., and Locker, D., "Effect of Aging on the High Strain Rate Mechanical Properties of SAC105 and SAC305 Lead free Alloys," Proceedings of the 63rd IEEE Electronic Components and Technology Conference, pp. 1277-1293, Las Vegas, NV, May 28-31, 2013.

[63] Skipor, A. and Leicht, L., "Mechanical Bending Fatigue Reliability and Its Application to Area Array Packaging," Proceedings of the 51st Electronic Components and Technology Conference, pp. 606-612, 2001.

[64] Leicht, L. and Skipor, A., "Mechanical Cycling Fatigue of PBGA Package Interconnects," Microelectronics Reliability, Vol. 40, pp. 1129-1133, 2000.

[65] Pang, J.H. and Che, F.X., "Isothermal Cyclic Bend Fatigue Test Method for Lead-Free Solder Joints," Journal of Electronic Packaging, Vol. 129, pp. 496-503, 2007.

[66] Syed, A., "Predicting Solder Joint Reliability for Thermal, Power, and Bend Cycle Within 25% Accuracy," Proceedings of the 51st Electronic Components and Technology Conference, pp. 255-263, 2001

[67] Tu, P.L., Chan, Y.C., Hung, K.C. and Lai, J.K., "Comparative Study of Micro-BGA Reliability under Bending Stress," IEEE transactions on advanced packaging, Vol. 23, pp. 750-756, 2000.

[68] Kim, I. and Lee, S.B., “Reliability and Failure Analysis of Lead-Free Solder Joints for PBGA Package under A Cyclic Bending Load” IEEE Transactions on Components and Packaging Technologies, Vol. 31, pp. 478-484, 2008.

[69] Rooney, D.T., Castello, N.T., Cibulsky, M., Abbott, D. and Xie, D., “Materials Characterization of the Effect of Mechanical Bending on Area Array Package Interconnects,” Microelectronics Reliability, Vol. 44, pp.275-285, 2004.

[70] Roberts, J., Motalab, M., Hussain, S., Suhling, J.C., Jaeger, R.C. and Lall, P., “Measurement of die stresses in microprocessor packaging due to thermal and power cycling,” IEEE 62nd Electronic Components and Technology Conference, pp. 756-770, 2012.

[71] Hong, B.Z. and Su, L.S., “On Thermal Stresses and Reliability of A PBGA Chip Scale Package,” Proceedings of the 48th Electronic Components and Technology Conference, pp. 503-510, 1998.

[72] Paul V. Bolotoff, 2010, Physical and Mechanical Properties of Solder Alloys, <file:///E:/Electronic%20Packaging/Properties/Solder%20Alloys_%20Physical%20and%20Mechanical%20Properties.html>

[73] Intel, Physical Constants of IC Package Materials: Databook, Ch. 5, <https://www.intel.com/content/dam/www/public/us/en/documents/packagingdatabooks/packaging-chapter-05-databook.pdf>

[74] Gregory K. Ovrebo, 2008, Thermal Simulation of Four Die-Attach Materials, < https://apps.dtic.mil/dtic/tr/fulltext/u2/a477372.pdf>

[75] Motalab, M., Mustafa, M., Suhling, J.C., Zhang, J., Evans, J., Bozack, M.J. and Lall, P., “Thermal Cycling Reliability Predictions for PBGA Assemblies that Include Aging Effects,” ASME International Technical Conference and Exhibition on Packaging and Integration of Electronic and Photonic Microsystems, pp. V001T05A008-V001T05A008, 2013.

[76] Basit, M., Ahmed, S., Motalab, M., Roberts, J.C., Suhling, J.C. and Lall, P., “The Anand parameters for SAC solders after extreme aging,” IEEE 15th Intersociety Conference on Thermal and Thermomechanical Phenomena in Electronic Systems (ITherm), pp. 440-447, 2016.

[77] Motalab, M., Cai, Z., Suhling, J.C., Zhang, J., Evans, J.L., Bozack, M.J. and Lall, P., “Improved Predictions of Lead Free Solder Joint Reliability that Include Aging Effects,” IEEE 62nd Electronic Components and Technology Conference, pp. 513-531, 2012.

[78] Basit, Munshi M., “Constitutive Model and Solder Joint Reliability Predictions for BGA Packages Subjected to Aging,” Ph.D. Thesis, Department of Mechanical Engineering, Auburn University, 2015.

[79] Che, F., X., Pang, J. H. L., Xiong, B. S., Xu, L., Low, T. H., “Lead Free Solder Joint Reliability Characterization for PBGA, PQPF and TSSOP Assemblies,” Proceedings of the 55th IEEE Electronic Components and Technology Conference, pp. 916-921, 2005.

[80] Basit, M., Motalab, M., Suhling, J.C. and Lall, P., “Viscoplastic Constitutive Model for Lead-Free Solder Including Effects of Silver Content, Solidification Profile, and Severe Aging,” International Technical Conference and Exhibition on Packaging and Integration of Electronic and Photonic Microsystems collocated with the ASME 2015 13th International Conference on Nanochannels, Microchannels, and Minichannels, pp. V002T01A002-V002T01A002. 2015.

[81] Intel, Ball Grid Array (BGA) Packaging, <https://www.intel.com/content/dam/www/public/us/en/documents/packaging-databooks/packaging-chapter-14-databook.pdf>

[82] Motalab, M., “A Constitutive Model for Lead Free Solder Including Aging Effects and Its Application to Microelectronic Packaging,” Ph.D. Thesis, Department of Mechanical Engineering, Auburn University, 2013.